Highlights of Fifty Years of Turbulent Boundary Layer Research

Turbulence Colloquium Marseille 2011

James Wallace

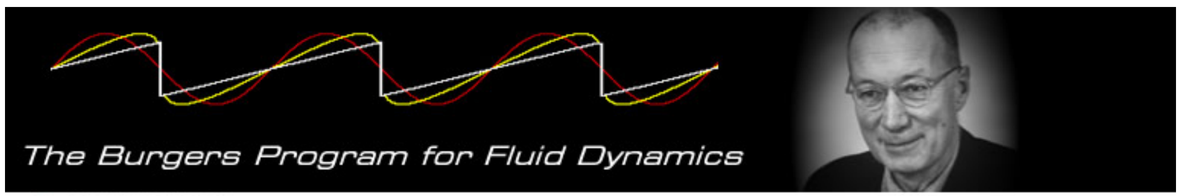

Landmarks of Turbulent Boundary Layer Research

Pre – 1961

Development of Hot-wire anemometry & measurement of statistical properties.

1960s

Visualization identifying organized (coherent) structures related to turbulence production.

1970s

Conditional sampling and averaging methods (quadrant analysis, VITA, etc.) developed to quantify properties and effects of organized structures.

1980s

First DNS of turbulent channel and boundary layer flows providing full spatial field properties and access to 3D structural information. First experimental measurements of velocity gradient tensor based properties: vorticity, dissipation rate, etc.

1990s

Development of better methods to identify vortices. Implementation of planar PIV providing new insights to flow structure. Development of field sites for experiments in the ASL at very high Reynolds numbers. Development of high Reynolds number laboratory facilities.

2000s

DNS at significantly higher Reynolds numbers and supersonic Mach numbers. Use of stereo-, tomographic- & holographic-PIV to provide additional insight about flow structure.

2010s

DNS for much higher Reynolds numbers and hypersonic flow (Re_θ ~ 11,000 & Mach ~ 12).

Pre - 1961

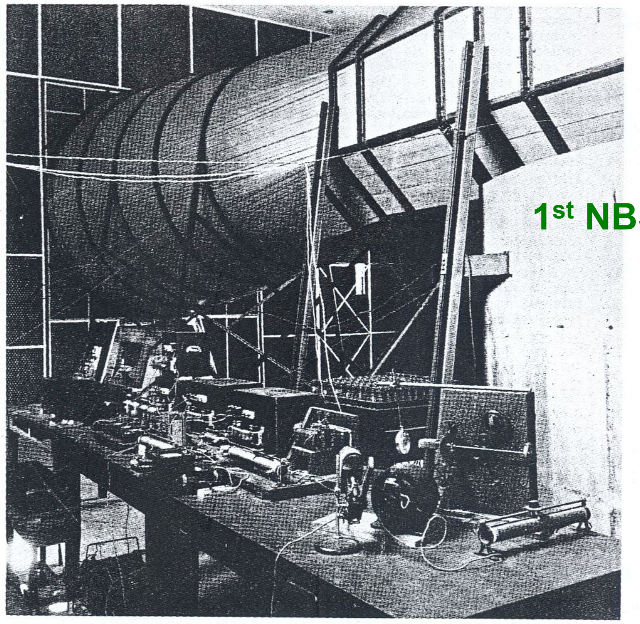

1st NBS hot-wire apparatus

Figure 1. General View of First NBS Hot-Wire Apparatus (Dryden and Kuethe, reference [6])

Dryden & Kuethe (1929) NACA TR 320

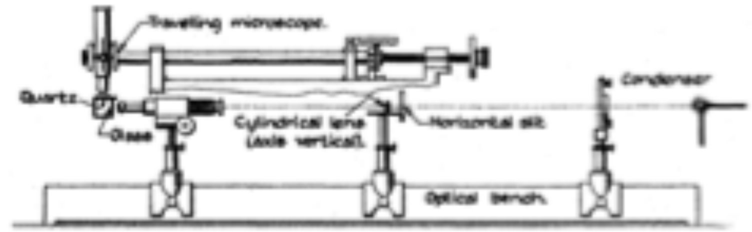

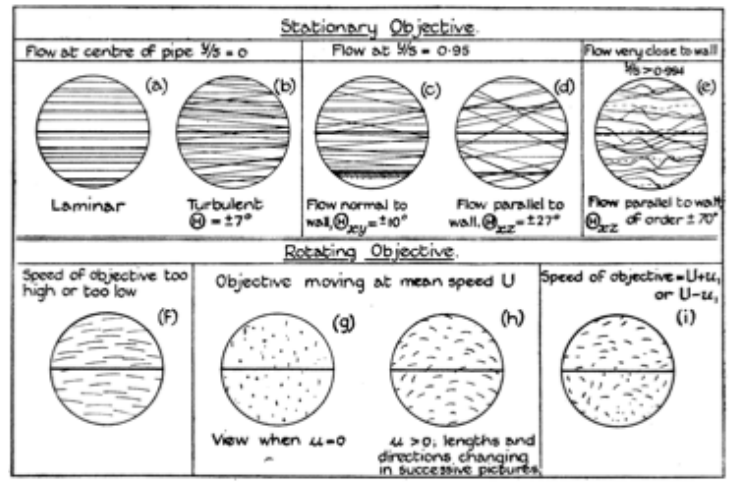

Fig. 2 (a)–(e).—Sketches of Paths of Particles as observed in the Ultramicroscope.

Fage & Townend (1932) Proc. Roy. Soc. Lond. A 135

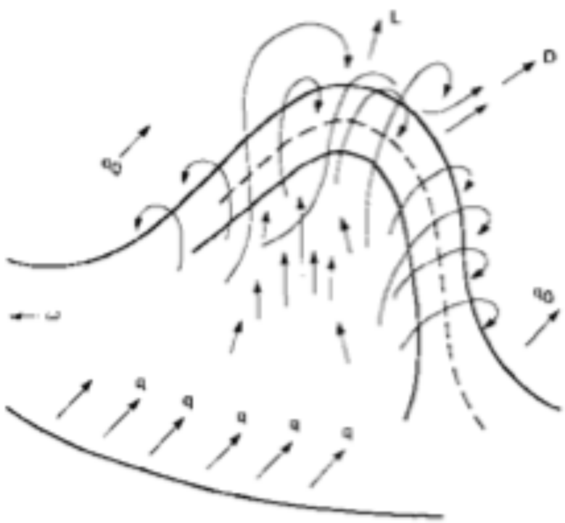

"horseshoe" structure of wall bounded turbulence

Theodorsen (1952) 2nd Midwestern. Conf. on Fl. Mech.

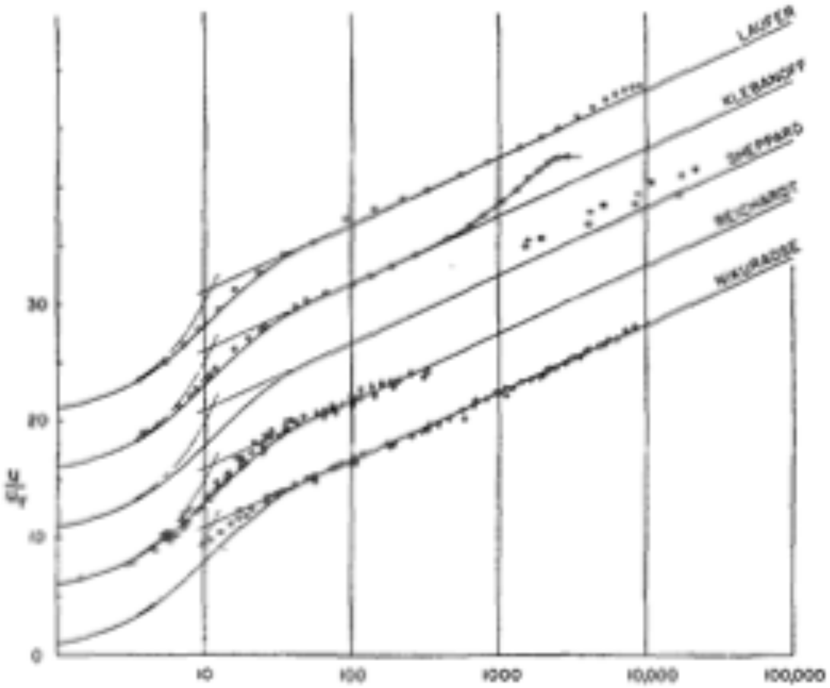

$\frac{yu_\tau}{\nu}$

Figure 1. The law of the wall.

$$\frac{u}{u_\tau} = \frac{1}{\kappa}\ln\left(\frac{yu_\tau}{\nu}\right) + c$$

Millikan (1938) 5th Int. Appl. Mech. Congress

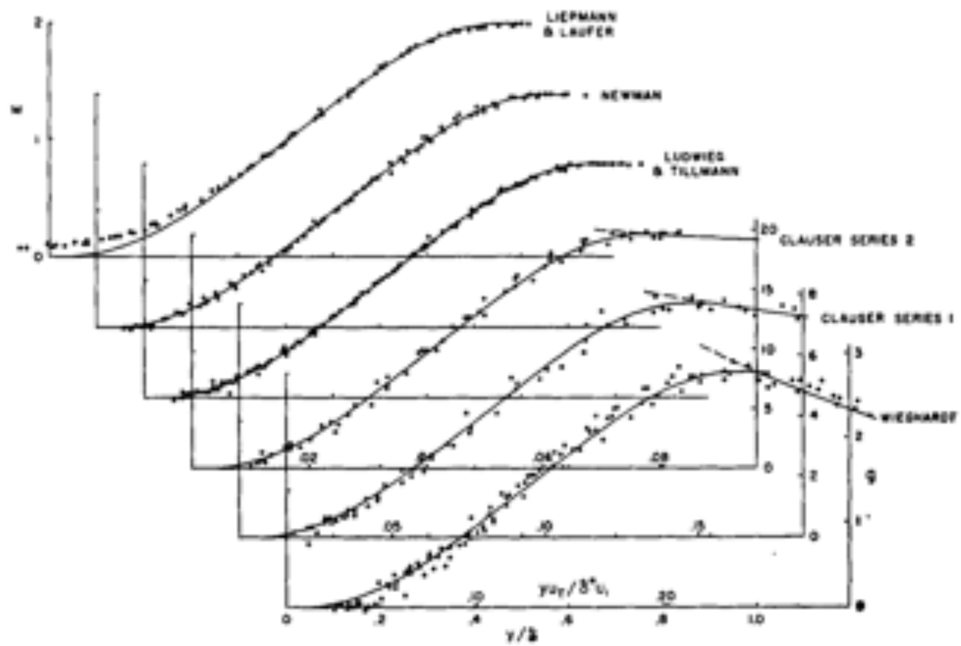

Figure 2. The law of the wake.

$$\frac{u}{u_\tau} = f\left(\frac{yu_\tau}{\nu}\right) + \frac{\Pi}{\kappa} w\left(\frac{y}{\delta}\right)$$

Coles (1956) JFM 1

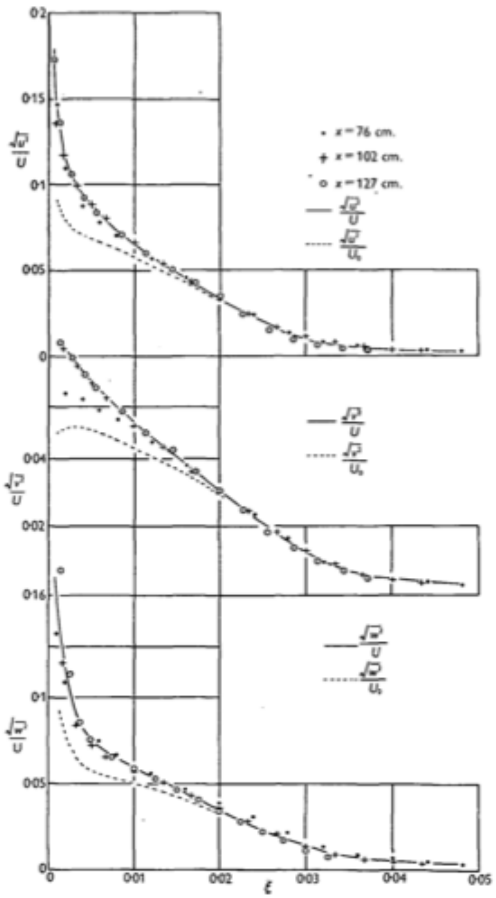

Fig. 3. Turbulent intensities.

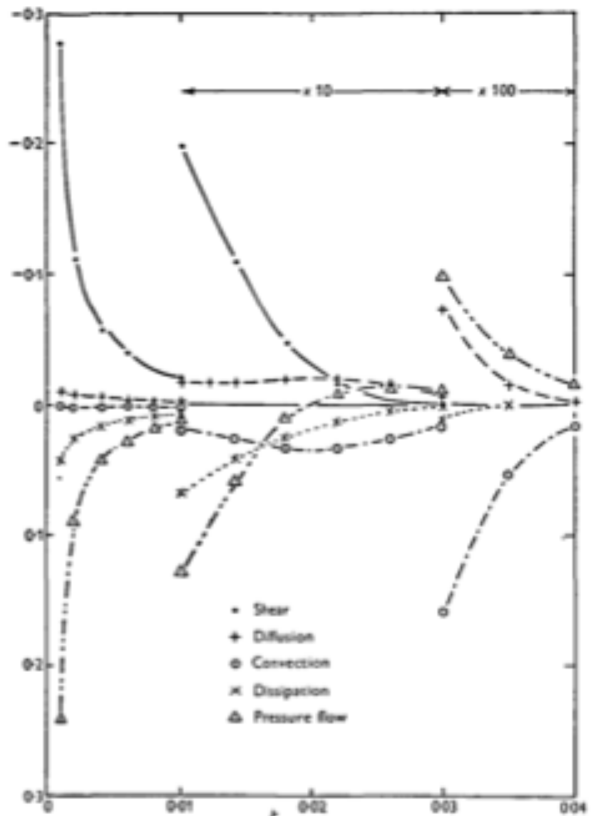

Fig. 7. Total energy balance.

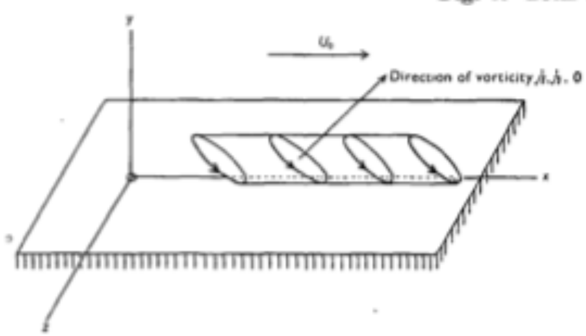

Fig. 12. Eddy structure.

Townsend (1951) Math. Proc. Cambridge Phi. Soc. 47

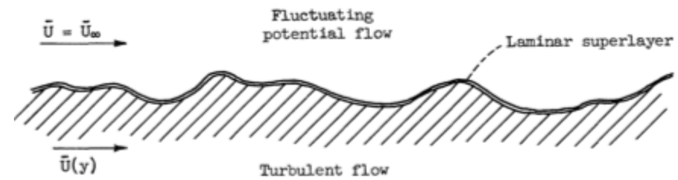

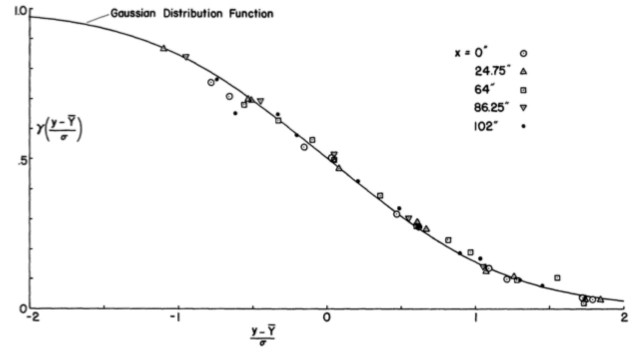

Figure 20.- Intermittency distributions for several x-stations in boundary layer.

Corrsin & Kistler (1954) NACA TN 3133

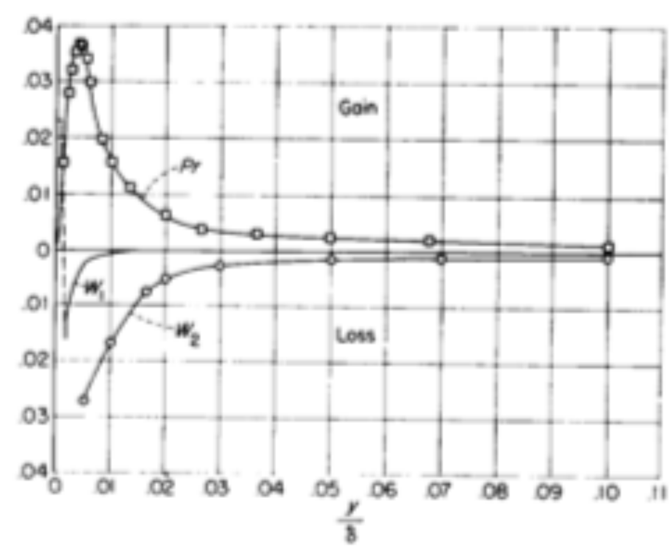

FIGURE 23.—Production and dissipation in region near wall.

Klebanoff (1955) NACA Rep. 1247

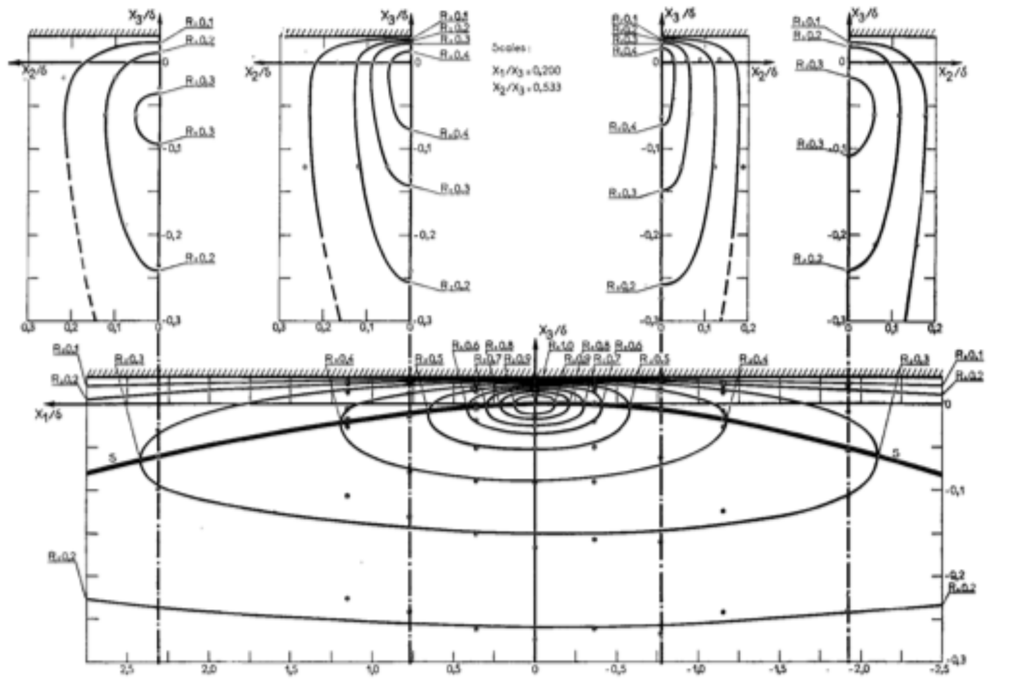

Figure 7. Space-time isocorrelation surfaces with optimum delay in the boundary layer on a flat plate; $\delta = 33$ mm, $R_\delta = 27900$, $y'/\delta = 0{\cdot}03$

Favre, Gaviglio & Dumas (1958) JFM 3

Grant (1958) JFM 4

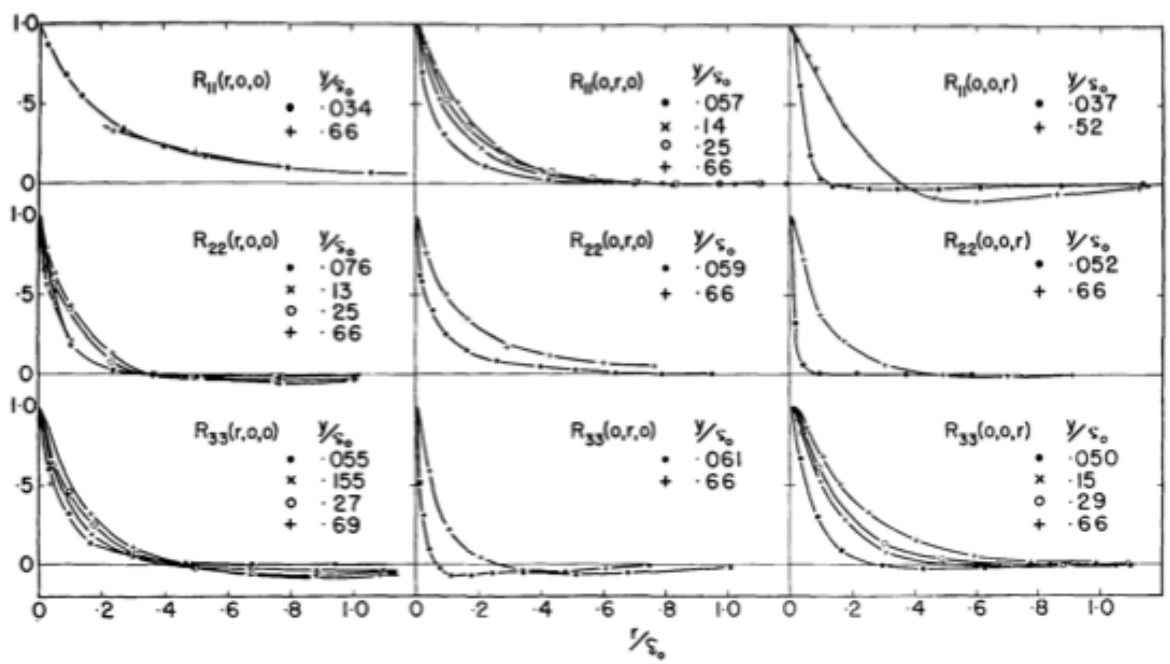

Figure 21. The nine correlations in the boundary layer.

1961 – 1970: Visualization & Measurement

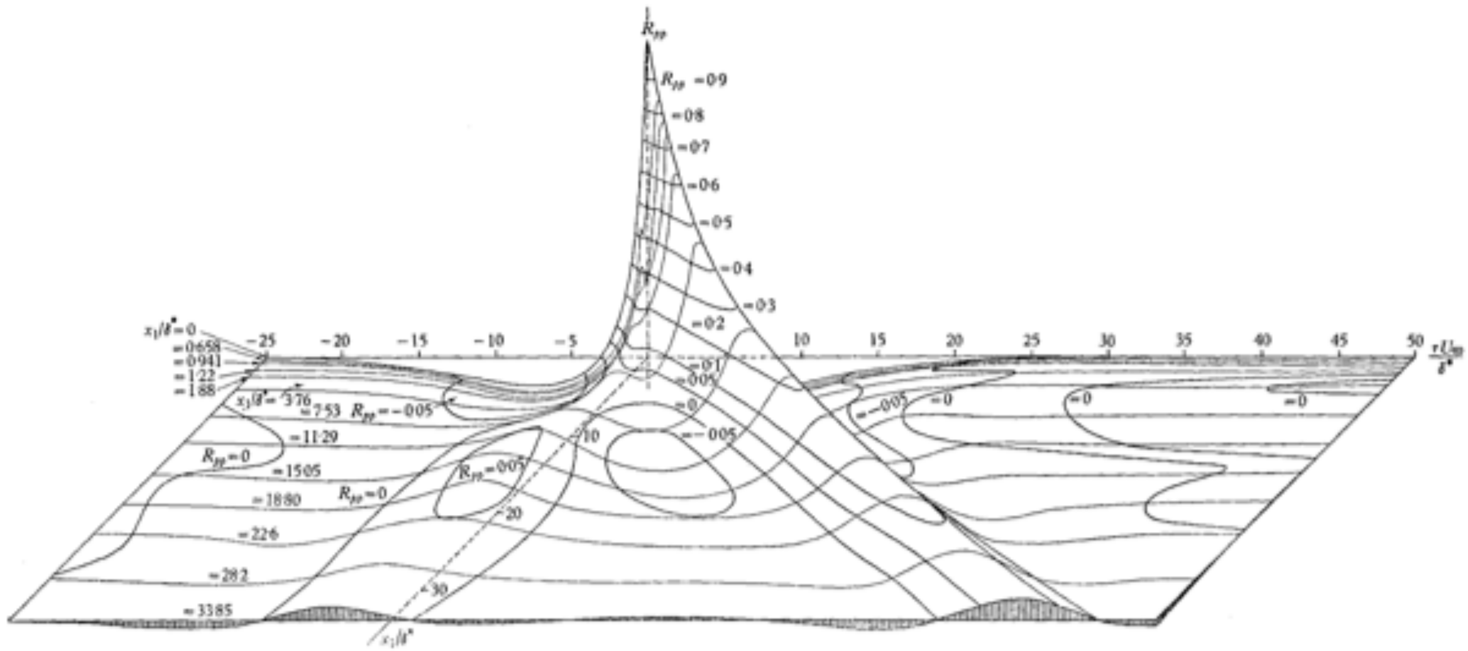

FIGURE 6. Longitudinal space-time correlation of the wall pressure displayed in three dimensions using the data of figure 5.

Willmarth & Wooldridge (1962) JFM 14

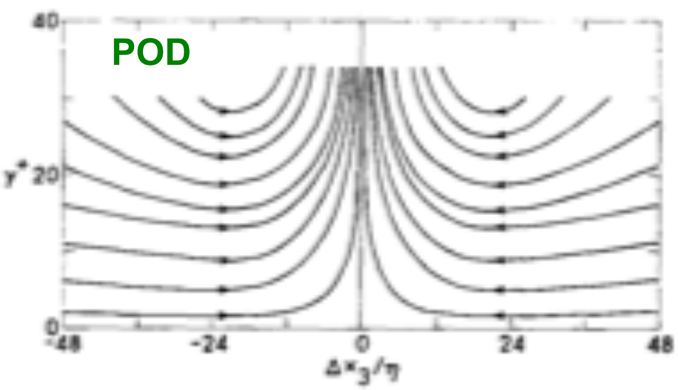

FIG. 11. Streamlines of the large eddy structure in a plane normal to the mean flow.

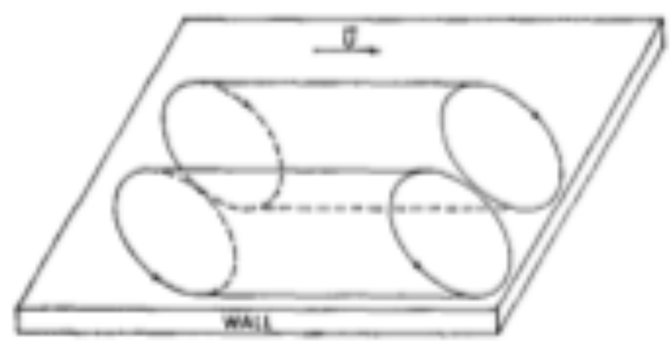

FIG. 12. Composite representation of the large eddy pairs.

Bakewell & Lumley (1967) Phys. Fl. 10

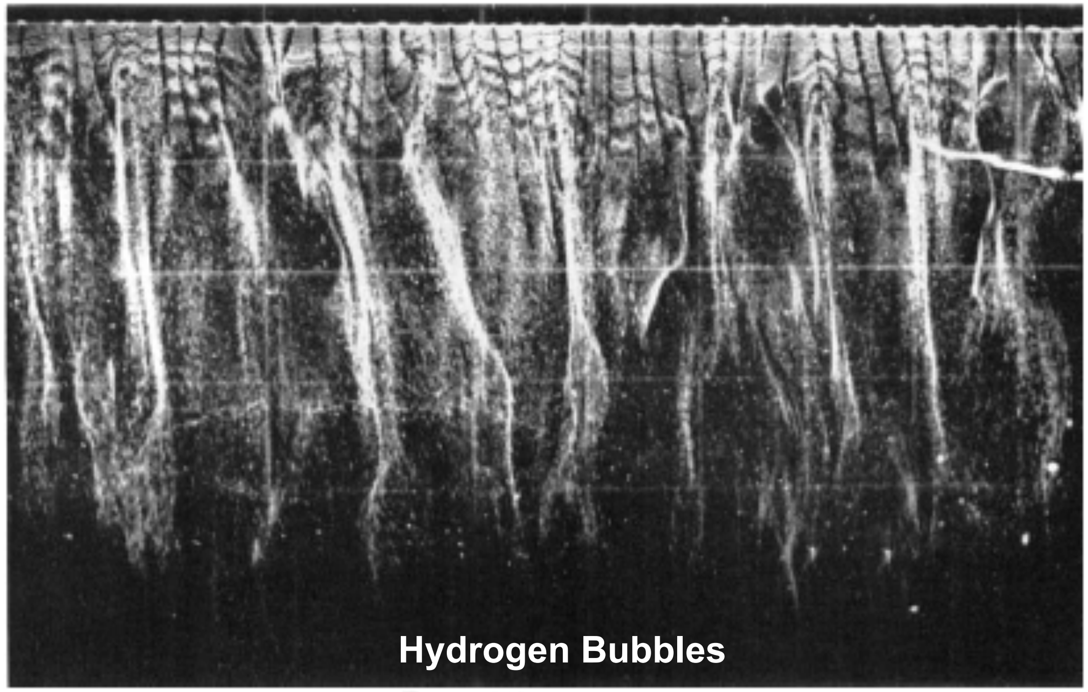

FIGURE 10b. $y^+ = 4{\cdot}3$.

FIGURE 10. Photographs of the structure of a flat plate turbulent boundary layer.

Kline, Reynolds, Schraub & Runstadler (1967) JFM 30

View Multi-media Fluid Mechanics videos 4192, 4497 & 4766 in the Media Library

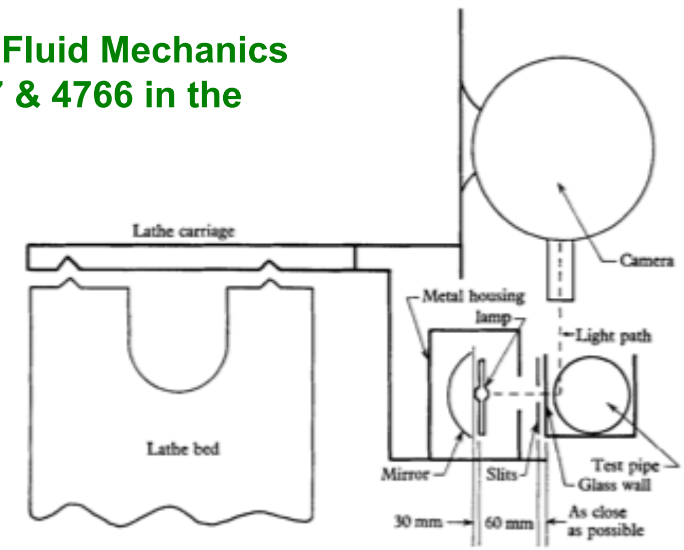

FIGURE 2. Optical system.

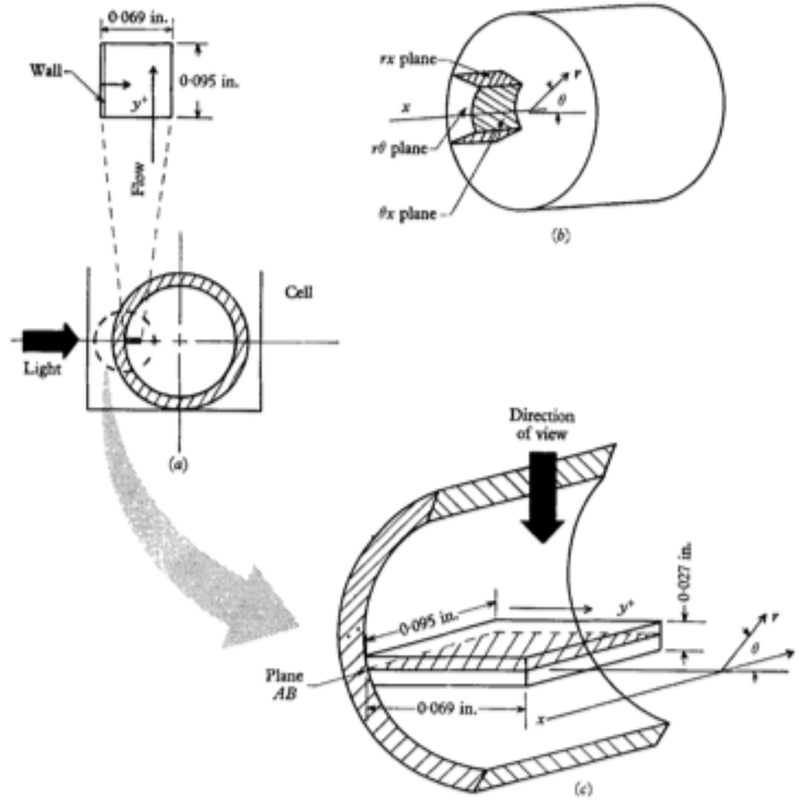

FIGURE 3. Wall view (dimensions for × 4·3).

Corino & Brodkey (1969) JFM 37

1970 – 1986: Conditional Processing of Measurements & Further Visualization

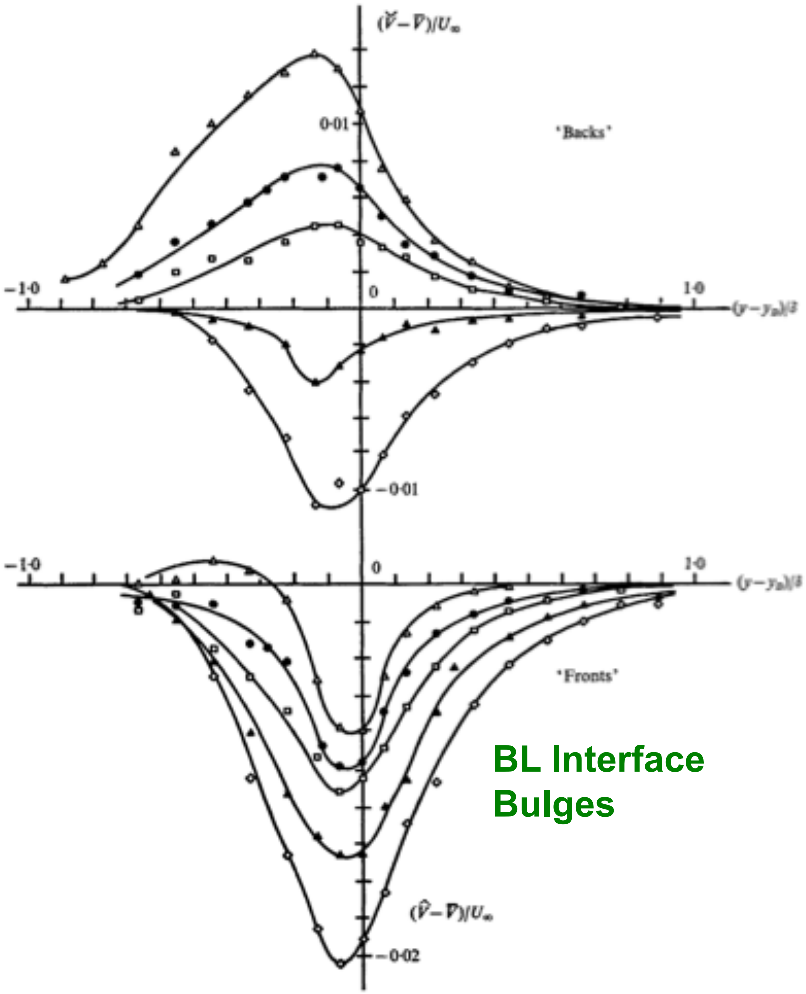

FIGURE 9. Point averages of the normal velocity component as a function of the distance from the interface. $\gamma(y_D)$: △, 0·1; ●, 0·3; □, 0·5; ▲, 0·7; ◇, 0·9.

BL Interface Bulges

Kovasznay, Kibens & Blackwelder (1970) JFM 41

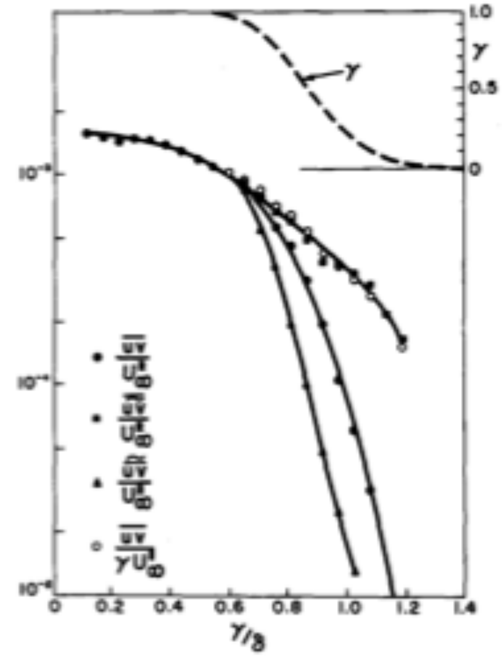

FIG. 1. Conditional averages of the Reynolds stress.

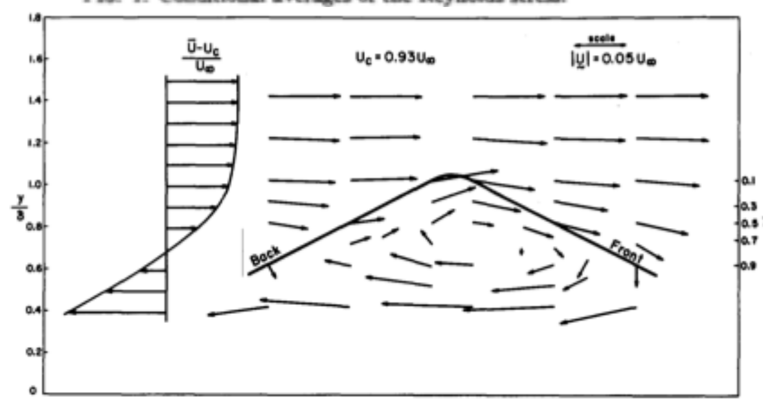

FIG. 3. Composite velocity distribution in the outer region of the boundary layer.

Blackwelder & Kovasznay (1972) Phys. Fl. 15

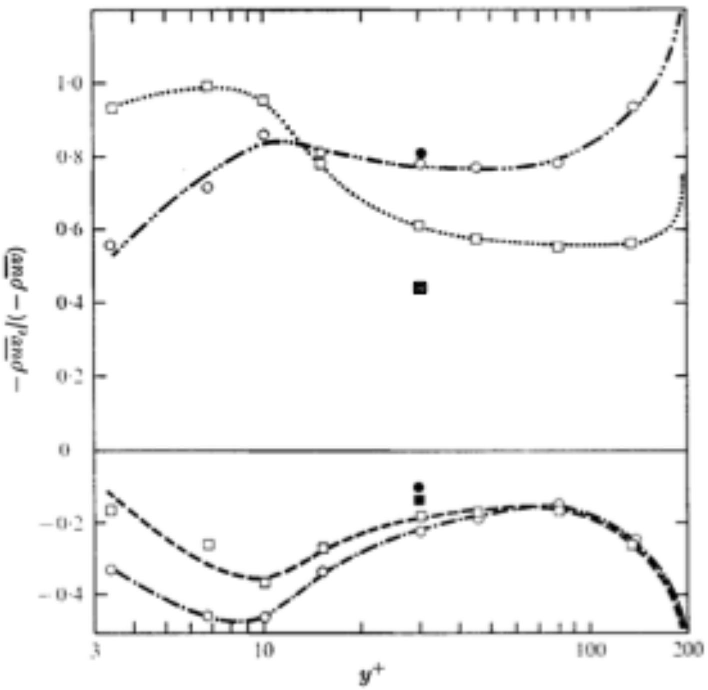

FIGURE 1. The classified Reynolds stresses normalized with the local average Reynolds stress. ●, ■, results of Willmarth & Lu (1972). ·····, sweep; —·—·—, ejection; —·—, i_o, outward interaction; – – –, i_w, wallward interaction.

Wallace, Eckelmann & Brodkey (1972) JFM 54
Brodkey, Wallace & Eckelmann (1974) JFM 63
Wallace & Brodkey (1977) Phys. Fl. 20

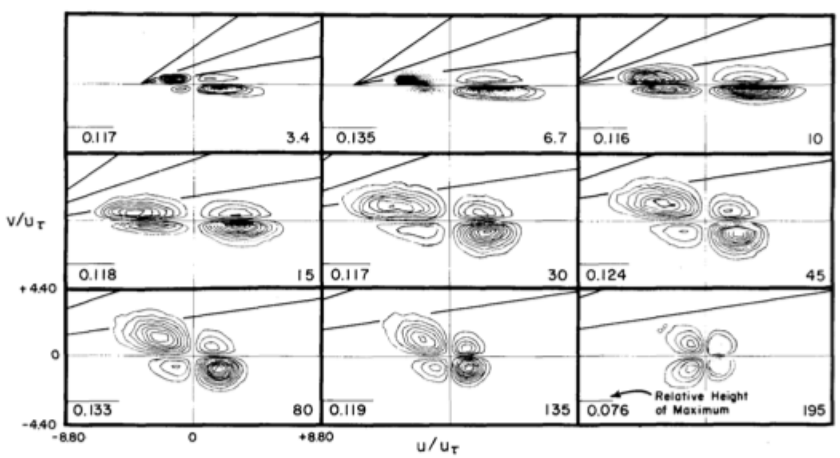

Quadrant Analysis

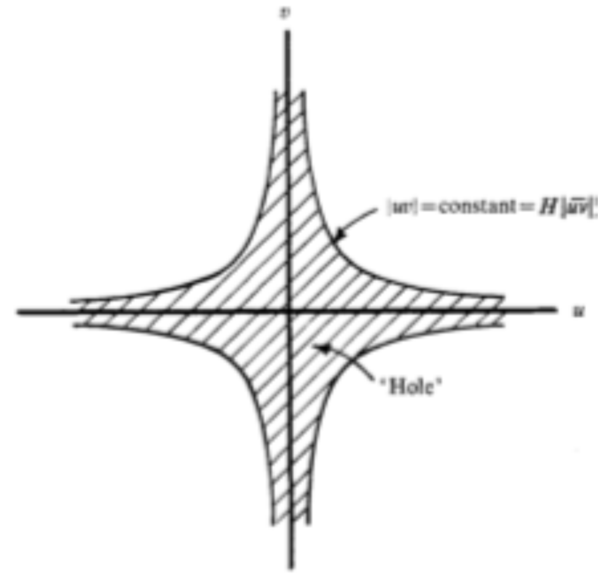

FIGURE 15. Sketch of 'hole' region in uv plane.

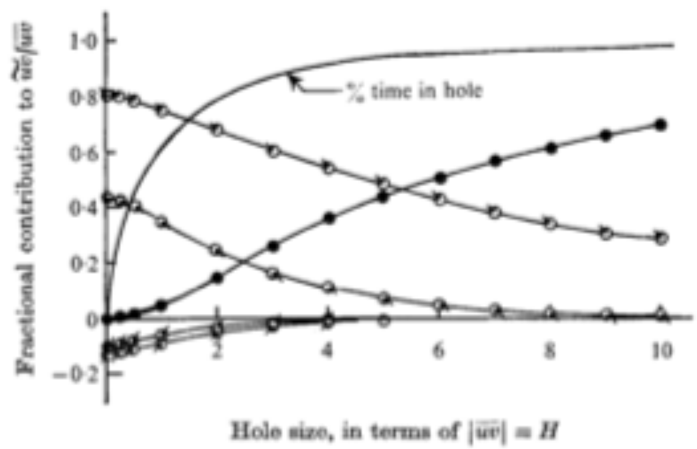

FIGURE 16. Contributions to Reynolds stress from truncated quadrants of u, v plane and percentage time spent in 'hole' as a function of 'hole' size, uv measured at $y^+ = 30$ in low-speed boundary layer; $U_\infty = 19{\cdot}7$ ft/s. Open circles indicate $|uv| >$ hole size: ○, $u > 0$, $v > 0$; ○, $u < 0$, $v > 0$; ○, $u < 0$, $v < 0$; ○, $u > 0$, $v < 0$. ●, 'hole', $|uv| <$ hole size.

Willmarth & Lu (1972) JFM 55
Lu & Willmarth (1973) JFM 60

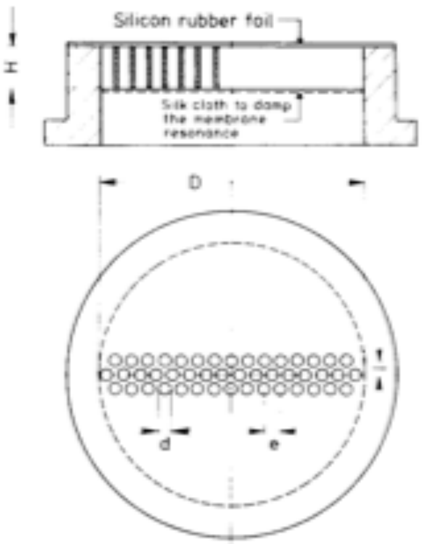

FIG. 1. Pressure transducer ($D = 97$ mm, $H = 6$ mm, $d = 2.5$ mm, $e = 3$ mm, $l = 2.6$ mm).

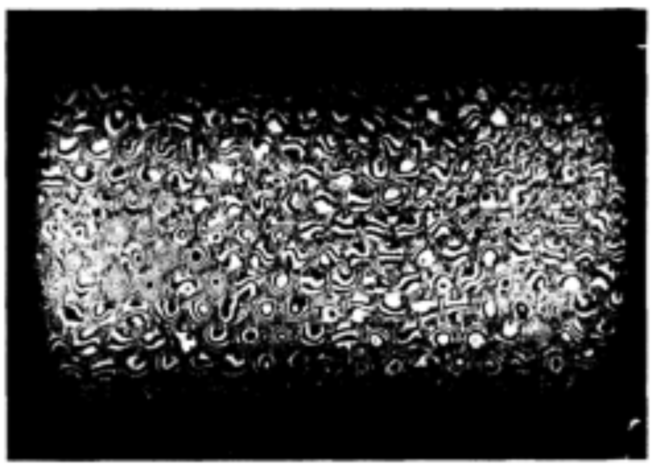

FIG. 9. Interference fringe pattern of one frame of a film taken with $U_\infty = 8.5$ m/sec and a frame rate of 7000 frames per second.

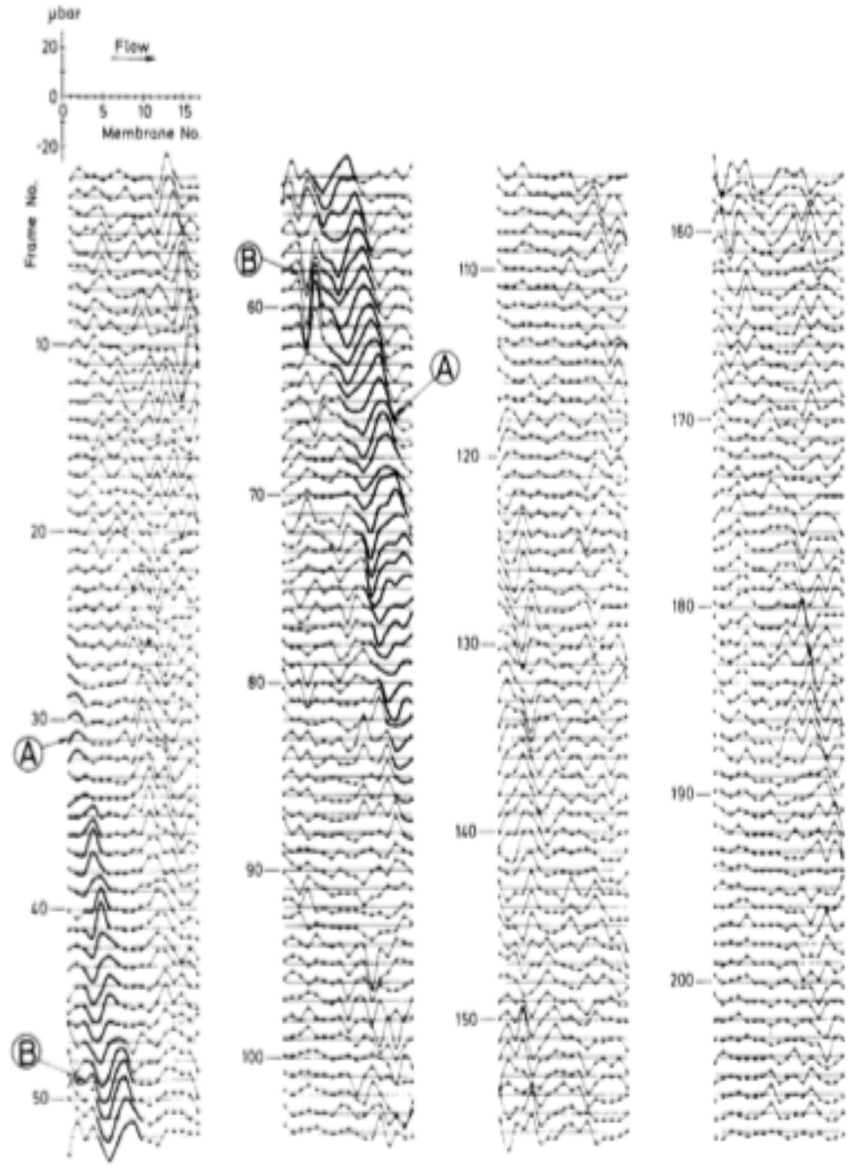

FIG. 11. Sequence of consecutive pressure distributions along one row of 17 membranes lying in flow direction one behind the other. (Flow from left to right, flow velocity $U_\infty = 8.5$ m/sec, time between consecutive maps $\Delta t = 0.14$ msec.)

Patterns ~ 1100 Δx+, 1.6δ

Emmerling (1973) MPI für Strömungsforschung Bericht No. 9

Dinkelacker, Hessel, Meier & Schewe (1977) Phys. Fl. 20

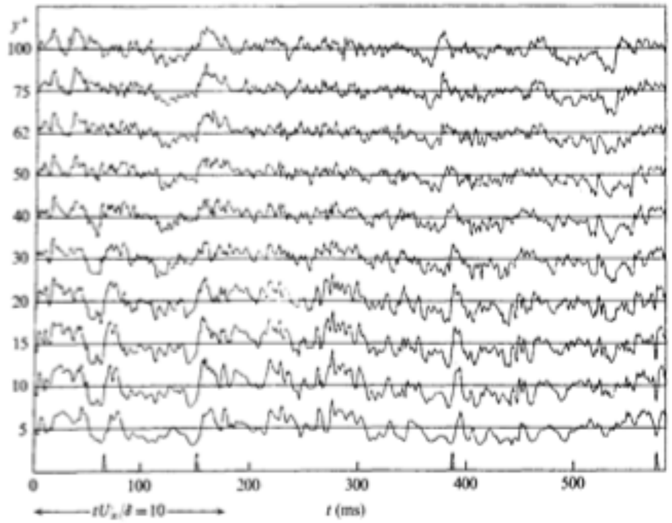

FIGURE 7. Instantaneous streamwise velocities as a function of the normal direction. The detector function obtained at $y^+ = 15$ is shown between the tick marks.

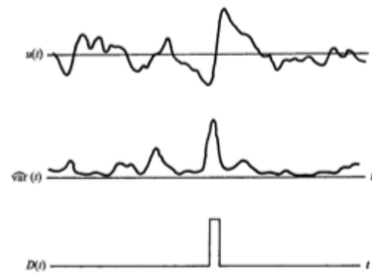

FIGURE 3. Schematic diagram of the detection process.

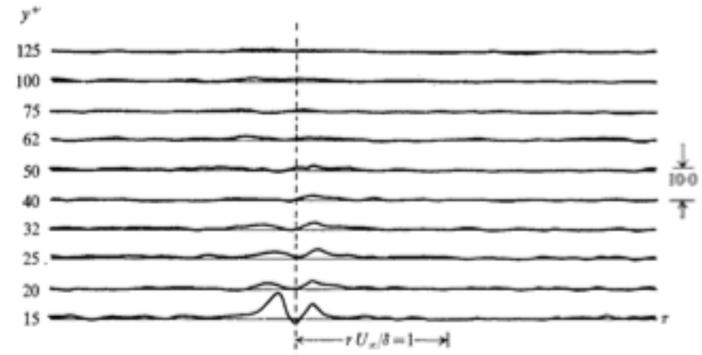

FIGURE 14. The conditional averages of the Reynolds shear stress at $\Delta x = 0$, $R_\theta = 2550$.

VITA Conditional Sampling

Blackwelder & Kaplan (1976) JFM 76

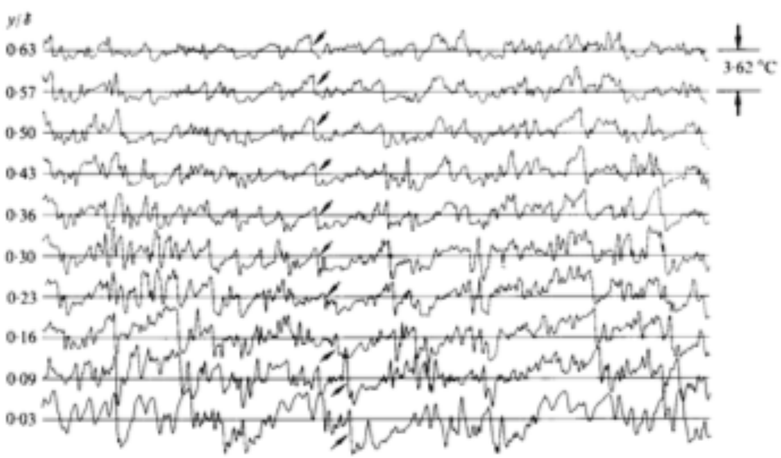

FIGURE 12. Simultaneous temperature signals from the ten-wire rake in the turbulent region. The horizontal time span is $18{\cdot}7 U_\infty \Delta t/\delta$. One particular temperature front is denoted by the arrows.

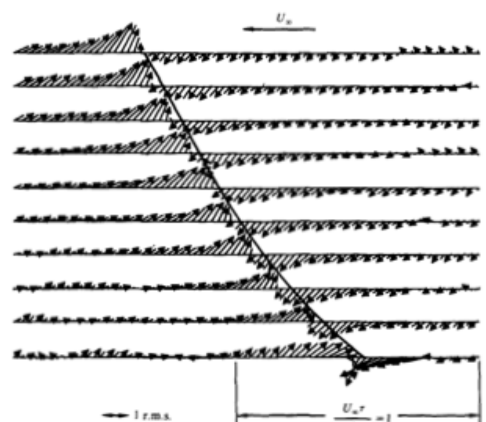

FIGURE 18. Composite picture of the velocity field associated with the internal front. The velocity components are normalized with their local fluctuation levels. The velocity magnitude and time scale are given at the bottom of the figure. For clarity only every other velocity vector has an arrowhead.

Chen & Blackwelder (1978) JFM 89

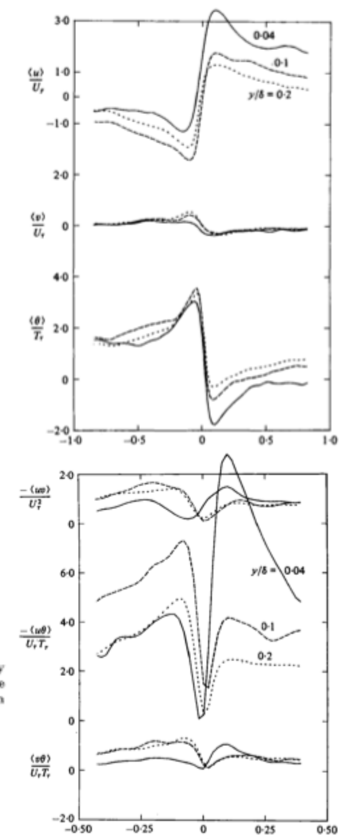

FIGURE 4. Conditional averages of products uv, $u\theta$, $v\theta$ in the inner layer

Antonia, Rajagopalan, Subramanian & Chambers (1977) JFM 121

Attached Eddies

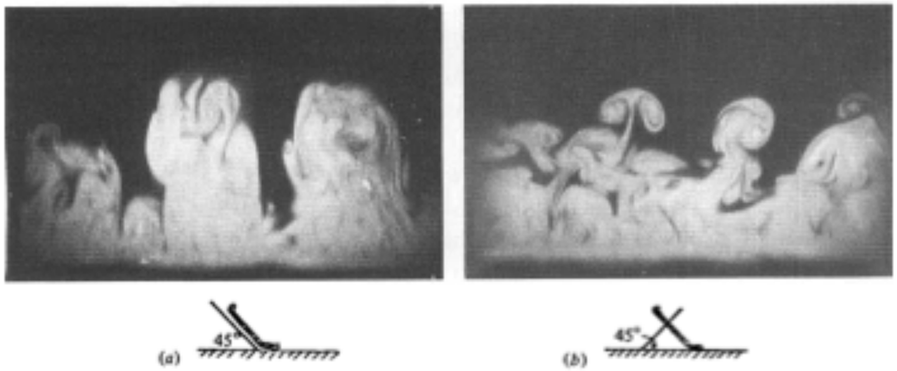

FIGURE 21. Comparison between views with transverse light plane inclined

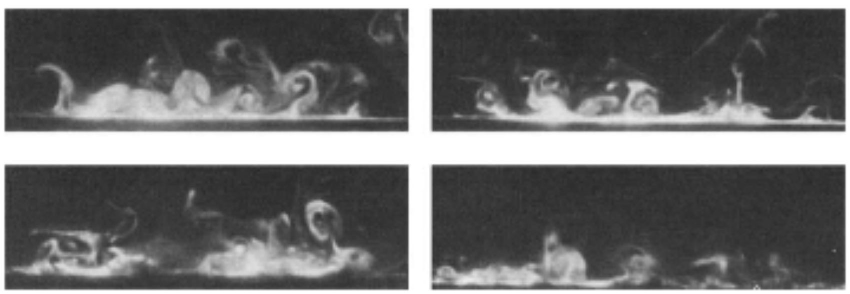

FIGURE 26. Examples of longitudinal vortices and vortex pairs in near-wall region.

Head & Bandyopadhyay (1981) JFM 107

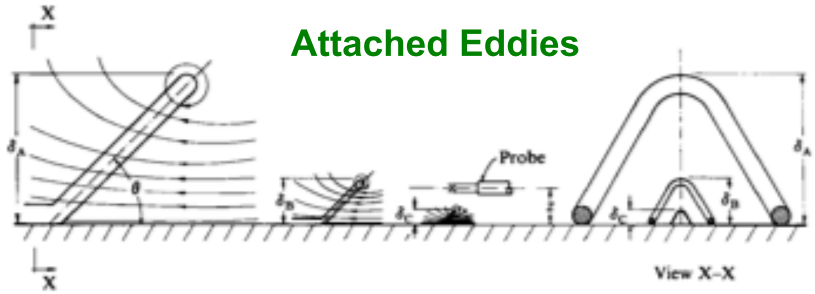

FIGURE 1. A sketch of three attached eddies of varying scales together with the instantaneous streamline pattern generated by each.

Townsend (1970, 1976)
Perry, Henbest & Chong (1986) JFM 165

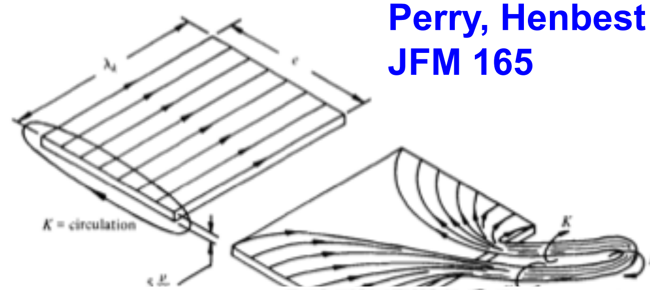

Perry & Chong (1982) JFM 119

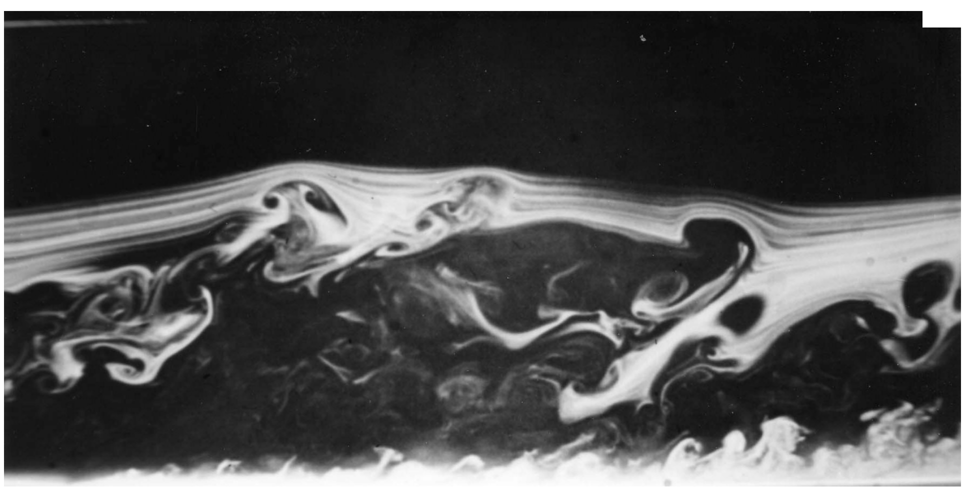

Balint, Ayrault & Wallace (1981)

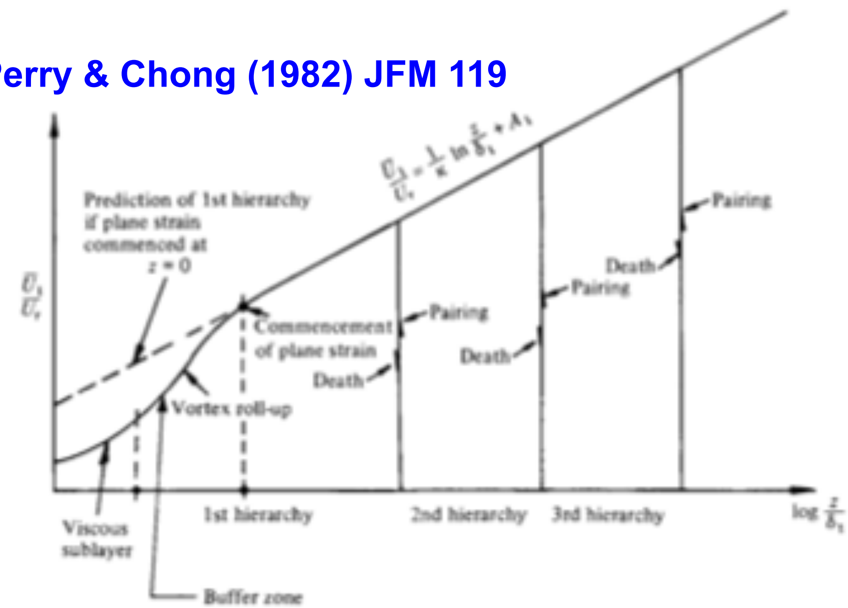

FIGURE 18. Mean-velocity profile interpreted in terms of quantum-jump model. A_1 is a universal constant.

1986 – 2011: DNS, Multi-Sensor Hot-Wire Probes & PIV Measurement

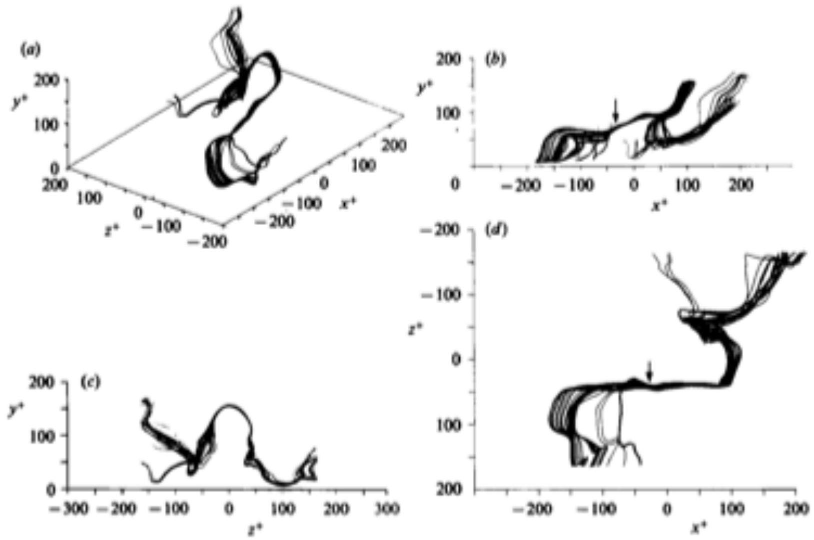

FIGURE 15. Vortex lines of an instantaneous vortical structure detected by QD-2: (a) oblique view; (b) side view; (c) end view; (d) top view.

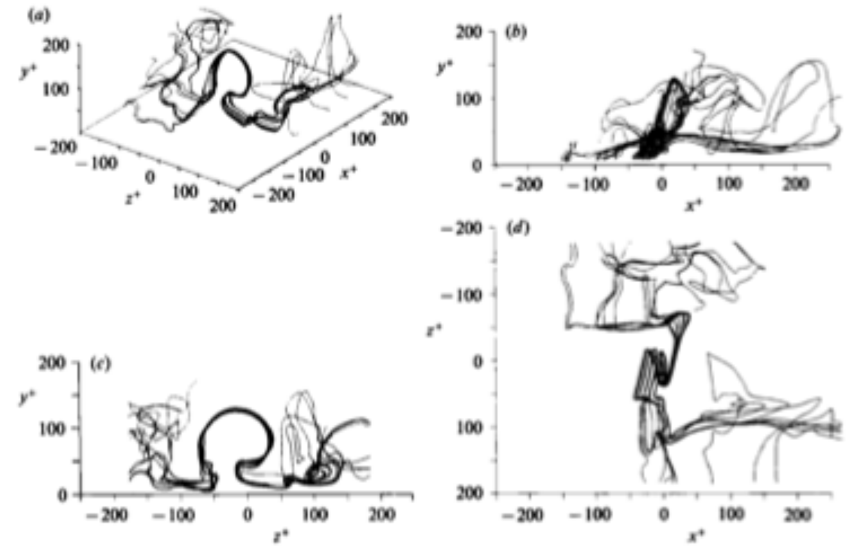

FIGURE 14. Vortex lines of an instantaneous vortical structure detected by QD-2: (a) oblique view; (b) side view; (c) end view; (d) top view.

Kim & Moin (1986) JFM 162

DNS R_T = 180

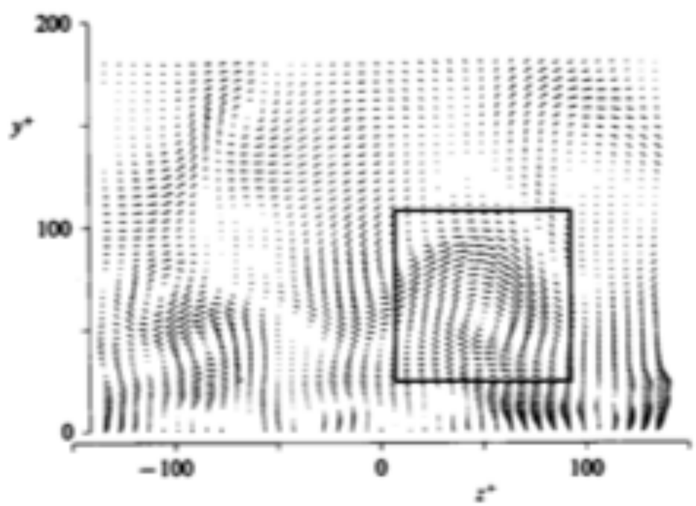

FIGURE 18. Velocity vectors in a (y, z)-plane. The streamwise location is indicated in figure 15(b), and the direction of the mean flow is into the figure.

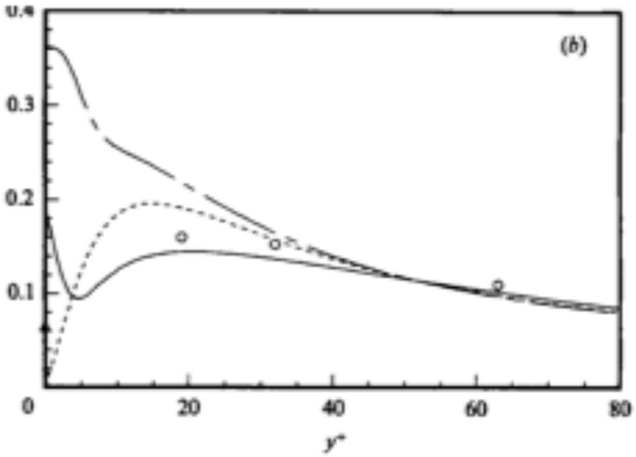

FIGURE 14. Root-mean-square vorticity fluctuations normalized by the mean shear. (a) In global coordinates: ——, $\omega_x \nu/u_\tau^2$; ----, $\omega_y \nu/u_\tau^2$; —·—, $\omega_z \nu/u_\tau^2$; (b) in wall cordinates: ○, ω_x from Kastrinakis & Eckelmann (1983). △, ω_z at the wall from Kreplin & Eckelmann (1979).

Kim, Moin & Moser (1987) JFM 177

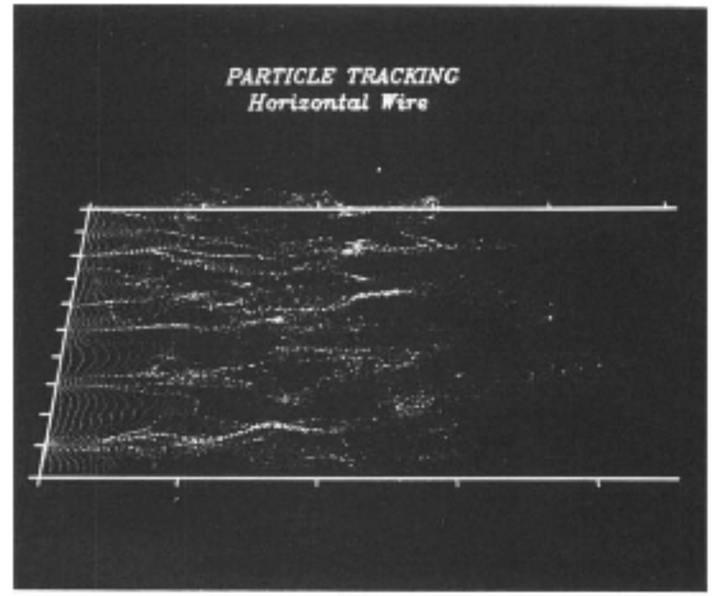

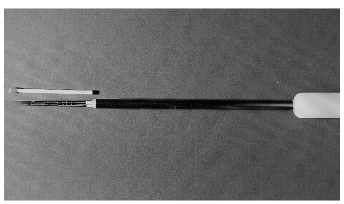

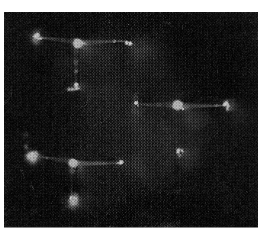

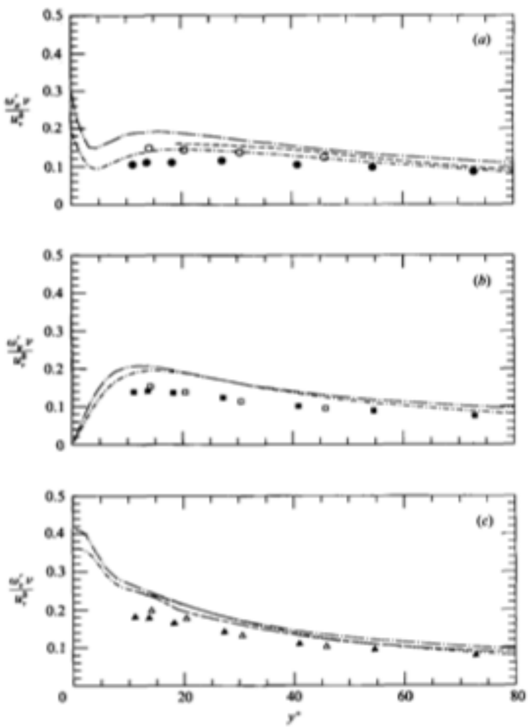

FIGURE 12. Measured r.m.s. fluctuating vorticity components normalized with inner scaling u_τ and ν and compared to other measured and simulated values. Symbols given in table 2.

Balint, Vukoslavčević & Wallace (1987) , (1991) JFM 228

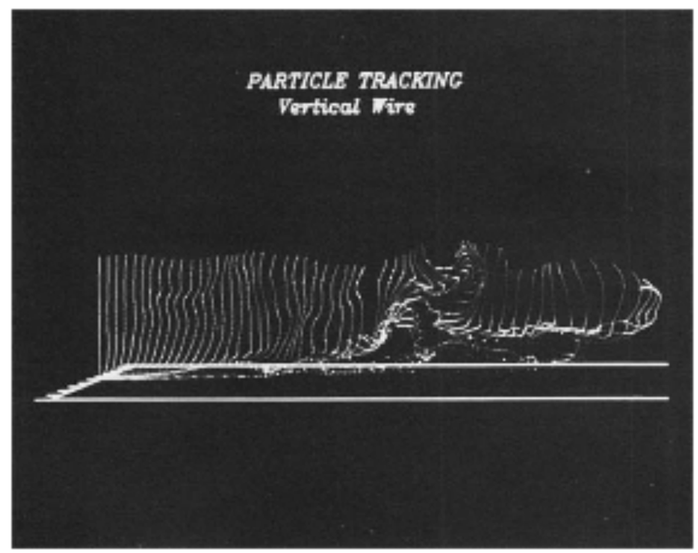

(c)

FIGURE 25. Flow structures visualized by fluid markers: (a) particles are generated along a line parallel to the z-axis at $y^+ \approx 10$ (oblique top view); (b) particles are initially distributed uniformly on a plane parallel to the wall at $y^+ \approx 10$ (top view); (c) particles are generated along a line parallel to the y-axis (side view).

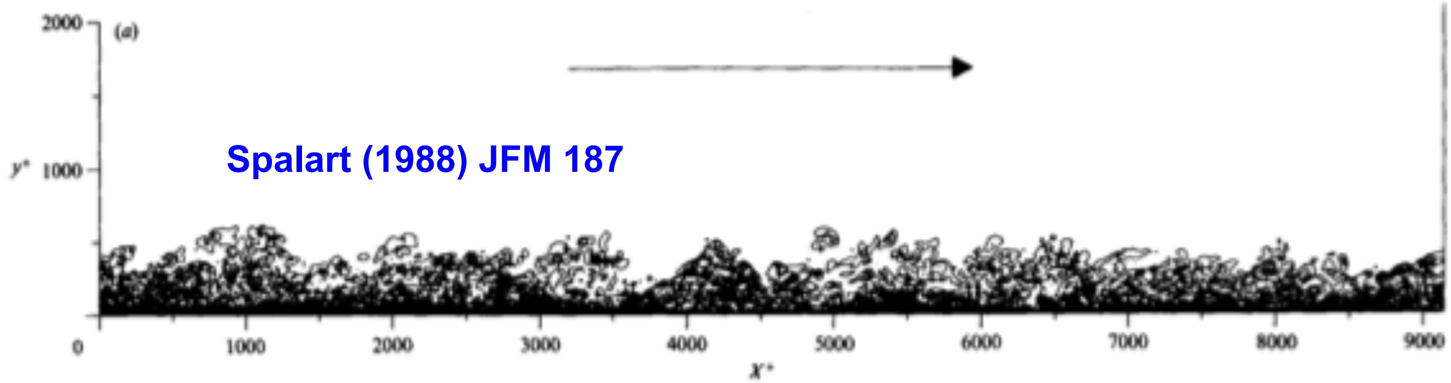

Spalart (1988) JFM 187

FIGURE 19. Vorticity contours, $R_\theta = 1410$. (a) streamwise plane; (b) spanwise plane; (c) downstream plane, at 45°; (d) upstream plane at 45°. Contour levels: $\|\omega\| (\delta\nu/u_\tau^3)^{\frac{1}{2}} = 1, 2, 3, \ldots$.

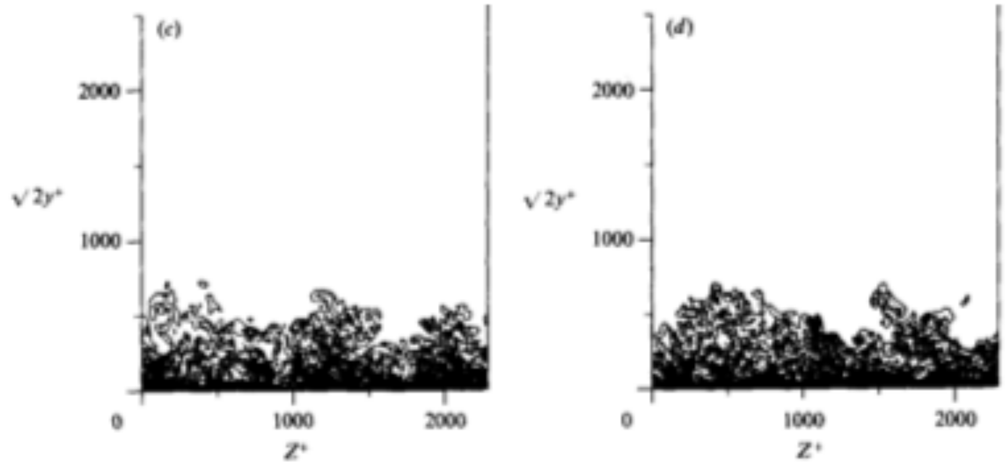

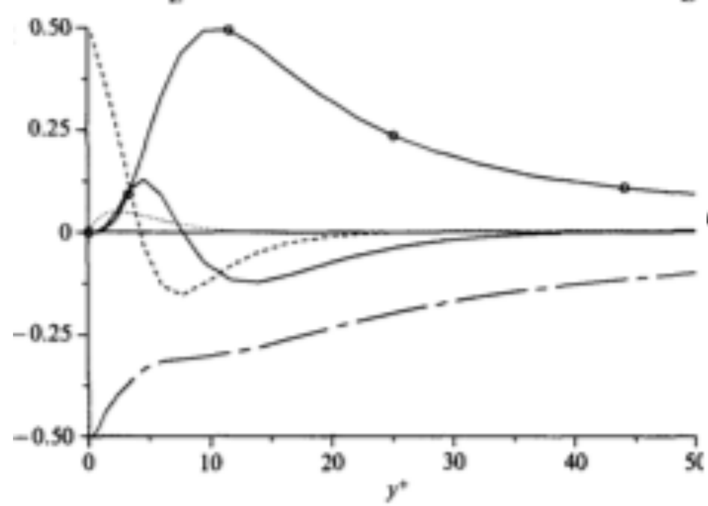

ll. Normalized by u_τ^4/ν.

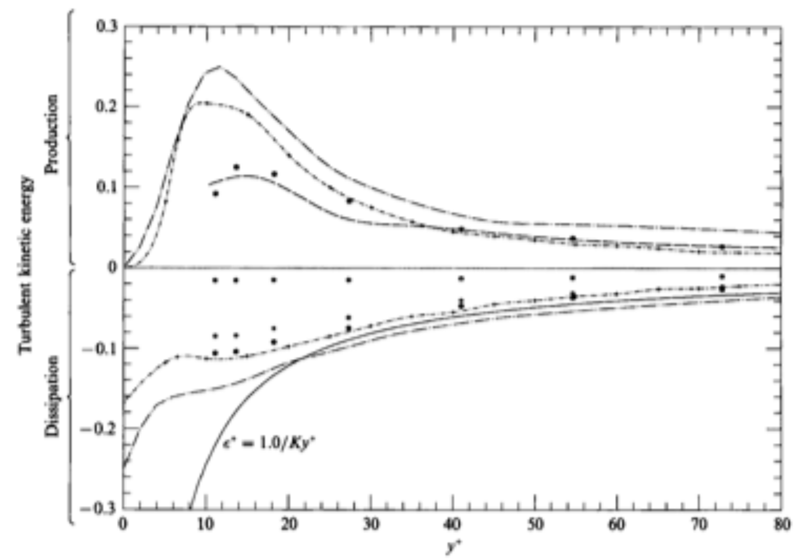

FIGURE 10. Measured turbulent kinetic energy production and dissipation rates normalized with inner scaling u_τ and ν and compared to other measured and simulated values. Symbols given in table 2 except for •, dissipation neglecting cross-product velocity gradient correlations and ✿, dissipation assuming isotropy.

Balint, Vukoslavčević & Wallace (1987) , (1991) JFM 228

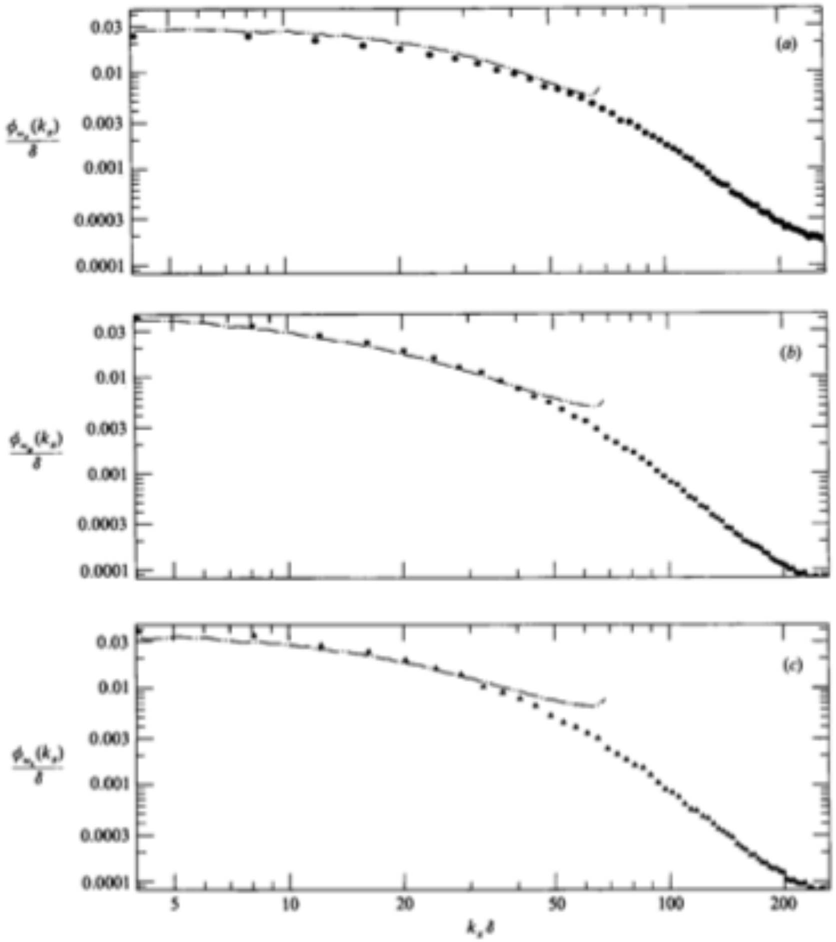

FIGURE 19. Measured one-dimensional fluctuating vorticity component spectra at $y^+ = 18$ compared to direct numerical simulations of P. R. Spalart (1990, private communication) at $y^+ = 15$.

Balint, Vukoslavčević & Wallace (1991) JFM 228

Spalart (1988) JFM 187

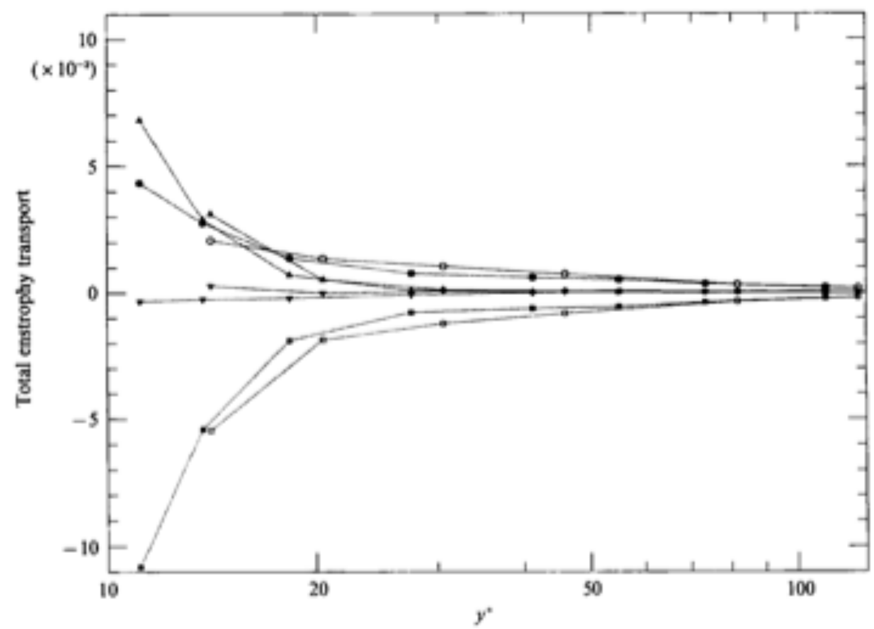

FIGURE 21. Measured terms in equation (7) for the transport of total enstrophy normalized with inner scaling u_τ and ν. Closed symbols, present measurements; open symbols, Balint *et al.* (1990); (▼, ▽), advection (term (7) I); (●, ○), rotation and stretching/compression (term (7) II); (▲, △), viscous diffusion (term (7) III); (■, □), viscous dissipation (term (7) IV).

$$\underbrace{\overline{U_j \frac{\partial}{\partial x_j}(\tfrac{1}{2}\Omega_i \Omega_i)}}_{\text{I}} = \underbrace{\overline{\Omega_i \Omega_j \frac{\partial U_i}{\partial x_j}}}_{\text{II}} + \underbrace{\nu \overline{\frac{\partial^2(\frac{1}{2}\Omega_i \Omega_i)}{\partial x_j \partial x_j}}}_{\text{III}} - \underbrace{\nu \overline{\left(\frac{\partial \Omega_i}{\partial x_j}\frac{\partial \Omega_i}{\partial x_j}\right)}}_{\text{IV}},$$

I: the rate of advection of total enstrophy;

II: the rate of rotation and stretching/compression of total enstrophy by the velocity gradient field;

III: the rate of viscous diffusion of total enstrophy; and

IV: the rate of viscous dissipation of total enstrophy.

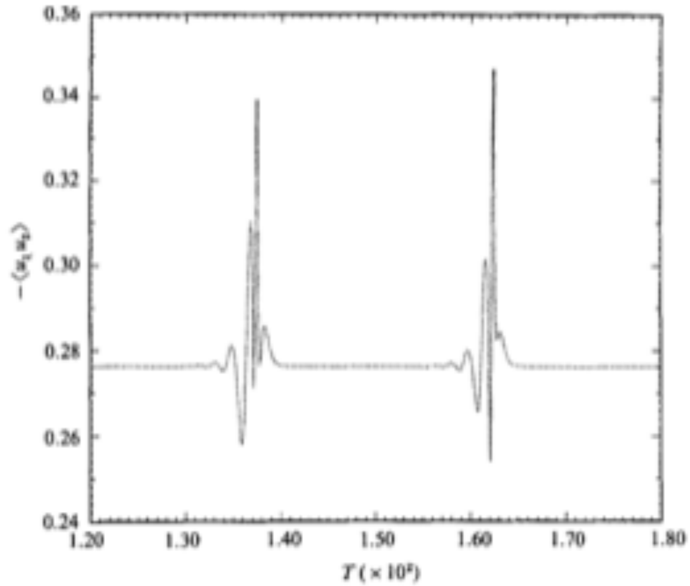

FIGURE 21. The Reynolds stress $\langle u_1, u_2\rangle$ at $y^+ = 35$ vs. time for Heisenberg paramet showing two bursts.

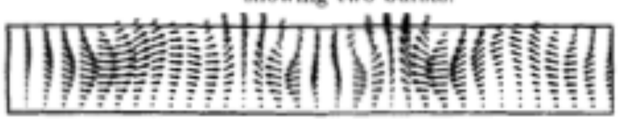

FIGURE 20. Vector representation of u_2, u_3 in a (x_2, x_3)-plane

Aubry, Holmes, Lumley & Stone (1988) JFM 192

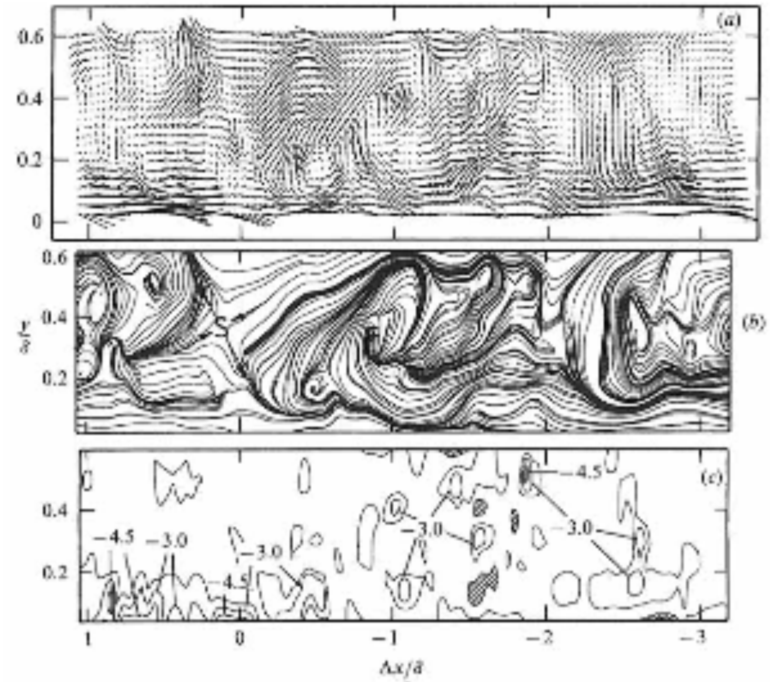

FIGURE 3. (a) Instantaneous velocity vectors, (b) sectional streamlines and (c) contours of approximate spanwise vorticity $\omega_z \delta / U_1$ calculated from the vectors in (a). The information is viewed in a frame of reference which translates to the left with $U_c = 0.8U_1$. $R_\theta = 1360$. Note: hatched contours have a value of +1.5. Unlabelled contours have a value of −1.5.

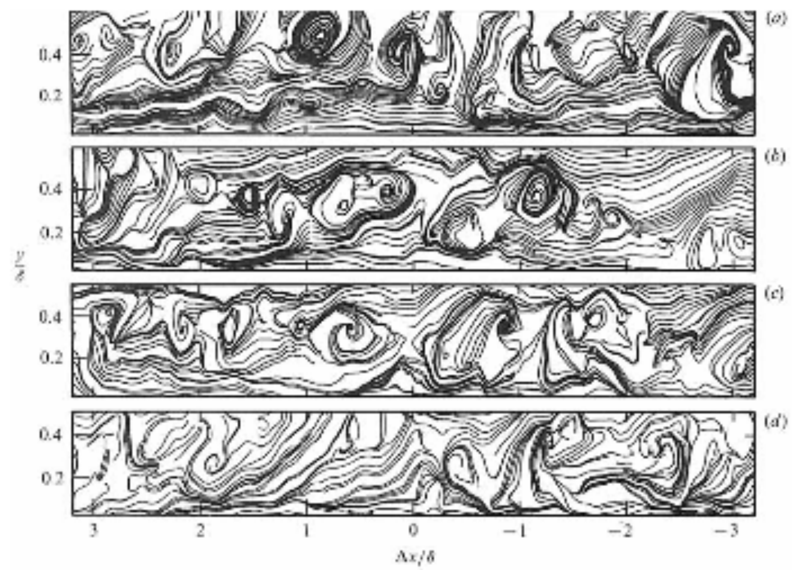

Antonia, Bisset & Browne (1990) JFM 213

FIGURE 5. Instantaneous sectional streamlines in a frame of reference translating to the left with a velocity $U_c = 0.8U_1$ for different Reynolds numbers. (a) $R_\theta = 1360$; (b) 2180; (c) 6030; (d) 9630.

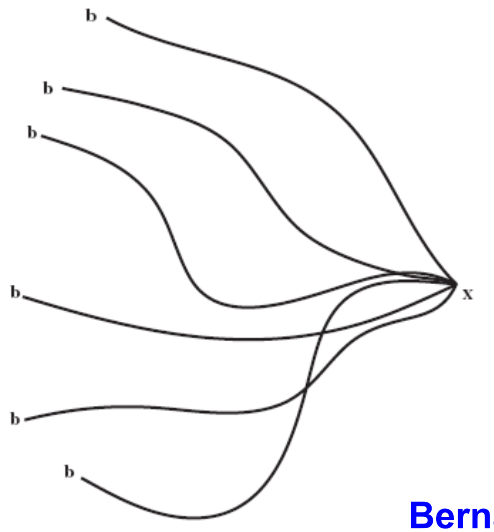

Fig. 6.2 *Ensemble of paths arriving at* x.

Bernard & Handler (1990) JFM 220

FIGURE 5. Quadrant breakdown of the p.d.f. of particle displacement at $y^+ = 12.0$: (*a*) Q1; (*b*) Q2; (*c*) Q3; (*d*) Q4; (*e*) total.

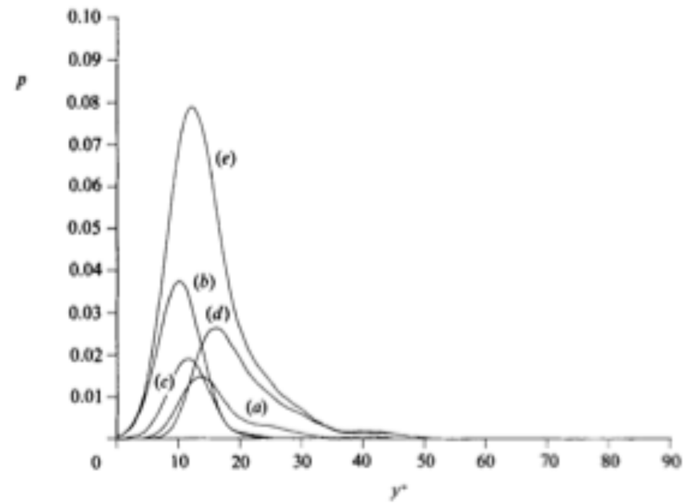

$$\overline{u_a v_a} = \overline{u_b v_a} + \overline{v_a(U_b - U_a)} - \int_{-\tau}^{0} \frac{1}{\rho}\, v(0) \frac{\partial p}{\partial x}(s)\,\mathrm{d}s + \int_{-\tau}^{0} \overline{\nu v(0)\, \nabla^2 U(s)}\,\mathrm{d}s.$$

Lagrangian decomposition of Reynolds stress

$$\overline{u_a v_a} = \overline{u_b v_a} + \overline{v_a(U_b - U_a)} + \overline{v_a(U_a - U_b)}$$

displacement transport **acceleration transport**

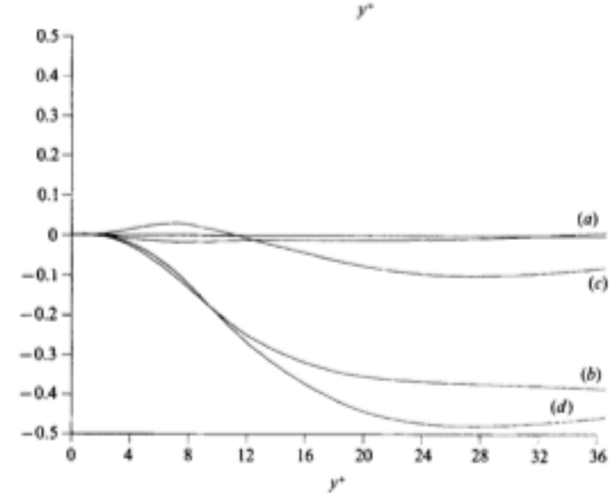

FIGURE 15. Spatial dependence of terms in Reynolds stress decomposition (7): (*a*) $\overline{u_b v_a}$; (*b*) $\overline{v_a(U_b - U_a)}$; (*c*) $\overline{v_a(U_a - U_b)}$; (*d*) $\overline{uv}$.

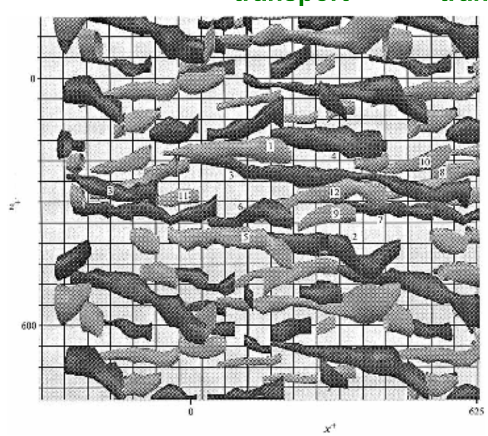

FIGURE 5. Plan view of complete set of vortices visualized using approximate core dimensions. Dark structures have negative streamwise vorticity, light structures have positive streamwise vorticity.

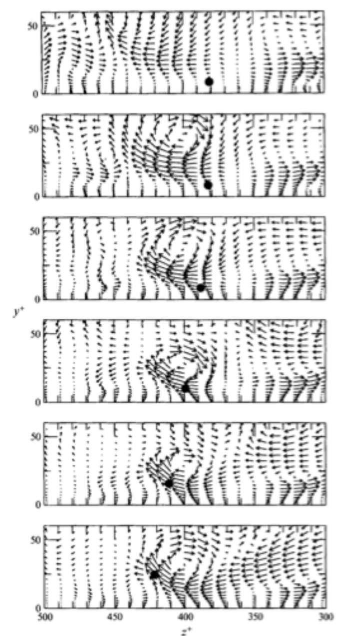

FIGURE 20. Ejection event in figure 19 viewed from end-on velocity vector plot.

Bernard, Handler & Thomas (1993) JFM 253

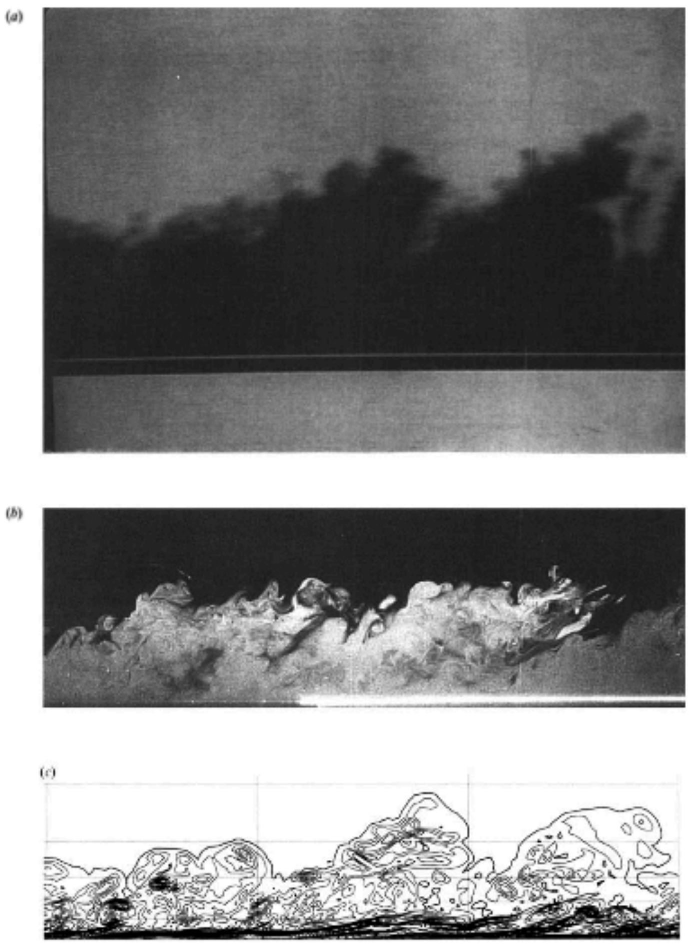

Figure 20. (a) Streamwise cross-section of a supersonic boundary layer with $Re_\theta = 25000$, obtained using Rayleigh scattering; Smith (1989). (b) Streamwise cross-section of a subsonic boundary layer with $Re_\theta = 4000$, obtained using oil droplet visualization; Falco (1977). (c) Streamwise cross-section of a computer-generated subsonic boundary layer with $Re_\theta = 670$, showing iso-vorticity contours. The flow is a direct Navier–Stokes turbulence simulation; Robinson (1989).

Spina, Donavan & Smits (1991) JFM 293

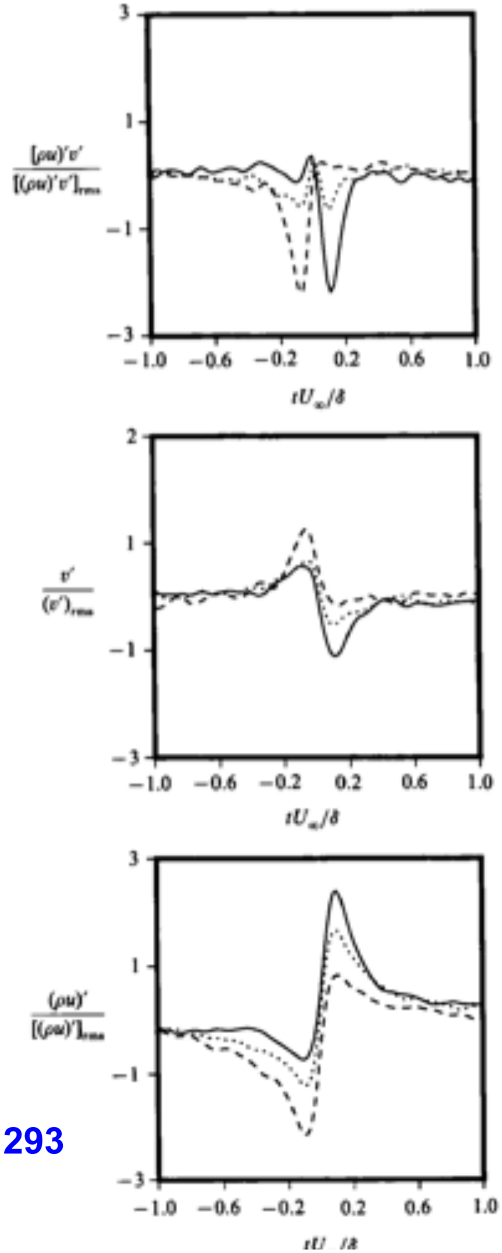

Figure 12. Ensemble-averaged $(\rho u)'$, v', and $(\rho u)'v'$ signatures based upon the positive VITA technique (detection on $(\rho u)'$). ——, $y/\delta = 0.2$; ……, $y/\delta = 0.5$; ---, $y/\delta = 0.8$.

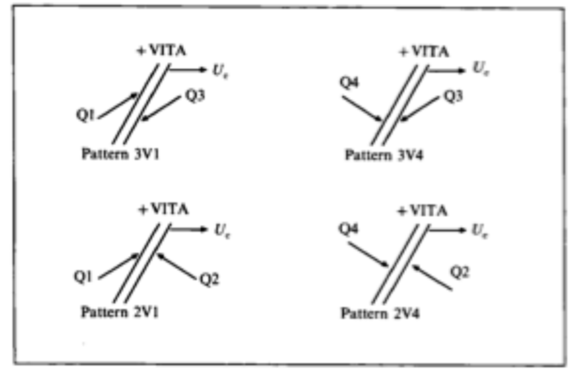

E 17. Schematic of the four possible triple event patterns showing the spatial location of the shear stress events relative to the +VITA event.

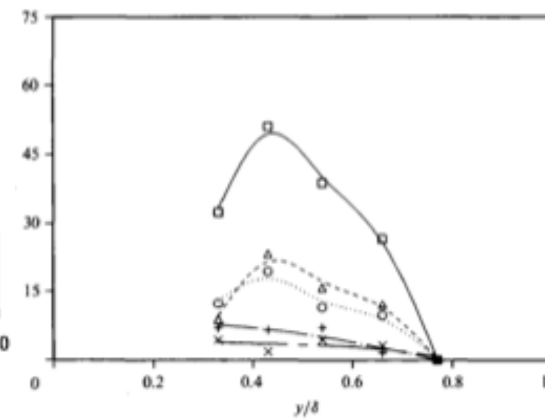

GURE 18. Percentage of +VITA events occurring in each of the triple event patterns defined by …resholding the shear stress. □——, Combined; ○……, 2V4; △----, 2V1; +—·—, 3V4; ×—·—, 3V1.

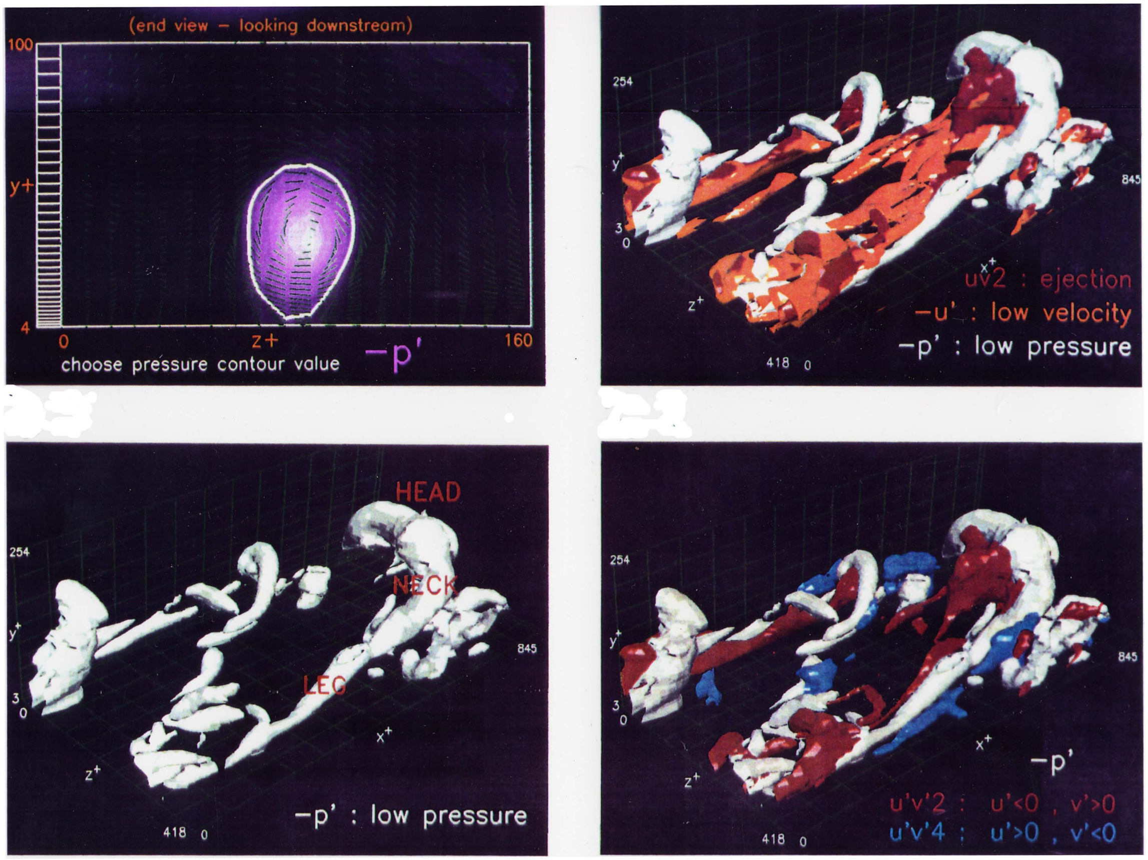

Robinson (1990)

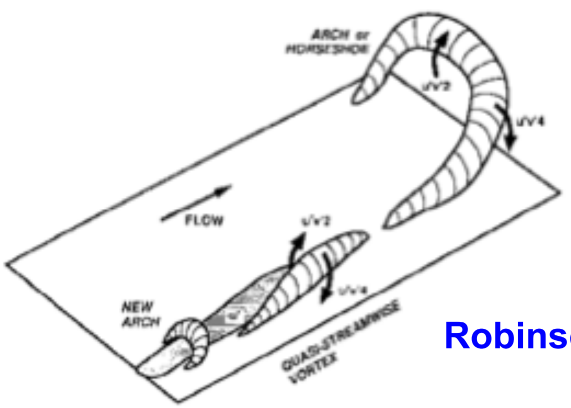

Figure 13b Conceptual model of the kinematical relationships between (1) ejection/sweep motions and quasi-streamwise vortices in the near-wall region and (2) ejection/sweep motions and arch-shaped vortical structures in the outer region. Model proposed for low-Reynolds-number boundary layers (from Robinson 1990).

Robinson (1991) Ann. Rev. Fl. Mech. 23

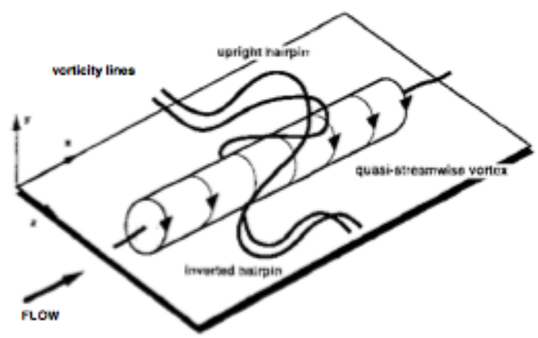

Figure 4 Vorticity lines traced from either side of a quasi-streamwise vortex in a boundary layer, showing upright- and inverted-hairpin shapes.

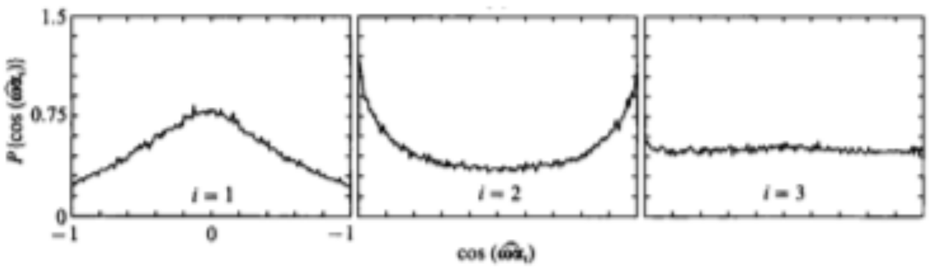

FIGURE 12. Probability density functions of cosine of the angle between vorticity vector and eigenvectors of the rate-of-strain tensor; $\alpha_1 < \alpha_2 < \alpha_3$; $x/M = 30$. (a) Grid flow, (b) boundary layer, $y/\delta = 0.2$

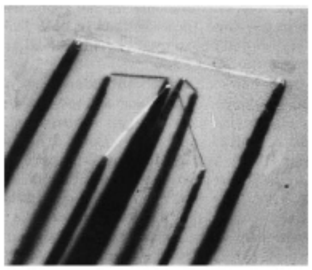

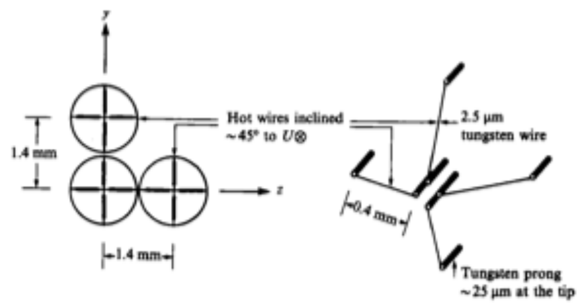

Tsinober, Kit and Dracos (1992) JFM 242

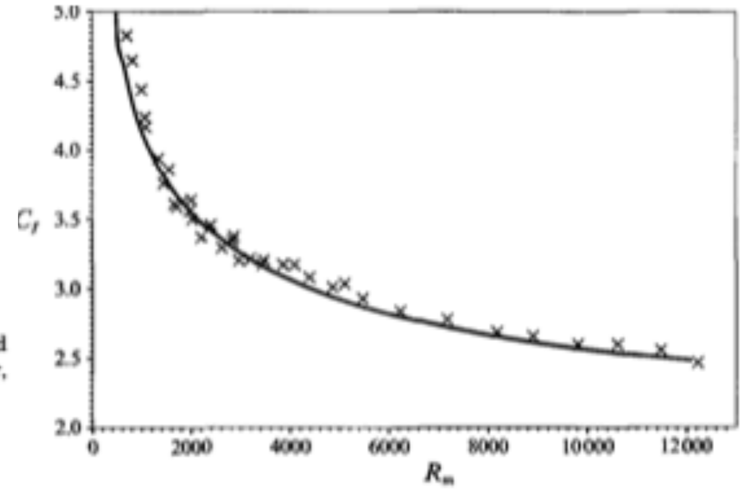

FIGURE 3. Friction coefficient in a zero-pressure-gradient boundary layer versus momentum-thickness Reynolds number. Experimental data is from Coles & Hirst; solid line is present model.

The exact Reynolds stress transport equation can be written

$$D_t \overline{u_i u_j} = \wp_{ij} + P_{ij} - \frac{\overline{u_i u_j}}{k}\epsilon - \partial_k \overline{u_k u_i u_j} - \frac{2}{3\rho}\delta_{ij}\partial_k \overline{u_k p} + \nu\nabla^2$$

where $$P_{ij} = -\overline{u_i u_k}\,\partial_k U_j - \overline{u_j u_k}\,\partial_k U_i$$

is the rate of turbulence production by mean velocity gradients,

$$\wp_{ij} = -\frac{1}{\rho}\overline{u_i \partial_j p} - \frac{1}{\rho}\overline{u_j \partial_i p} + \frac{2}{3\rho}\delta_{ij}\partial_k \overline{u_k p} - \epsilon_{ij} + \frac{\overline{u_i u_j}}{k}\epsilon$$

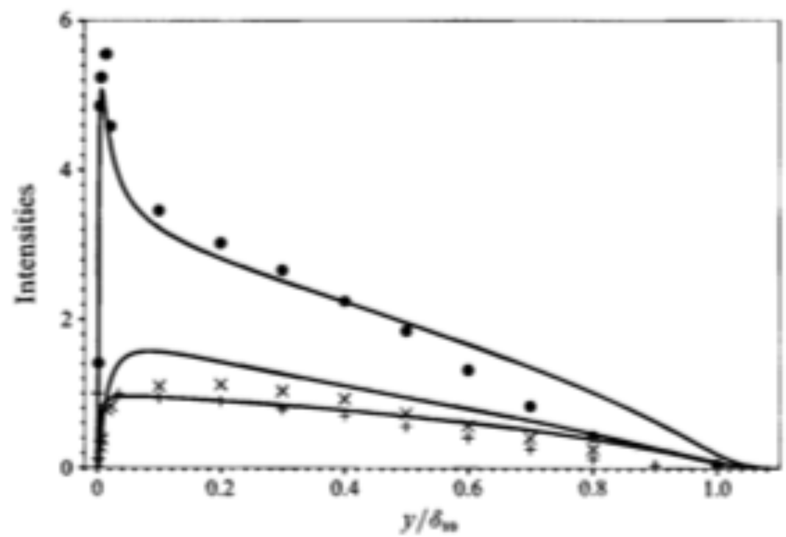

FIGURE 4. Profiles of k (●), $\overline{v^2}$ (×) and $-\overline{uv}$ (+) at $R_m = 7150$ in a zero-pressure-gradient boundary layer. Experimental data were transcribed from Klebanoff.

Tensorially consistent near wall 2nd order closure model without ad hoc damping functions

Durbin (1993) JFM 249

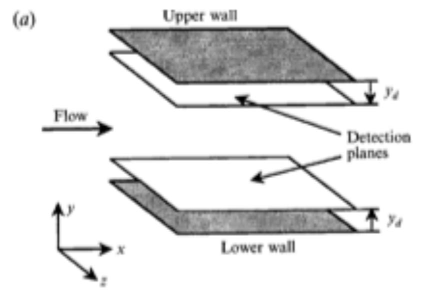

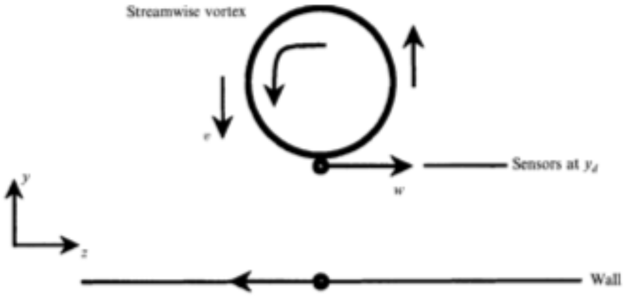

FIGURE 4. Schematic diagram of out-of-phase w-control.

Choi, Moin & Kim (1993) JFM

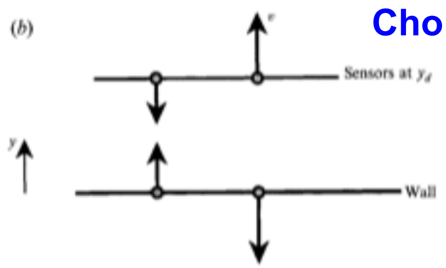

FIGURE 1. (a) Three-dimensional view of detection planes (b) schematic diagram of out-of-phase v-control.

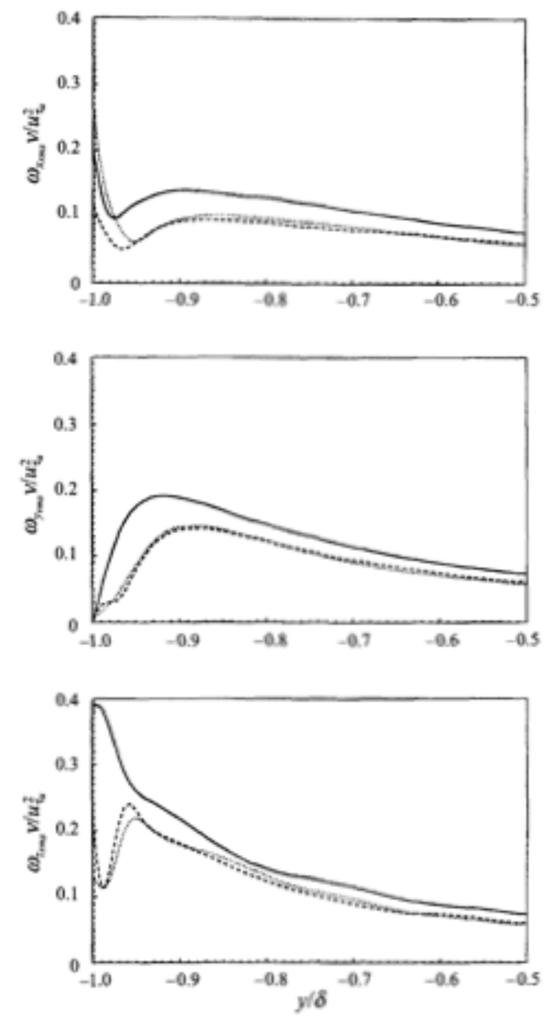

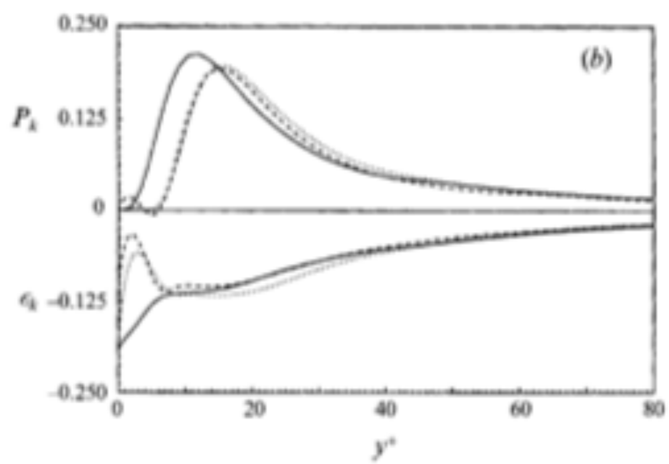

FIGURE 10. Production (P_k) and dissipation (ϵ_k) of the turbulence kinetic energy: —, no co[illegible] ——, v-control; ········, w-control. (a) In global coordinates; (b) in wall coordinates. In coordinates, values are non-dimensionalized by the actual wall-shear velocity.

FIGURE 14. Root-mean square vorticity fluctuations normalized by the wall-shear velocity in global coordinates: —, no control; ——, v-control; ········, w-control. Note that $y/\delta = -1$ corresponds to the lower location.

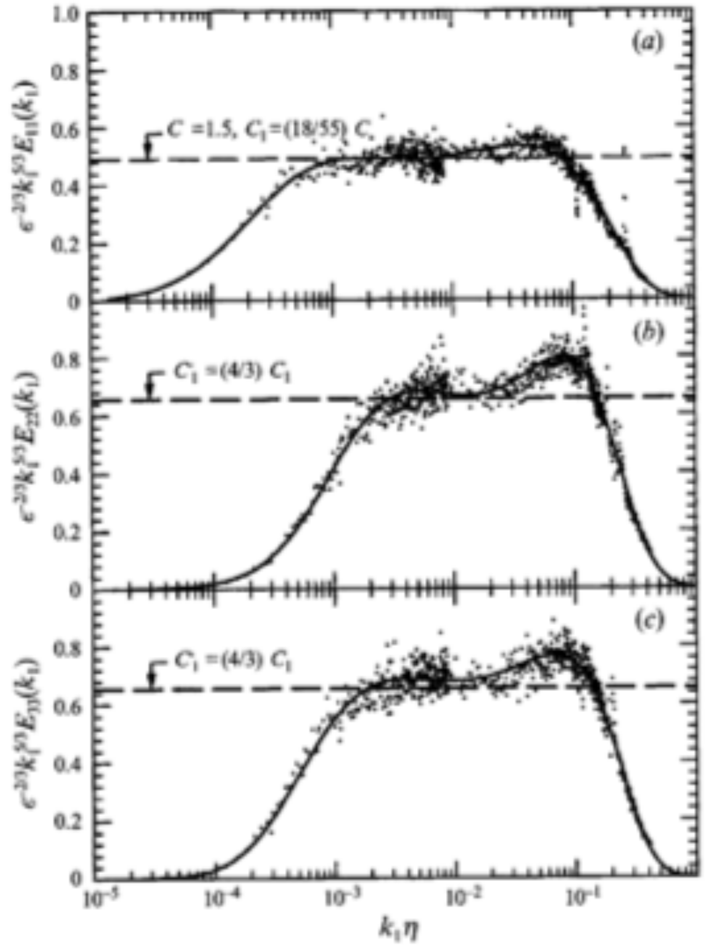

FIGURE 13. Compensated longitudinal and transverse spectra measured at mid-layer for the high-speed case ($y = 400$ mm, $y^+ \approx 62000$, $R_\lambda \approx 1450$). Only the data for wavenumber range $k_1\eta < 0.25$ can be accepted. Solid lines are the ninth-order, least-square, log-log polynomial fits to the spectral data. (*a*) u_1-spectrum; (*b*) u_2-spectrum; (*c*) u_3-spectrum.

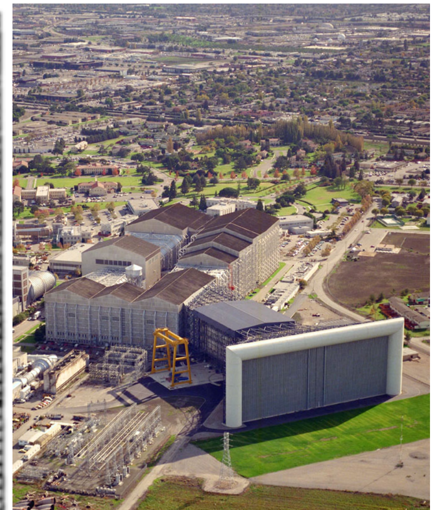

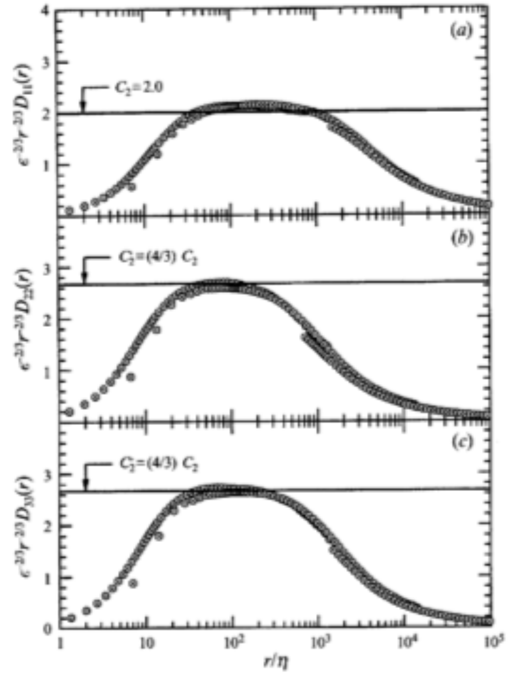

FIGURE 17. Compensated second-order structure functions for longitudinal and transverse velocity fluctuations measured at mid-layer for the low-speed case ($y = 515$ mm, $y^+ \approx 16200$, $R_\lambda \approx 600$). Dissipation is from the third-order structure function. (*a*) u_1-structure function; (*b*) u_2-structure function; (*c*) u_3-structure function.

Saddoughi & Veeravalli (1994) JFM 268

$$E_{\omega_y}(k_x) = E_{\omega_z}(k_x) = \frac{1}{4}\int_{k_x}^{\infty} \frac{E(k)}{k}(k^2 + k_x^2)\,dk$$

Wallace & Ong (2008) Phys. Fl. 20

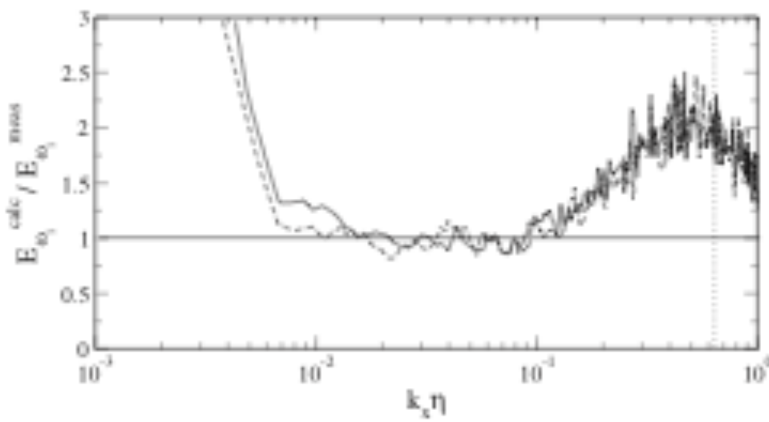

FIG. 6. Distributions of the ratios of wall normal and spanwise vorticity spectra calculated from Eq. (21) to their measured values: (——) $i=y$; (---) $i=z$.

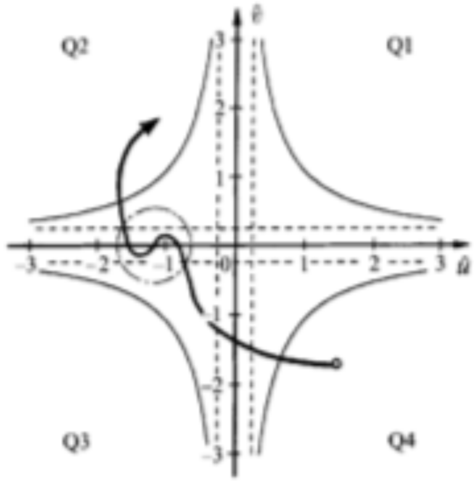

FIGURE 3. Trajectory analysis technique (TRAT) based on quadrant-sequences on the (u, v)-plane. ———, $H = 1.07$; – – – –, $h = 0.25$.

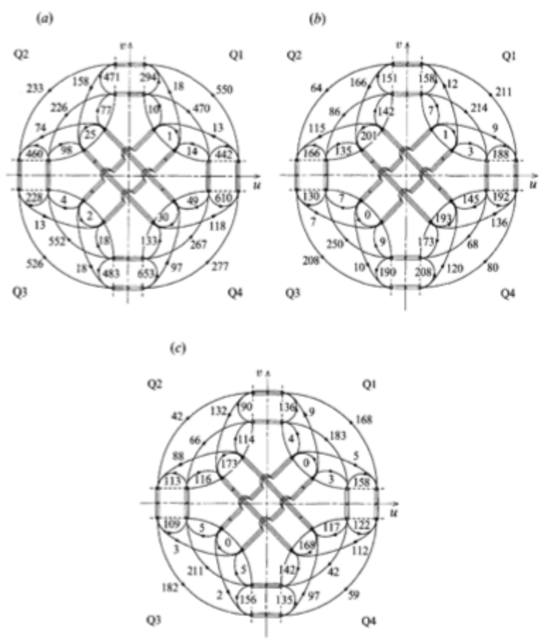

FIGURE 5. Trajectories of turbulent motions in the near-wall region ($y^+ = 18.5$). (a) $(h, H) = (0, 0)$, $N_{total} = 7712$; (b) $(h, H) = (0.25, 0)$, $N_{total} = 4155$; (c) $(h, H) = (0.25, 1.07)$, $N_{total} = 3267$.

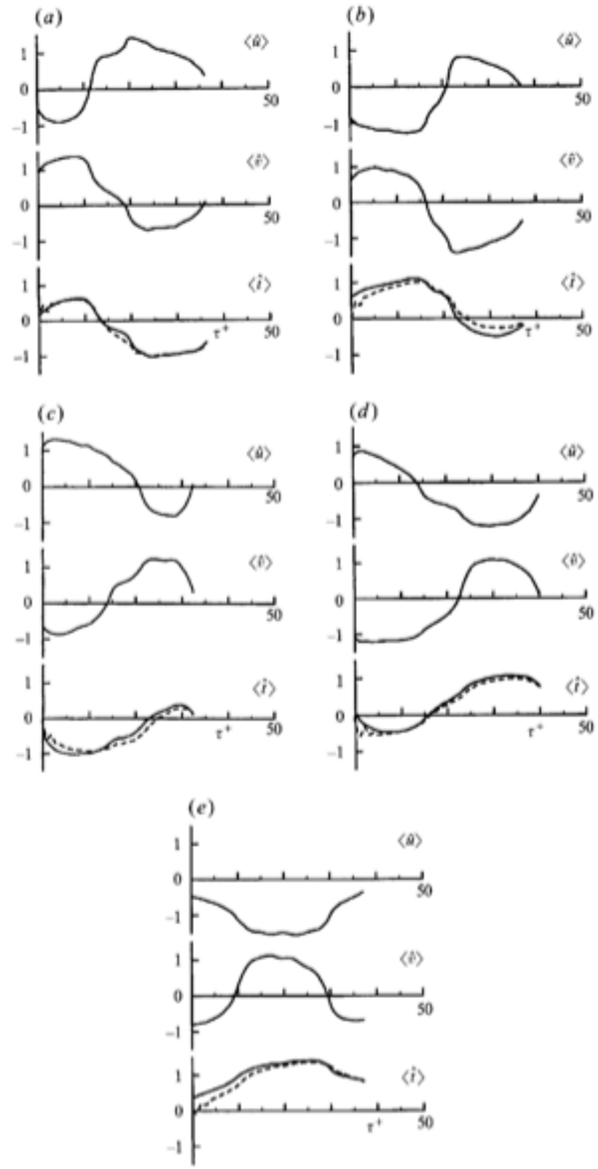

FIGURE 13. Predictions of near-wall temperature fluctuations associated with the key flow patterns using the autoregressive (AR) model: ———, measurements; – – – –, AR model prediction. (a) Q2-Q1-Q4; (b) Q2-Q3-Q4; (c) Q4-Q1-Q2; (d) Q4-Q3-Q2; (e) Q3-Q2-Q3.

Nagano & Tagawa (1995) JFM 305

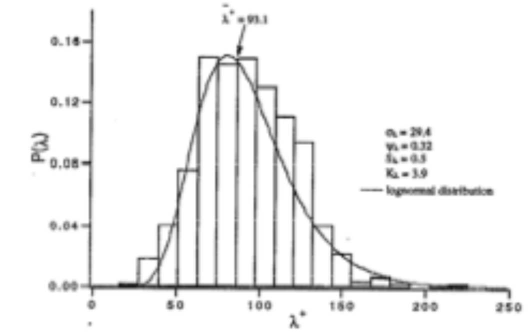

FIG. 4. Probability density histogram of spanwise streak spacing at $R_\theta \sim 1.5\times10^6$, with a sample size of 1072. The symbols σ_λ, ψ_λ, S_λ, and K_λ define the standard deviation, coefficient of variation (σ_λ/λ^+), skewness, and kurtosis, respectively. The dotted line describes a lognormal distribution using λ^+ and ψ_λ, as suggested by Smith and Metzler.[3]

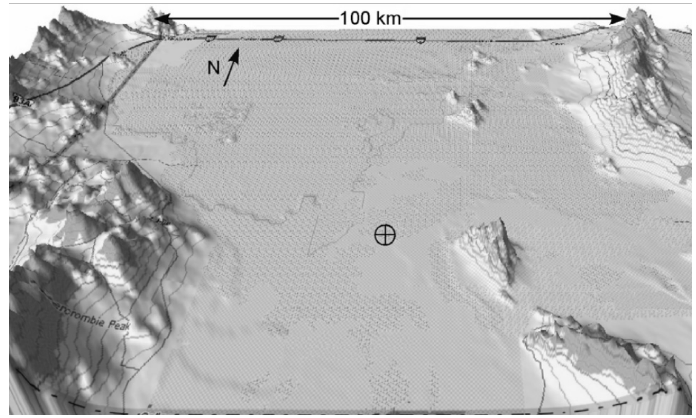

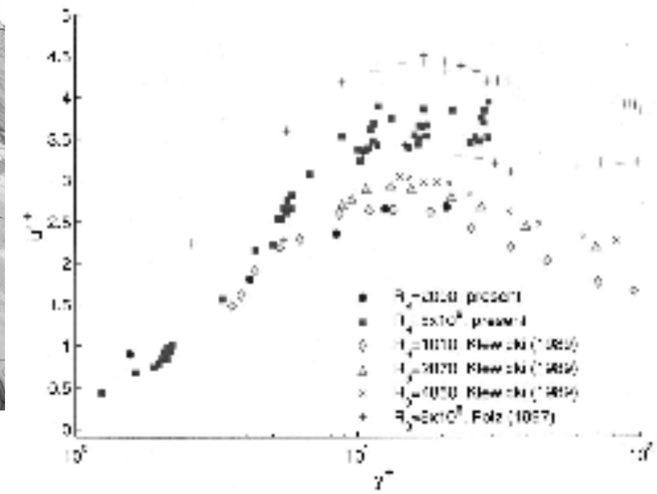

FIG. 3. Inner normalized plot of rms streamwise velocity vs position above the surface.

Klewicki, Metzger, Keiner & Thurlow (1995) Phys. Fl. 7

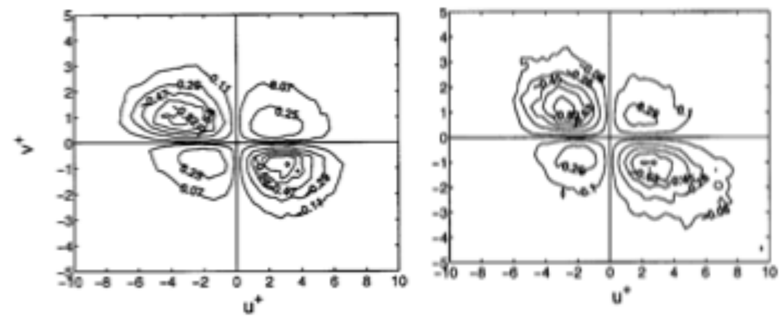

(b) $R_\theta = 4850$

(c) $R_\theta = 2\times10^6$, $k^+ \approx 25 \sim 50$

Priyadarshana & Klewicki (2004) Phys. Fl. 16

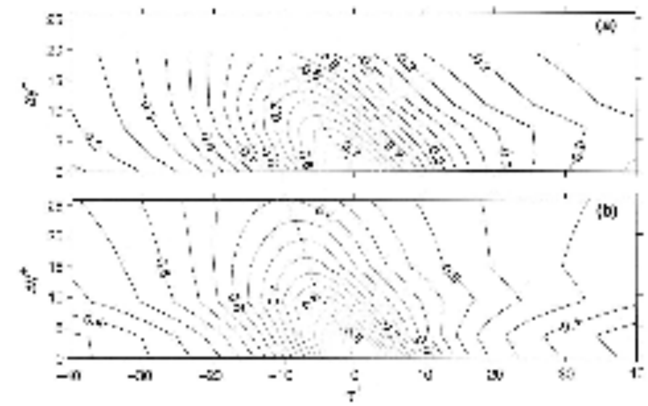

FIG. 15. Space–time autocorrelations of u. Dotted lines denote the locus of maximum correlation. Reference locations are identical to those used in Fig. 11. (a) $R_\theta = 2\times10^3$. (b) $R_\theta \sim 5\times10^6$.

Metzger & Klewicki (2001) Phys. Fl. 13

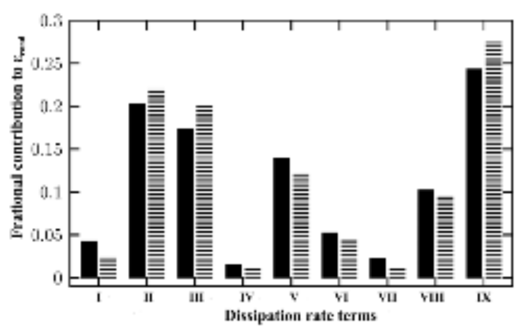

Fig. 14. Average fractional contribution of each of the nine squared velocity gradients [Roman numeral subscripted terms in [8]] to ε during periods of high ε at $R_\theta \sim 10^6$ and $y^+ = 45$. Solid bars are based on all values exceeding the ε threshold; hashed bars also require that ε exceed the threshold for at least 1.33 ms.

$$\overline{\varepsilon}/\nu = 2\overline{\left(\frac{\partial u}{\partial x}\right)^2}_{I} + \overline{\left(\frac{\partial u}{\partial y}\right)^2}_{II} + \overline{\left(\frac{\partial u}{\partial z}\right)^2}_{III} + \overline{\left(\frac{\partial v}{\partial x}\right)^2}_{IV} + 2\overline{\left(\frac{\partial v}{\partial y}\right)^2}_{V} + \overline{\left(\frac{\partial v}{\partial z}\right)^2}_{VI} + \overline{\left(\frac{\partial w}{\partial x}\right)^2}_{VII} + \overline{\left(\frac{\partial w}{\partial y}\right)^2}_{VIII} + 2\overline{\left(\frac{\partial w}{\partial z}\right)^2}_{IX} + 2\overline{\left(\frac{\partial u}{\partial y}\right)\left(\frac{\partial v}{\partial x}\right)}_{X} + 2\overline{\left(\frac{\partial u}{\partial z}\right)\left(\frac{\partial w}{\partial x}\right)}_{XI} + 2\overline{\left(\frac{\partial v}{\partial z}\right)\left(\frac{\partial w}{\partial y}\right)}_{XII}$$

Folz & Wallace (2010) Physica D 239

Jeong, Hussain, Schoppa & Kim (1997) JFM 332

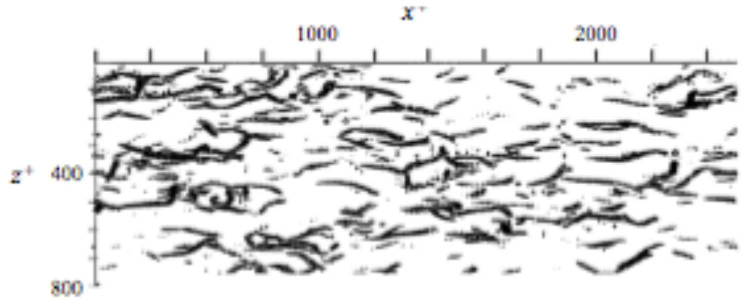

FIGURE 2. Top view of the isosurfaces of $\lambda_2 = -0.03$ in the range $0 < y^+ < 60$.

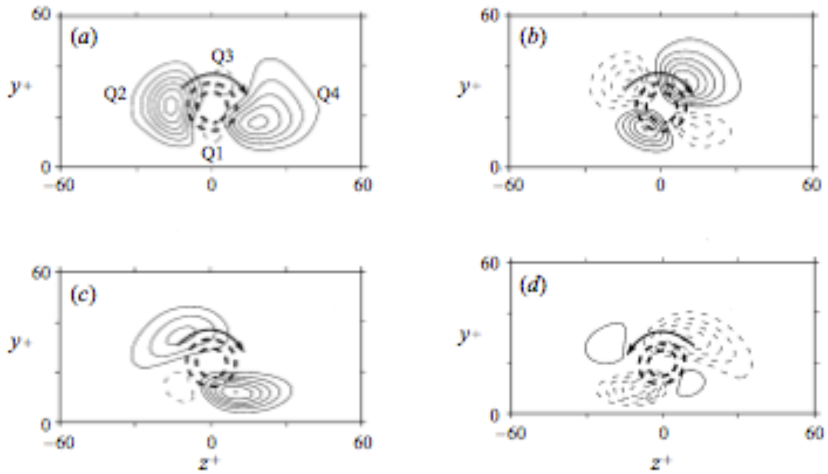

FIGURE 13. Coherent Reynolds stresses at $x = 0$ in E1: (a) $-\langle u - U \rangle \langle v \rangle$ for SP, contour levels = (0.3, −0.534, 1.94); (b) $-\langle v \rangle \langle w \rangle$ for SP, contour levels = (0.2, −0.868, 1.22); (c) $-\langle u - U \rangle \langle w \rangle$ for SP, contour levels = (0.7, −1.34, 4.23); (d) $-\langle u - U \rangle \langle w \rangle$ for SN. Relative locations of Q1, Q2, Q3 and Q4 events with respect to the CS center are shown in (a).

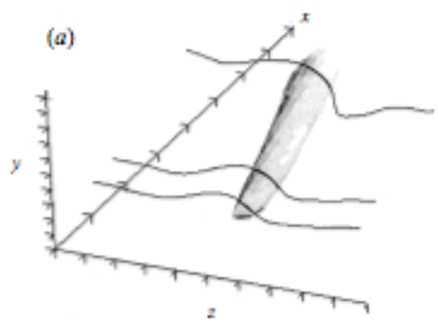

FIGURE 14. (a) Vortex lines traced outside CS

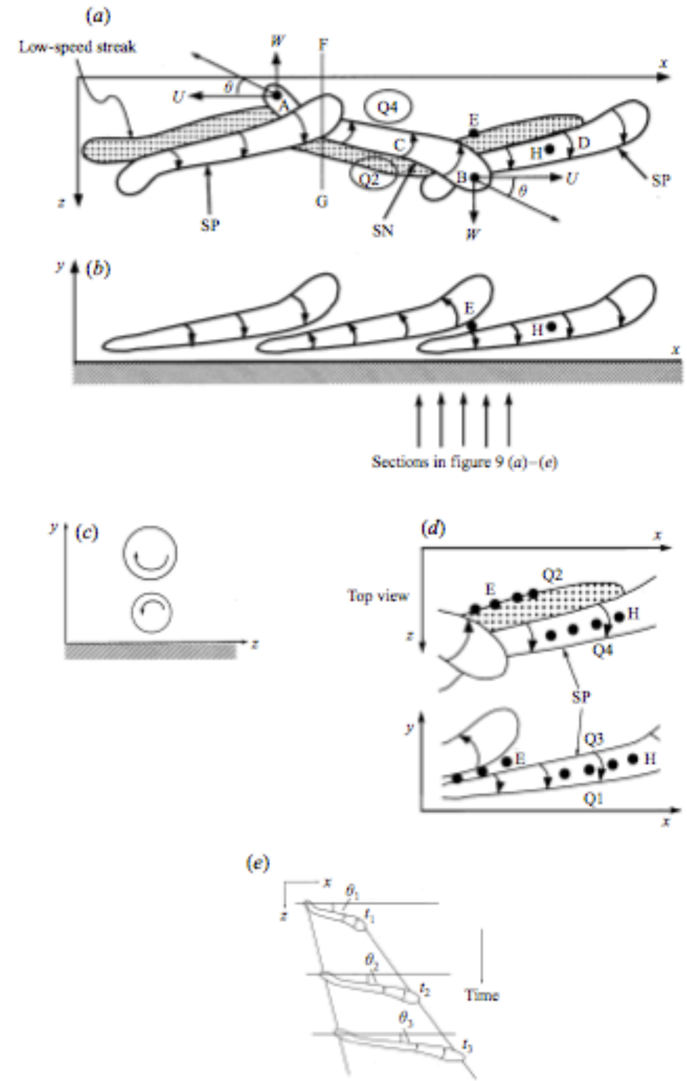

FIGURE 10. Conceptual model of an array of CS and their spatial relationship with experimentally observed events discussed in the text: (a) top view; (b) side view; (c) structures at cross-section FG in (a); (d) expanded views of structures C and D in (a,b), showing the relative locations of Q1, Q2, Q3, Q4, E and H. A schematic demonstrating the counteracting precession of SN in the (x, z)-plane due to background shear is shown in (e). The arrows in (b) denote the sections of figure 9(a–e).

Schoppa & Hussain (2002) JFM 453

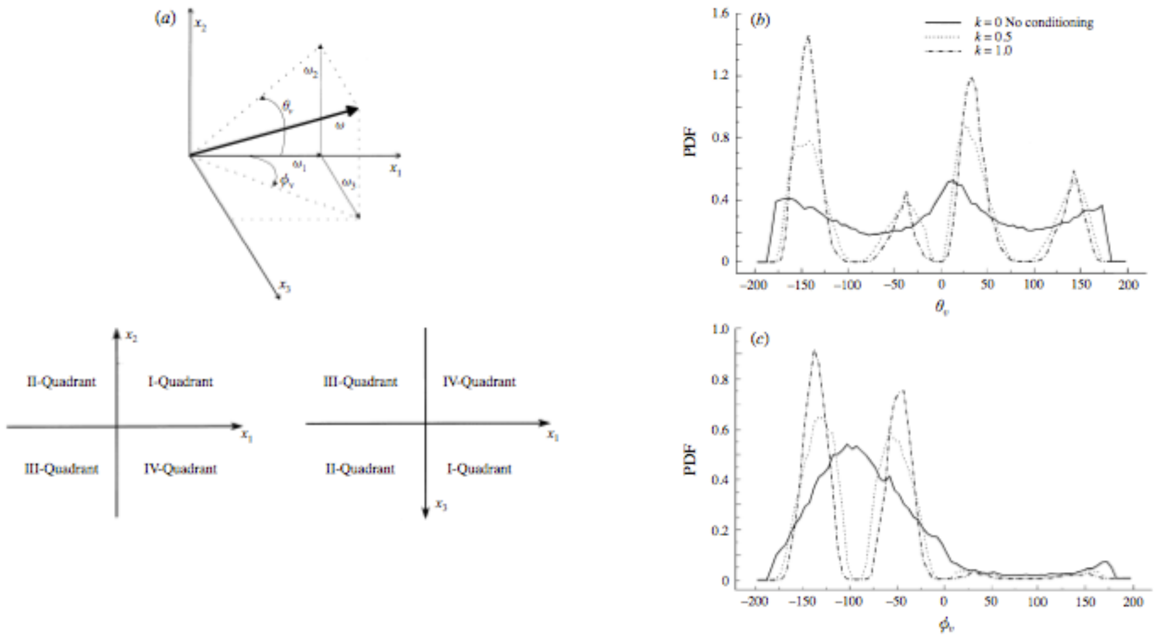

FIGURE 30. (*a*). Angular orientation of vorticity vector and definition of quadrants on vertical and horizontal planes. (*b*) Probability density function of vorticity vector orientation angle θ_v in the (x_1, x_2)-plane at $x_2^+ = 12.5$, for threshold levels 0, 0.5 and 1. r.m.s. of ω_1 and for ω_2. (*c*) Probability density function of vorticity vector orientation angle ϕ_v in the (x_1, x_3)-plane at $x_2^+ = 12.5$, for threshold levels 0, 0.5 and 1 r.m.s. of ω_1 and ω_3.

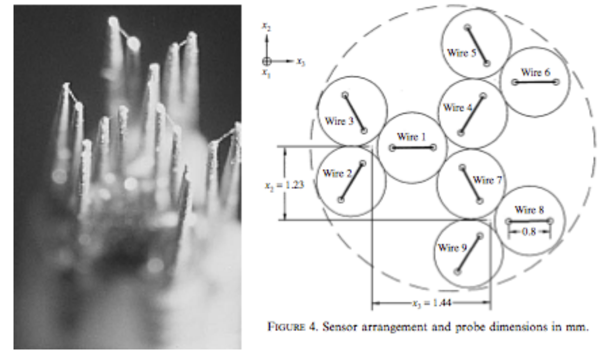

FIGURE 4. Sensor arrangement and probe dimensions in mm.

Honkan & Andreopolous (1997) JFM 350

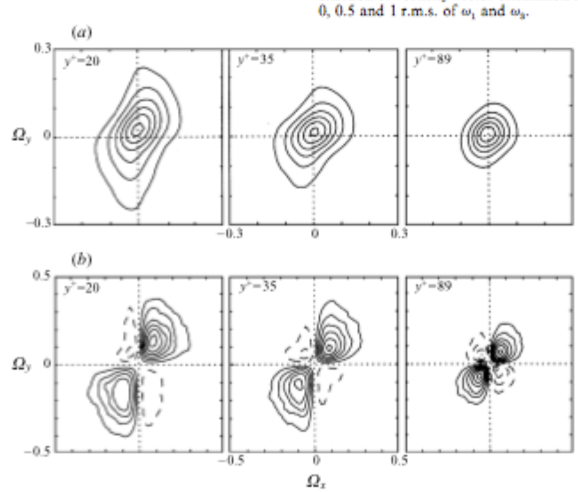

FIGURE 11. (*a*) JPDFs and (*b*) covariance integrands of Ω_x and Ω_y, non-dimensionalized by ν/u_τ^2. All vorticity and velocity gradients are normalized by this time scale here and in the following figures. Contour increments (for $y^+ = 20$, 35 and 89, respectively) are (*a*) 3.3, 4.5, 9.0 and (*b*) 3.4×10^{-6}, 2.9×10^{-6}, 1.4×10^{-6}. The outer contours are one increment above zero.

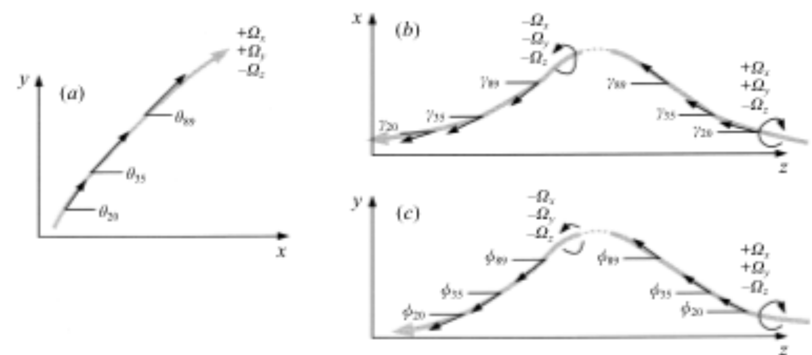

FIGURE 15. Projections of vorticity filament segments making the largest contributions to $\overline{\Omega_x\Omega_y}$, $\overline{\Omega_x\Omega_z}$ and $\overline{\Omega_y\Omega_z}$ at $y^+ = 20$, 35 and 89. (*a*) Projection on (x, y)-plane where $\theta = \tan^{-1}(\Omega_y/\Omega_x)$: $\theta_{20} \approx 58°$(or $-118°$) at $y^+ = 20$, $\theta_{35} \approx 48°$ (or $-136°$) at $y^+ = 35$ and $\theta_{89} \approx 48°$ (or $-137°$) at $y^+ = 89$. (*b*) Projection on (x, z)-plane where $\gamma = \tan^{-1}(\Omega_x/\Omega_z)$: $\gamma_{20} \approx \pm 16°$, $\gamma_{35} \approx \pm 27°$ and $\gamma_{89} \approx \pm 42°$. (*c*) Projection on (y, z)-plane where $\phi = \tan^{-1}(\Omega_y/\Omega_z)$: $\phi_{20} \approx \pm 27°$, $\phi_{35} \approx \pm 35°$ and $\phi_{89} \approx \pm 37°$.

$$\overline{\Omega_x\Omega_y} = \iint_{-\infty}^{\infty} \Omega_x\Omega_y P(\Omega_x, \Omega_y)\,\mathrm{d}\Omega_x\,\mathrm{d}\Omega_y$$

Ong & Wallace (1998) JFM 367

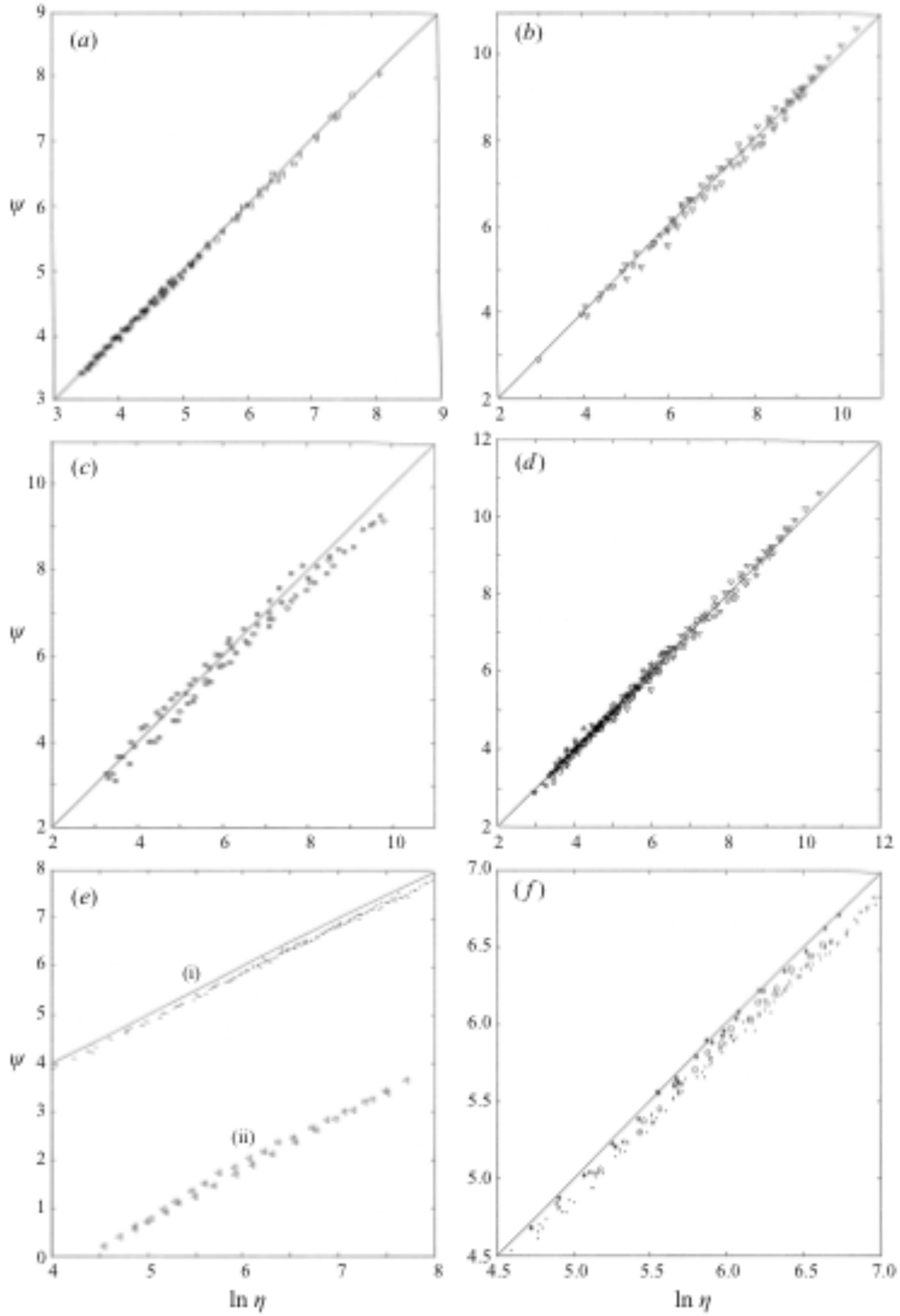

$$\eta = u_* y/\nu$$

$$\phi = \frac{u}{u_*} = \left(\frac{1}{\sqrt{3}}\ln Re + \tfrac{5}{2}\right)\eta^{3/2\ln Re}$$

$$\psi = \frac{1}{\alpha}\ln\left(\frac{2\alpha\phi}{\sqrt{3}+5\alpha}\right) = \ln\eta, \quad \alpha = \frac{3}{2\ln Re}$$

Barenblatt, Chorin & Prostokishin (2000) JFM 410

FIGURE 16. (*a*) The experiments of: ∗, Erm & Joubert (1991); □, Smith (1994); ◁, Krogstad & Antonia (1998); and ▷, Petrie *et al.* (1990). (*b*) ∇, The data of Winter & Gaudet (1973). (*c*) ∗, The data of Bruns *et al.* (1973) and Fernholz *et al.* (1995). (*d*) The data of all experiments except of those by Naguib (1992) and Nagib & Hites (1995), Bruns *et al.* (1992) and Fernholz *et al.* (1995): ○, Collins *et al.* (1978); ▷, Petrie *et al.* (1990); +, Erm (1988); ◇, Putell *et al.* (1981); ∗, Djenidi & Antonia (1993); ×, Warnack (1994); ◁, Krogstad & Antonia (1998); ∇, Winter & Gaudet (1973). All the data in (*a*–*d*) collapse on the bisectrix of the first quadrant in accordance with the universal form (14) of the scaling law (5). (*e*) (i) The data of Naguib (1992) and Nagib & Hites (1995) show a systematic deviation from the bisectrix of the first quadrant. (ii) The data of Krogstad & Antonia (1998) related to rough walls: the experimental points lie much lower than bisectric. For the evaluation of ψ the value $\alpha = 3/2\ln Re_1$ was taken. (*f*) The data of Hancock & Bradshaw (1989) show the parallel shift from the bisectrix of the same order as in the experiments by Nagib & Hites: ●, Nagib & Hites; ∗, Hancock & Bradshaw, $u'/U = 0.0003, 0.024, 0.026$; ×, Hancock & Bradshaw, $u'/U = 0.040, 0.041$; ○, Hancock & Bradshaw, $u'/U = 0.058$.

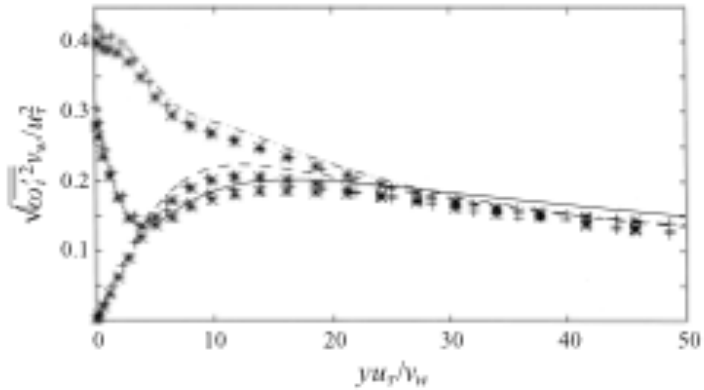

FIGURE 8. RMS of vorticity fluctuations. Lines correspond to the compressible simulation: ——, $\overline{\omega_1'^2}$; - - - -, $\overline{\omega_2'^2}$; —·—, $\overline{\omega_3'^2}$; +, Spalart ($Re_\theta = 1410$); ∗, Spalart ($Re_\theta = 670$).

$Re_\theta = 1577$
Mach = 2.5

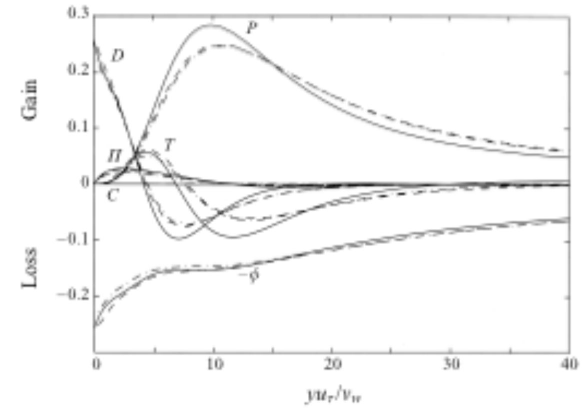

FIGURE 22. Turbulent kinetic energy budget: ——, simulation data; - - - -, Spalart's data $Re_\theta = 1410$; —·—, Spalart's data $Re_\theta = 670$. Symbols are: C, Convective term; P, Generation term; T, Turbulent transport; Π, Pressure terms; D, Viscous transport; $-\phi$, Viscous dissipation.

Guarini, Moser, Shariff & Wray (2000) JFM 414

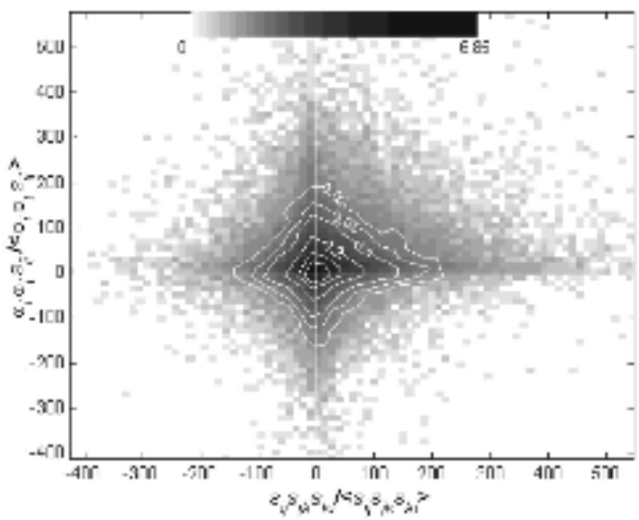

$R_\lambda \sim 10^4$

FIG. 2. Joint PDF/scatter plot of enstrophy production, $\omega_i\omega_j s_{ij}$, versus the production of strain $-(4/3)s_{ij}s_{jk}s_{ki}$. The density of the image corresponds to lg number of events.

Kholmyanshy, Tsinober & Yorish (2001) Phys. Fl. 13

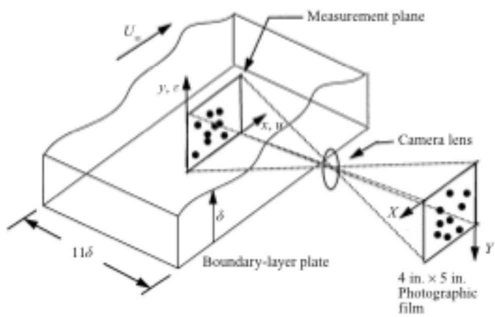

FIGURE 1. Schematic of PIV photographic recording system. The streamwise–wall-normal plane of a zero-pressure-gradient boundary layer is illuminated by a vertical laser light sheet and imaged by a side-viewing 4 in. × 5 in. photographic camera.

PIV

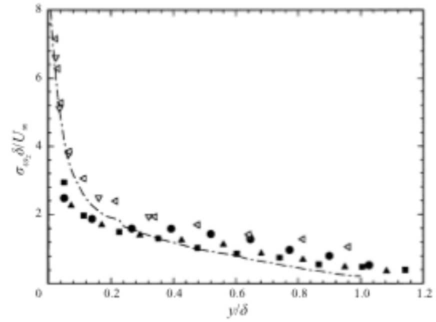

FIGURE 7. Root-mean-square spanwise vorticity scaled and plotted with outer variables ■, $Re_\theta = 930$; ▲, 2370; ●, 6845; ▽, Balint *et al.* (1991); ◁, Klewicki (1989) $Re_\theta = 2870$; — · —, Spalart (1988) $Re_\theta = 1410$.

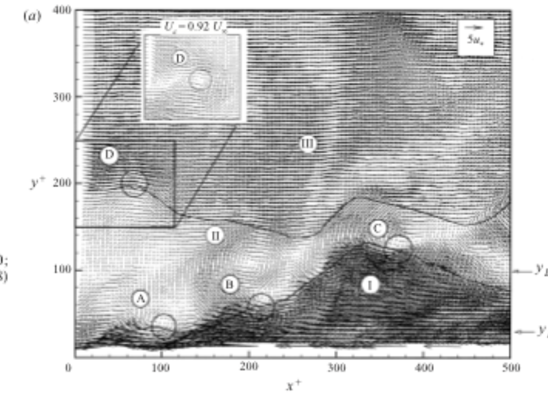

FIGURE 14. Realization of the $Re_\theta = 930$ boundary layer showing hairpin vortex heads along the boundaries separating regions of uniform-momentum fluid. The black lines separate the flow field into zones, labelled I, II and III, in which the streamwise momentum is nearly uniform: (*a*) instantaneous velocity vector map viewed in a convecting frame of reference $U_c = 0.8U_\infty$ and scaled with inner variables, (*b*) contours of constant *u*-momentum.

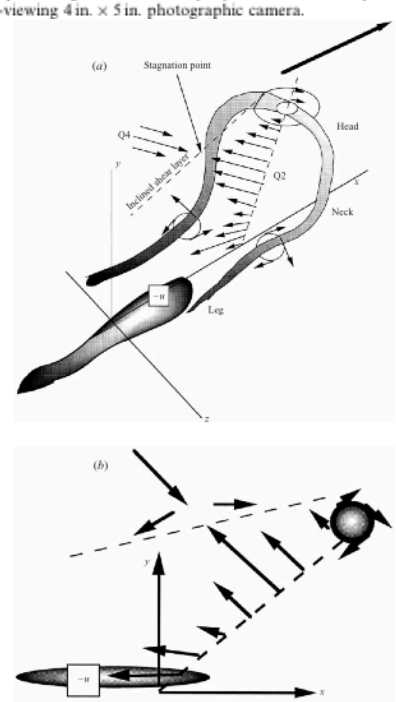

FIGURE 10. (*a*) Schematic of a hairpin vortex attached to the wall and the induced motion. (*b*) Signature of the hairpin vortex in the streamwise–wall-normal plane. The
to the spanwise location of the plane, until it intersects the concentrated cor
the hairpin.

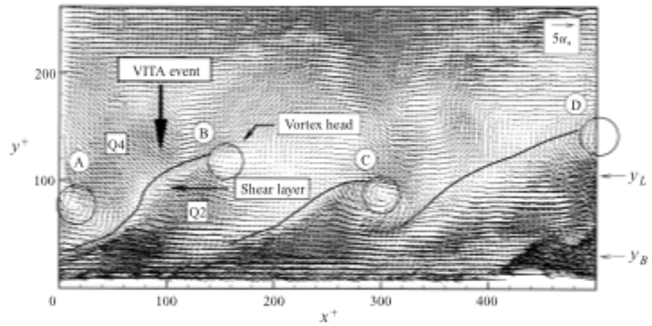

FIGURE 11. Near-wall realization at $Re_\theta = 930$ showing four hairpin vortex signatures aligned in the streamwise direction. Instantaneous velocity vectors are viewed in a frame-of-reference moving at $U_c = 0.8U_\infty$ and scaled with inner variables. Vortex heads and inclined shear layers are indicated schematically, along with the elements triggering a VITA event.

Adrian, Meinhart & Tompkins (2000) JFM 422

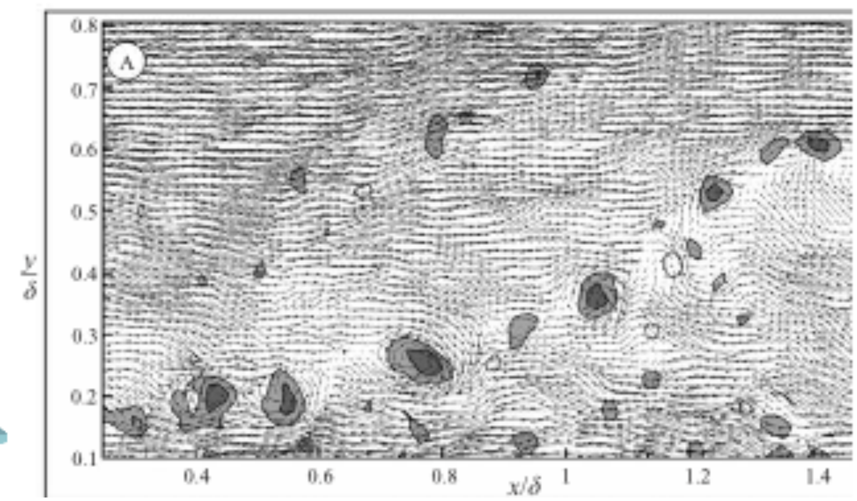

Adrian (2007) Phys. Fl. 19

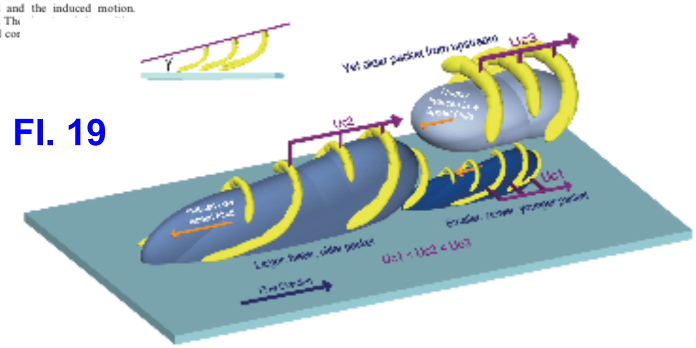

hairpin “packet”

$$A_{ij} = \partial U_i / \partial x_j$$
$$\lambda^3 + P\lambda^2 + Q\lambda + R = 0,$$
$$P = -A_{ii},$$
$$Q = \tfrac{1}{2}P^2 - \tfrac{1}{2}A_{ik}A_{ki},$$
$$R = -\tfrac{1}{3}P^3 + PQ - \tfrac{1}{3}A_{ik}A_{kn}A_{ni}.$$
$$D = \tfrac{27}{4}R^2 + Q^3$$

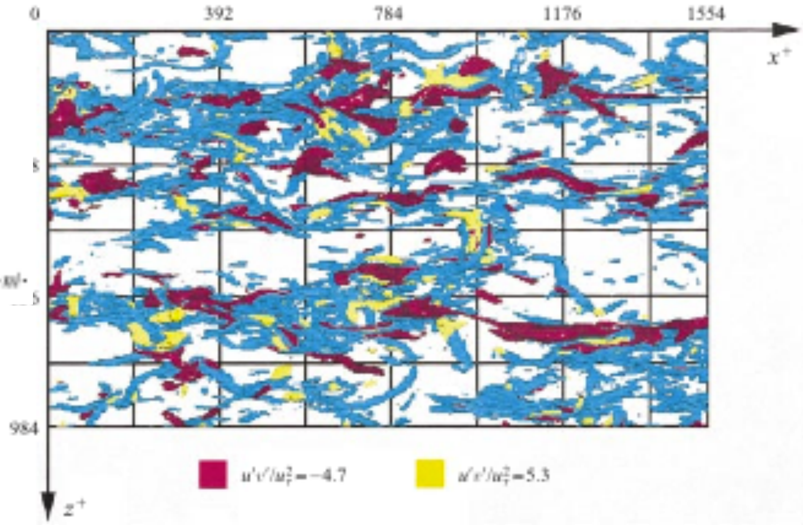

FIGURE 5. Top view of the computational domain showing regions of positive discriminant and their spatial association with Reynolds stress events ($u'v'$).

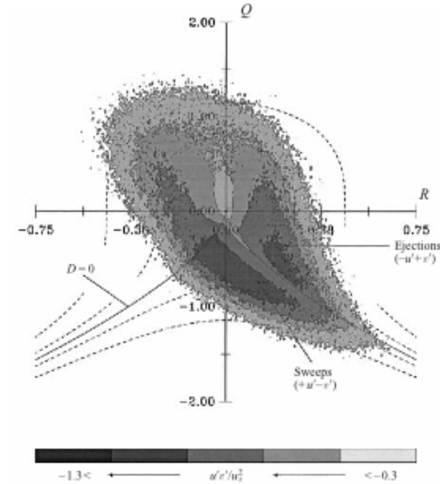

FIGURE 7. Time-averaged Reynolds-shear-stress ($u'v'$) generating events associated with the four incompressible flow patterns. Data taken from the entire boundary layer.

Chacin & Cantwell (2000) JFM 404

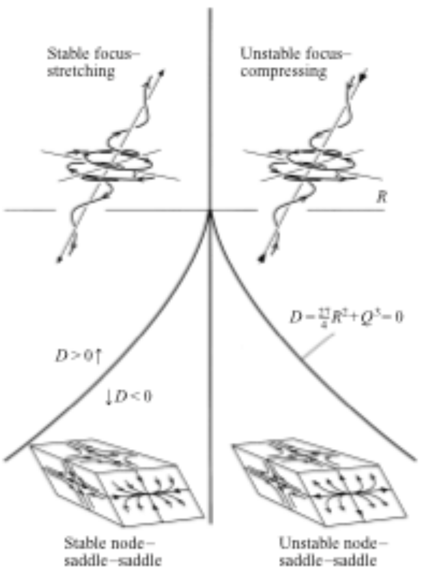

FIGURE 1. Summary of three-dimensional, incompressible flow patterns (from Soria *et al.* 1994).

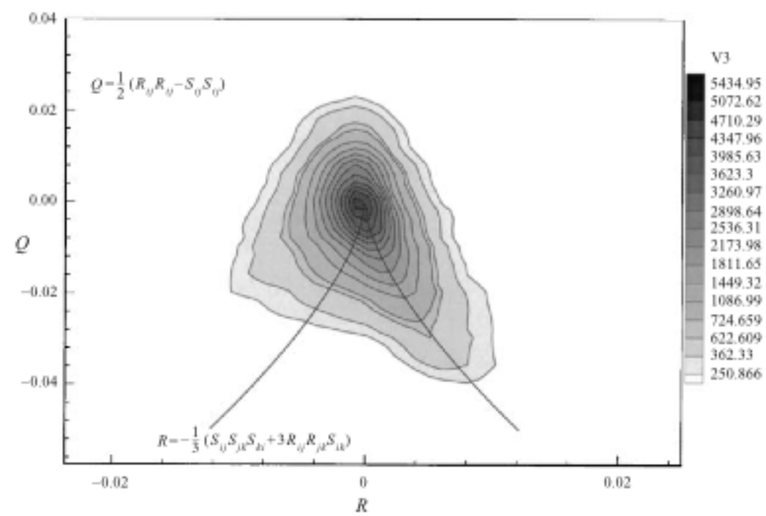

FIGURE 19. Joint probability density function of the Q and R invariants of velocity gradient tensor at $x_2^+ = 12.5$.

Andreopolous & Honkan(2001) JFM 439

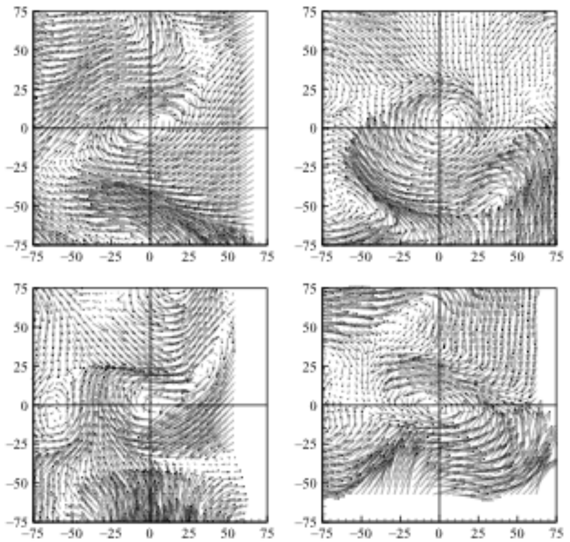

FIGURE 22. Examples of accepted eddy structures in the $(\boldsymbol{e}_z, \boldsymbol{e}_u)$-plane at $R_\theta = 7500$.

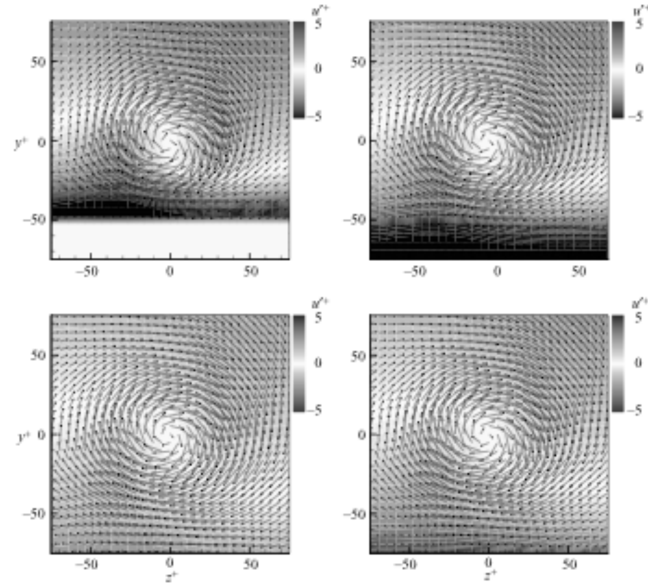

FIGURE 25. Averaged eddy structures in the $(\boldsymbol{e}_z, \boldsymbol{e}_y)$ normal to the wall plane at R $y_o{}^+ = 50$, 75, 100 and 125 (clockwise from the top left-hand side). The grey scale out-of-plane component.

PIV

R_θ = 7,500

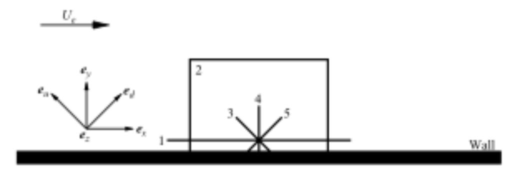

FIGURE 10. Orientations of the various planes used in the two series of PIV measurements: 1, $(\boldsymbol{e}_x, \boldsymbol{e}_z)$; 2, $(\boldsymbol{e}_x, \boldsymbol{e}_y)$; 3, $(\boldsymbol{e}_z, \boldsymbol{e}_u)$; 4, $(\boldsymbol{e}_z, \boldsymbol{e}_y)$; 5, $(\boldsymbol{e}_z, \boldsymbol{e}_d)$.

R_θ	$(\boldsymbol{e}_x, \boldsymbol{e}_y)$ V_-	$(\boldsymbol{e}_x, \boldsymbol{e}_y)$ V_+	$(\boldsymbol{e}_z, \boldsymbol{e}_u)$ V_-	$(\boldsymbol{e}_z, \boldsymbol{e}_u)$ V_+	$(\boldsymbol{e}_z, \boldsymbol{e}_y)$ V_-	$(\boldsymbol{e}_z, \boldsymbol{e}_y)$ V_+	$(\boldsymbol{e}_z, \boldsymbol{e}_d)$ V_-	$(\boldsymbol{e}_z, \boldsymbol{e}_d)$ V_+
7500	3613	1726	2386	2393	10 979	10 871	800	822
10 500	–	–	2096	2123	–	–	586	639
13 500	–	–	2423	2408	–	–	852	832
19 000	–	–	2303	2342	–	–	756	769

TABLE 6. Number of eddy structures detected.

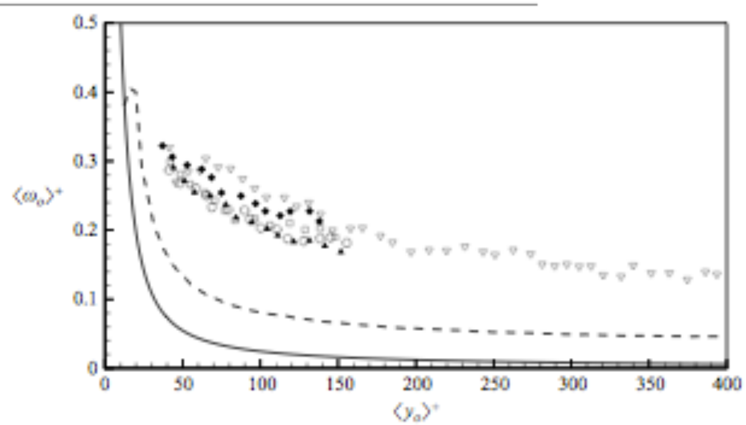

FIGURE 30. Mean vorticity profiles of eddy structures: ∇, $(\boldsymbol{e}_x, \boldsymbol{e}_y)$-plane and $R_\theta = 7500$; ◆, $(\boldsymbol{e}_z, \boldsymbol{e}_u)$-plane and $R_\theta = 7500$; □, $(\boldsymbol{e}_z, \boldsymbol{e}_u)$-plane and $R_\theta = 10\,500$; ▲, $(\boldsymbol{e}_z, \boldsymbol{e}_u)$-plane and $R_\theta = 13\,500$; ○, $(\boldsymbol{e}_z, \boldsymbol{e}_u)$-plane and $R_\theta = 19\,000$; - - -, r.m.s. spanwise vorticity; ———, Van Driest profile.

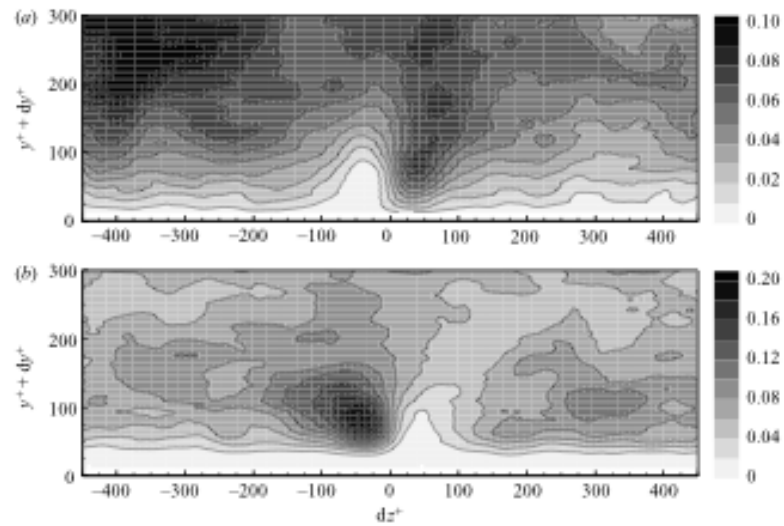

FIGURE 34. Probability map of the location of ejection compared to positive eddy structure and positive eddy structure compared to ejection at $y^+ = 50$ and $R_\theta = 7500$ in the $(\boldsymbol{e}_z, \boldsymbol{e}_y)$-plane. (*a*) Fixed point positive eddy structure; moving point, ejection. (*b*) Fixed point, ejection; moving point, positive eddy structure.

Carlier & Stanislas (2005) JFM 535

VLSMs

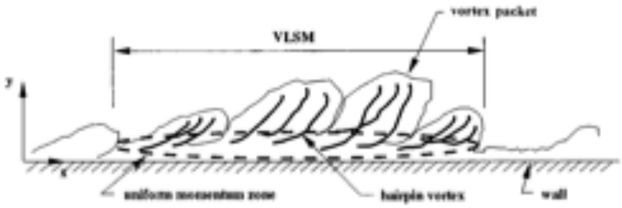

FIG. 7. The conceptual model of the process that creates very large-scale motions. Hairpins align coherently in groups to form long packets, and packets align coherently to form very large-scale motions.

Kim & Adrian (1999) Phys. Fl. 11

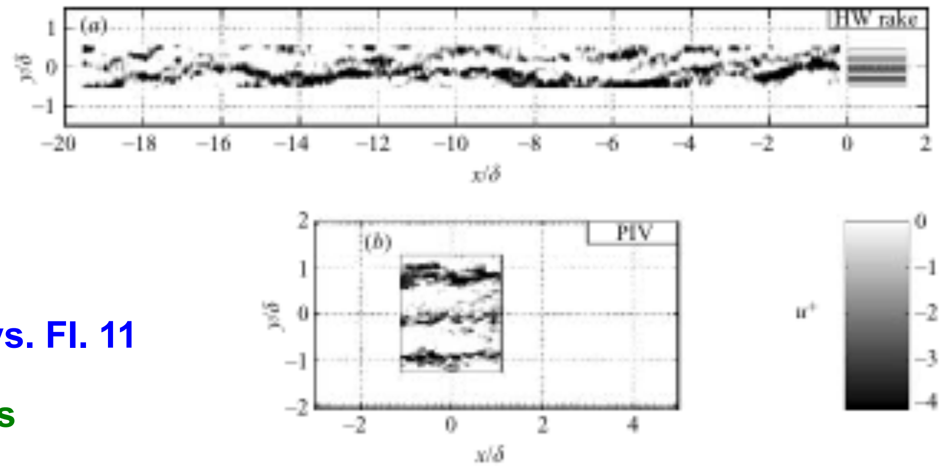

FIGURE 4. (*a*) Example of rake signal at $z/\delta = 0.15$ for $Re_\tau = 14\,380$. The x-axis is reconstructed using Taylor's hypothesis and a convection velocity based on the local mean, $\overline{U} = 15.9\,\mathrm{m\,s^{-1}}$. (*b*) Typical PIV frame for comparison at $Re_\tau = 1100$, $z/\delta = 0.087$. Shading shows only negative u fluctuations (see grey-scale).

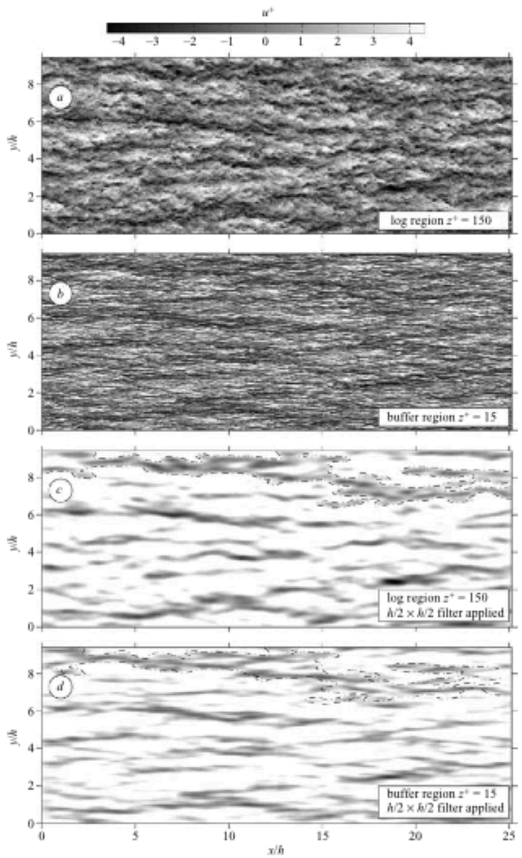

FIGURE 7. Instantaneous flow fields from $Re_\tau = 934$ channel simulations (del Álamo *et al.* 2004). Shading shows u fluctuations (*a*) at $z^+ = 150$; (*b*) at $z^+ = 15$ (see upper grey-scale). Plots (*c*) and (*d*) show the filtered data at the same respective heights (shading shows negative u fluctuations, grey-scale as figure 4).

Del Alamo, Jimenez, Zandonade & Moser (2004) JFM 500

Hutchins & Marusic (2007) JFM 579

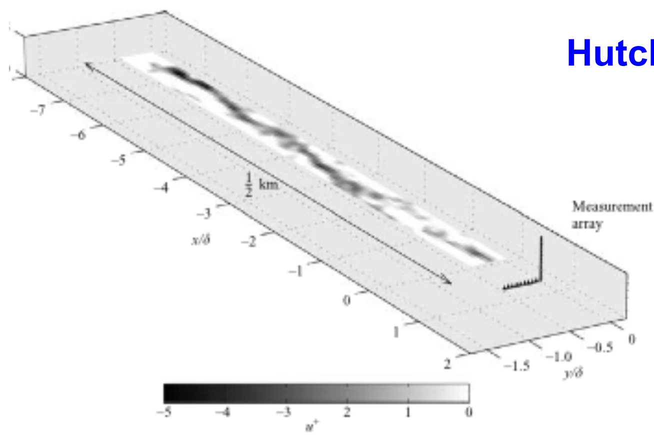

14. Example of signal across the spanwise array of sonic anemometers at SLTEST, 037, $Re_\tau = 660\,000$. The x-axis is reconstructed using Taylor's hypothesis and a ion velocity based on the local mean, $\overline{U} = 5.46\,\mathrm{m\,s^{-1}}$. Shading shows only negative ations (see grey scale).

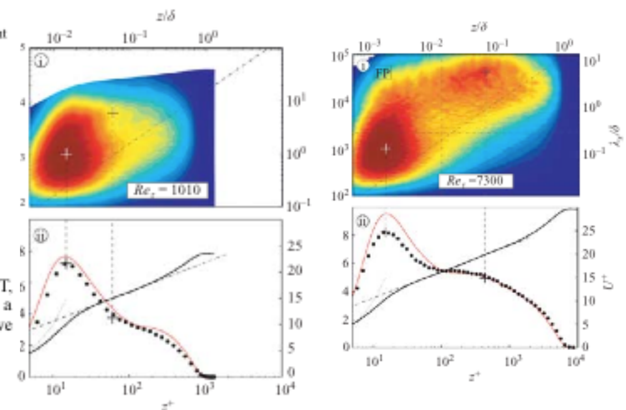

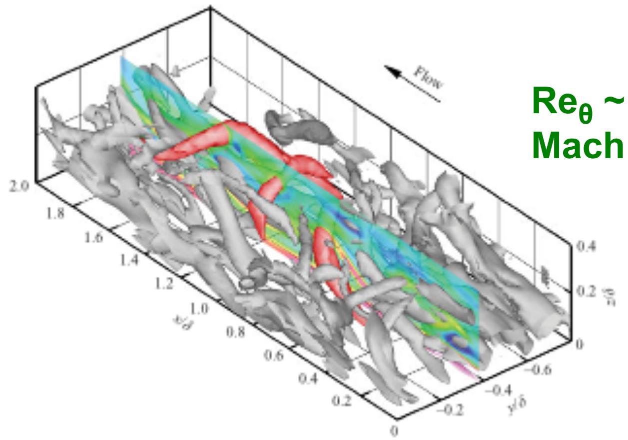

FIGURE 5. Hairpin packet from figure 4 visualized using an iso-surface of $\lambda_{ci} = 3.5\overline{\lambda_{ci}}$. The (x, z)-plane data of figure 4 are included at 50% translucency for reference. Portions of the packet hairpins not obscured by the reference plane have been coloured red.

Re_θ ~ 2600
Mach ~ 3

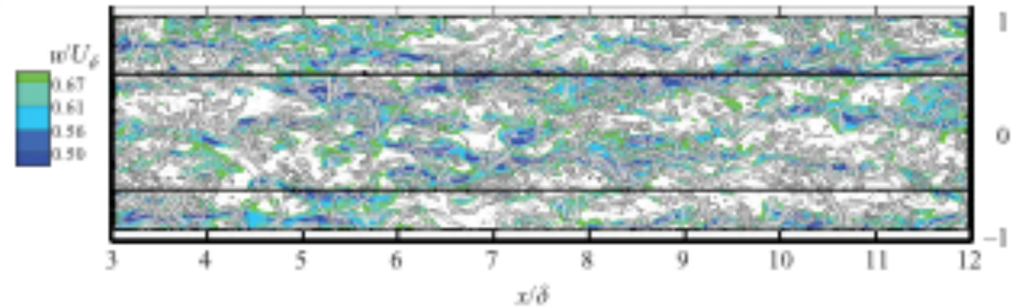

FIGURE 7. Instantaneous visualization connecting the large-scale low-speed regions with hairpin packets; see text for description.

Ringuette, Wu & Martin (2008) JFM 594

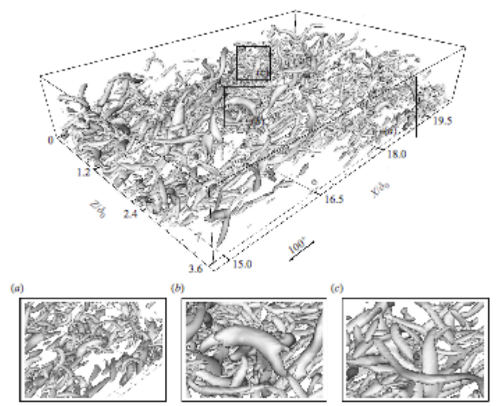

FIGURE 3. Perspective view of coherent structures in the boundary layer ($\lambda_{ci}^2 = 5u_\infty^2/\delta_0^2$). ($a$–$c$) Enlargements of corresponding parts in the main figure.

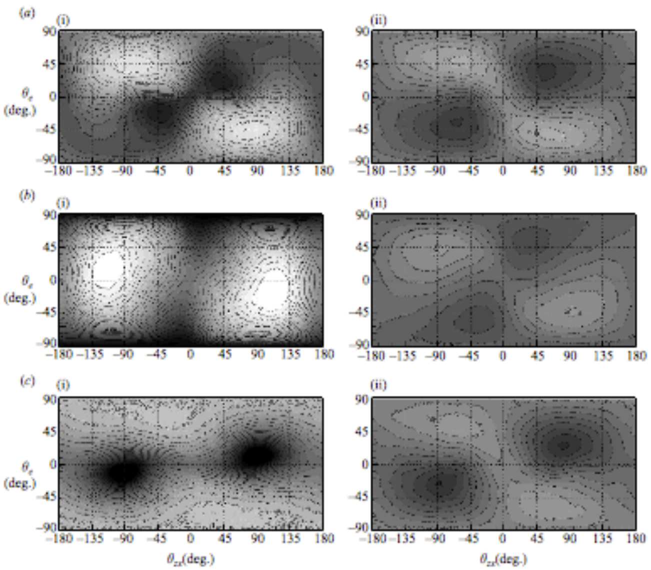

FIGURE 7. Scaled joint p.d.f. of vortex orientation ($\tilde{P}(\theta_{zx}, \theta_e)$) for various vortex orientation criteria. (a) $\hat{\omega}$-criterion; (b) $\hat{\mathbf{v}}_{\omega s}$-criterion; ($c$) $\hat{\mathbf{v}}_r$-criterion. Twenty-four equally spaced contour levels from 10^{-6} to 10^{-4} (grey shades indicate larger values). (i) Viscous + buffer layer ($y^+ \leqslant 40$). (ii) Log-layer + wake ($y^+ \geqslant 40$).

Re_θ = 950 - 1350
Mach = 2

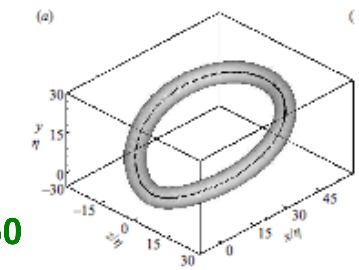

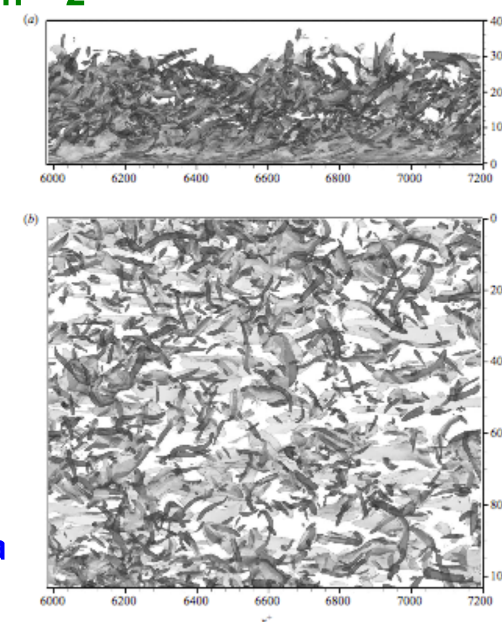

FIGURE 3. Iso-surfaces of tubes strength ($\omega_t/\omega' = 2$, dark grey) and sheets strength ($\omega_s/\omega' = 2$, light grey) projected onto the x–y and x–z planes.

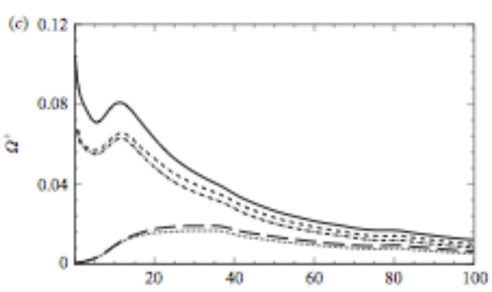

FIGURE 12. Distribution of turbulence kinetic energy (a), turbulent shear stress (b) and enstrophy (c) as a function of wall distance in wall units: DNS (——); strong vorticity events (- - - -); vortex sheets (- · - · -); vortex tubes (– – – –); 'roll-up' events (· · · · ·).

Pirozzoli, Bernadini & Grasso (2008) JFM 613
(2010) JFM 648a

T

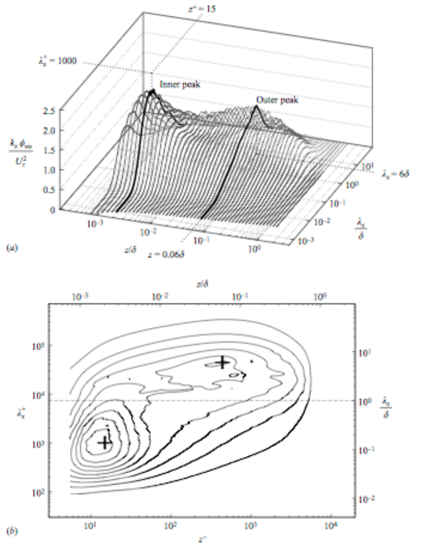

FIGURE 1. Pre-multiplied energy spectra of streamwise velocity fluctuation $k_x\phi_{uu}/U_\tau^2$ ($Re_\tau = 7300$). (a) Three dimensional surface plot for all wall-normal locations and (b) isocontour representation in which levels are from 0.2 to 1.8 in steps of 0.2; the '+' symbols mark the inner ($z^+ = 15$, $\lambda_x^+ = 1000$) and outer ($z/\delta = 0.06$, $\lambda_x/\delta = 6$) peaks. The horizontal dot-dashed line in (b) shows the location of the spectral filter ($\lambda_x = \delta$).

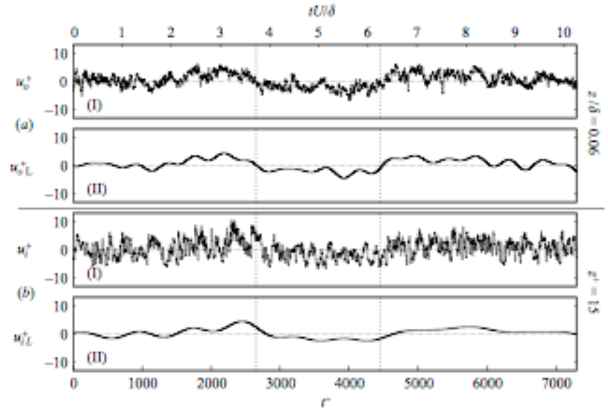

FIGURE 5. Example of large-scale decomposition on the fluctuating u velocity signal: (a) inner-peak location $z^+ = 15$; (b) outer-peak location $z/\delta = 0.06$; (I) raw signals, with 37 % of correlation; (II) large-scale components, with 72 % of correlation. Dashed vertical lines show region of negative large-scale u_{OL}^+ fluctuation.

Mathis, Hutchins & Marusic (2009) JFM 628

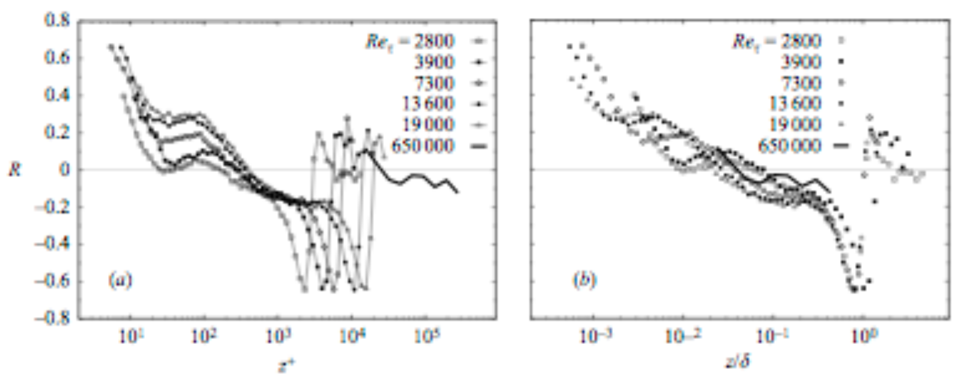

FIGURE 13. Comparison of correlation coefficient between the large-scale component and the filtered envelope of the small-scale component: (a) R plotted in inner-scale z^+ unit; (b) R plotted in outer-scale z/δ unit.

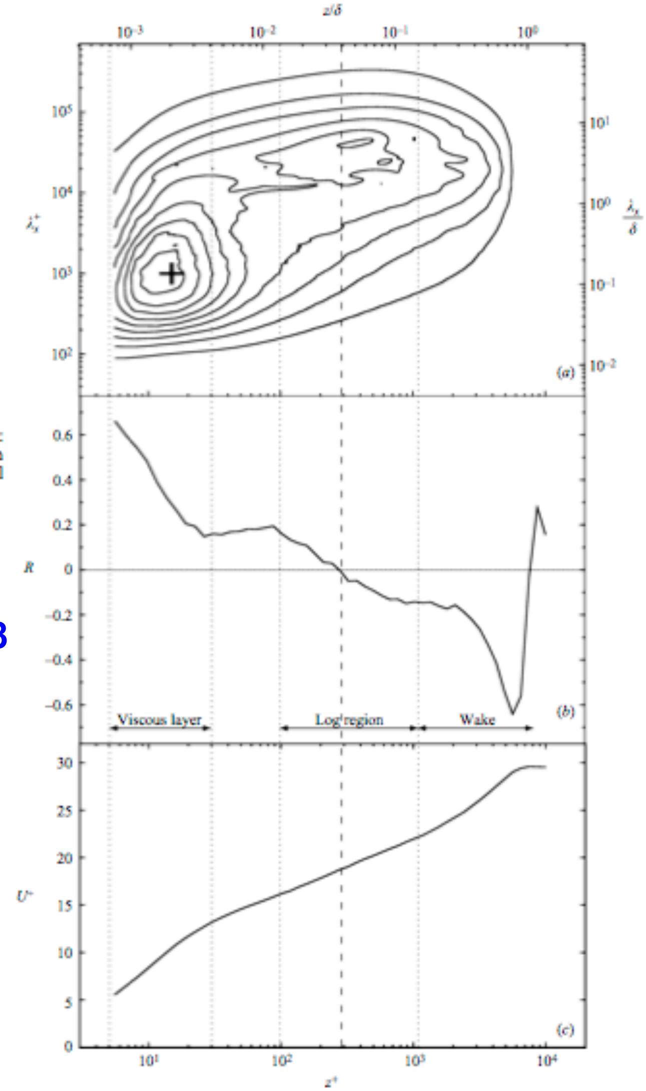

FIGURE 8. Wall-normal evolution of the degree of amplitude modulation: (a) pre-multiplied energy spectra of the streamwise velocity fluctuation $k_x\phi_{uu}/U_\tau^2$; (b) correlation coefficient $R(z^+)$ between the large-scale component and the filtered envelope of the small-scale component; (c) mean velocity profile; $Re_\tau = 7300$.

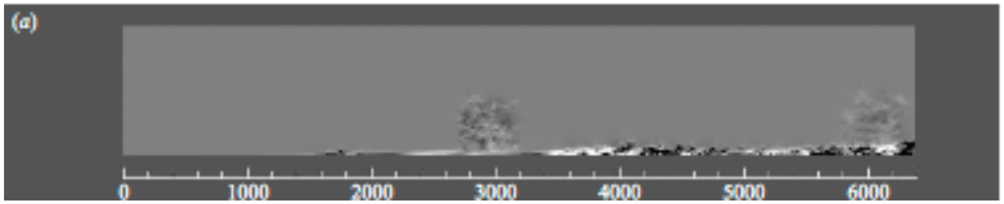

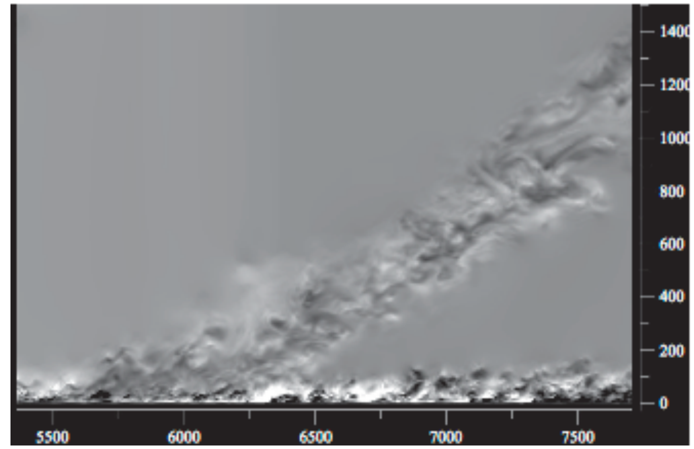

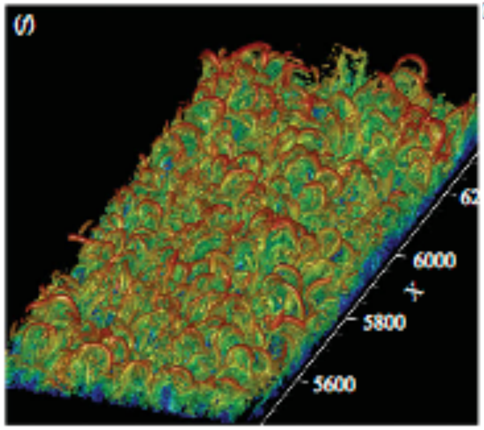

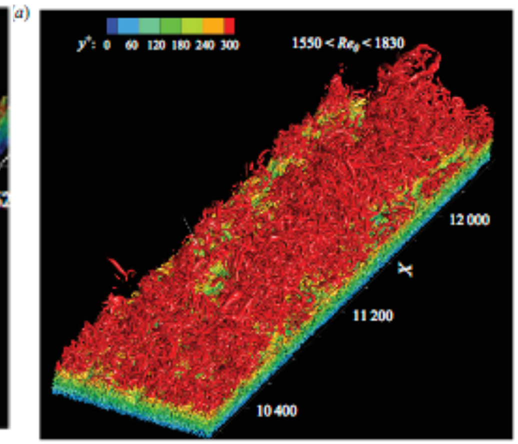

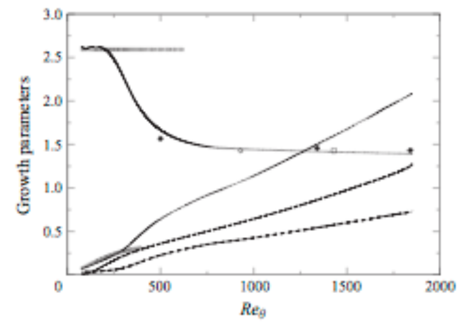

URE 2. Growth parameters of the present boundary layer with free-stream passing wakes. es are DNS results. Dotted, $10^{-2}\delta/\theta_0$; dashed, $10^{-4}x/\theta_0$; solid, H; dash-dotted, $10^{-3}Re_\tau$. s, Blasius solutions; diamond, Purtell, Klebanoff & Buckley (1981); circle, Adrian *et al.* 00); square, DeGraaff & Eaton (2000).

Wu & Moin (2009) JFM 630

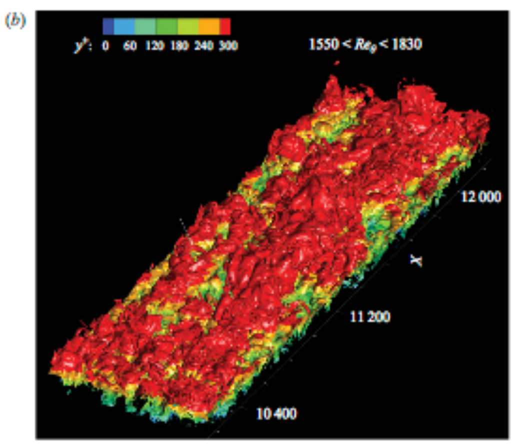

mparison of structures resolved using Q and temperature over $1550 <$ the boundary layer with passing wakes at $t = 46\mathscr{T}$. Iso-surfaces are coloured es of y^+. (*a*) $Q \approx 0$ and (*b*) $\phi = 0.05$.

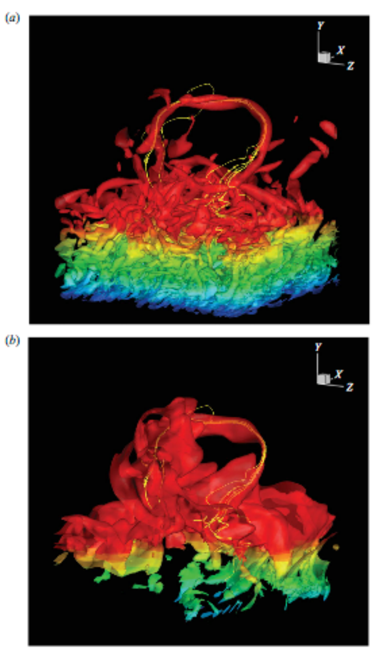

FIGURE 15. Zoomed view of the highlighted hairpin structure in figure 14 overlaid with local instantaneous vortex lines. (*a*) $Q \approx 0$ and (*b*) $\phi = 0.05$.

Wu (2010) JFM 664

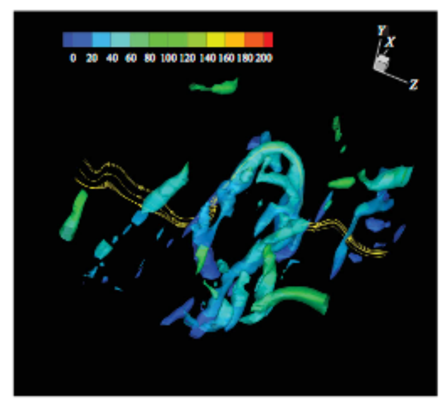

FIGURE 17. Zoomed view of the highlighted near-wall small structure in figure 16 overlaid with local instantaneous vortex lines. Iso-surfaces are coloured using y^+.

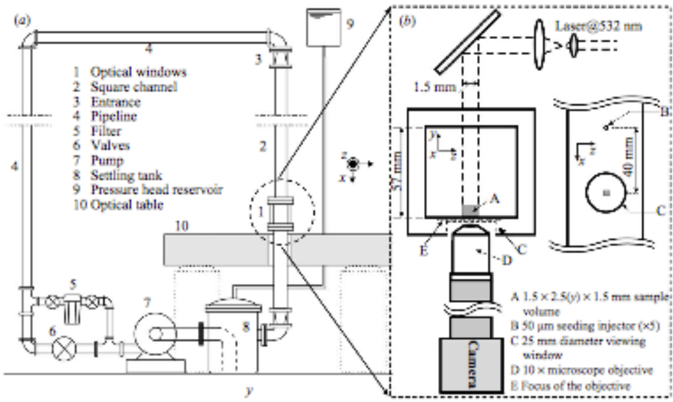

FIGURE 1. Test facility and DHM set-up.

Sheng, Malkiel & Katz (2009) JFM 633

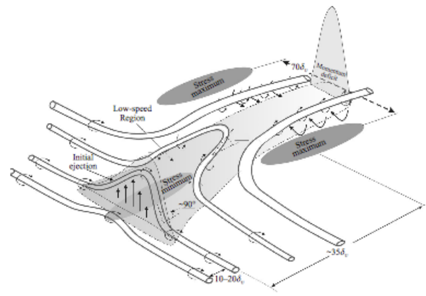

FIGURE 21. A conceptual model illustrating the process of spanwise vortex lifting and the resulting formation of a counter-rotating vortex pair, regions with wall stress extremes and low-momentum region.

Re_τ = 1470

Digital Holography

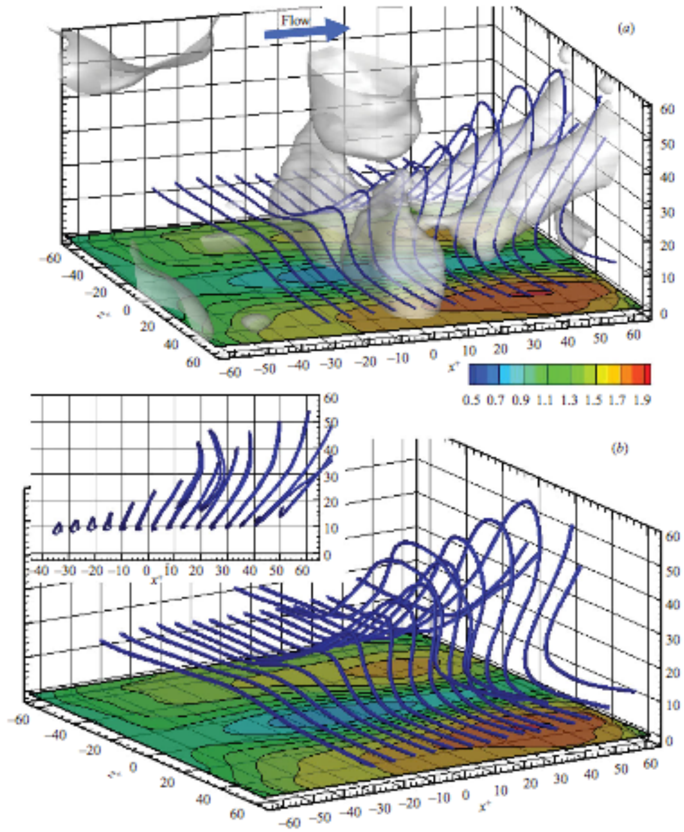

FIGURE 7. Conditionally averaged three-dimensional flow structure and wall stress based on a local stress minimum, $\tau_{xy} < 0.6\langle\tau_{xy}\rangle$, at $x^+ = z^+ = 0$. (*a*) Isosurface of $\lambda_2 = -350$, selected (blue) vortex lines and distribution of $\hat{\tau}_{xy}^{min}(\Delta x, 0, \Delta z)/\langle\tau_{xy}\rangle$. (*b*) Conditionally averaged near-wall vortex lines and distribution of $\hat{\tau}_{xy}^{min}(\Delta x, 0, \Delta z)/\langle\tau_{xy}\rangle$. Insert: x–y projection of the vortex lines.

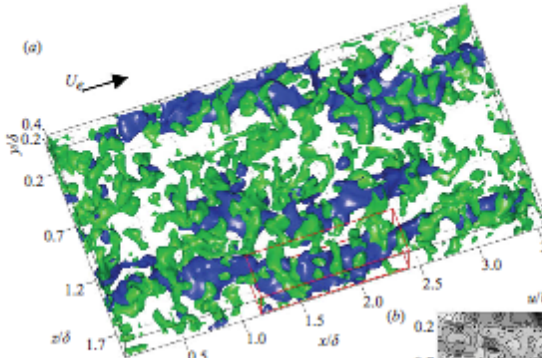

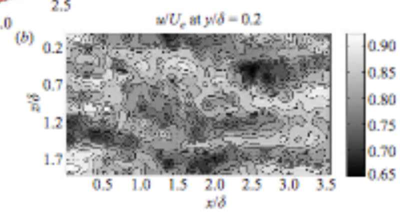

Elsinga, Adrian, Oudheusden & Scarano (2010) JFM 644

FIGURE 2. (*a*) Instantaneous vortex distribution detected by the Q criterion (green) and low-speed zones (blue, $u < 0.80U_e$) for $0.15 < y/\delta < 0.47$. (*b*) A contour plot of the u component of velocity at $y/\delta = 0.20$.

Tomographic PIV

Re_θ =34,000
Mach = 2

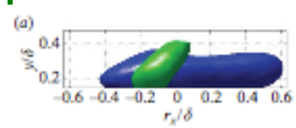

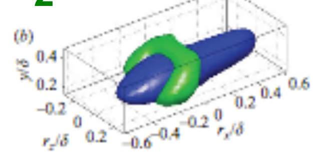

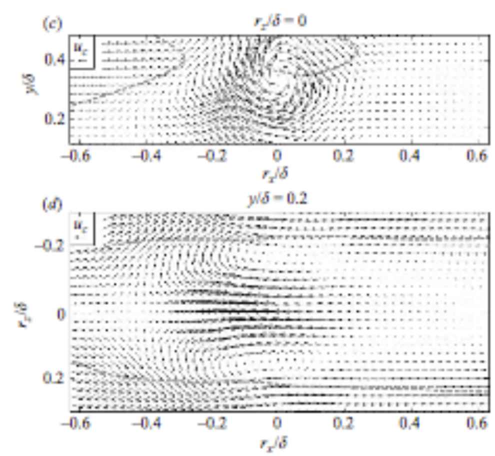

FIGURE 6. Conditional eddy (*a*, *b*) given a negative spanwise swirling event at $y/\delta = 0.35$ visualized using the Q vortex detection criterion (green) and low velocity region (blue, $\hat{u}' < u_c'$) with corresponding velocity vector plot in the x, y plane at $r_z = 0$ and x, z cross-sections at $y/\delta = 0.2$ (*c*, *d*). The velocity vectors are relative to the eddy convective velocity u_c', at $y/\delta = 0.35$ indicated in the upper left corner of each plot. The dashed lines indicate $\hat{u}' = 0$.

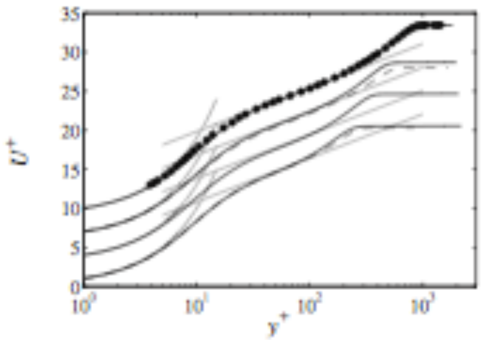

FIG. 2. Mean velocity profile U^+ in viscous units for (—) present DNS at Re_θ=671, 1000, 1412, 2512, (●) present measurements at Re_θ=2541. (- - -) DNS by Spalart (Ref. 4) at Re_θ=670, 1410. The profiles are shifted by U^+=3 for increasing Re_θ. The linear and logarithmic regions are indicated by a thin line, using $1/\kappa \log y^+ + B$ with κ=0.41 and B=5.2.

Re_θ ~ 2500

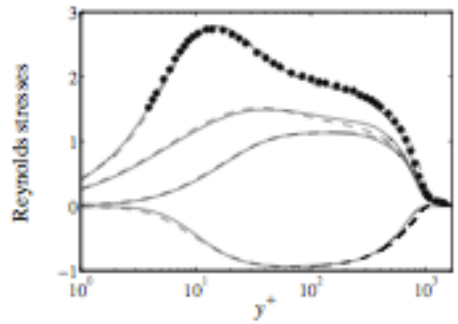

FIG. 3. Turbulent fluctuations u^+_{rms}, w^+_{rms}, v^+_{rms}, and shear stress $\langle u'v' \rangle^+$ (from top). (—) Present DNS at Re_θ=2512, (●) experiments at Re_θ=2541. (- - -) Correlations based on the attached-eddy hypothesis (Refs. 14–16).

Schlatter, Örlü, Li, Brethouwer, Fransson, Johansson, Alfredsson, & Henningson (2009) Phys. Fl. 21

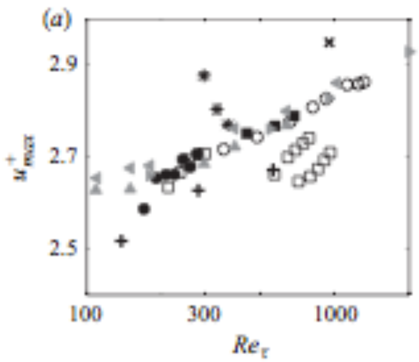

FIGURE 4. Near-wall behaviour of inner-scaled streamwise velocity fluctuation. (*a*) Value and (*b*) wall-normal position of maximum. Corresponding channel-flow DNS values are depicted in filled grey symbols (see figure 3*b* for references).

as function of the friction Reynolds number. Best fit to data by Komminaho & Skote (2002), Simens *et al.* (2009), Schlatter *et al.* (2009*a*): $\tau^+_{w,rms} = 0.298 + 0.018 \ln Re_\tau$. Channel-flow DNS data (filled grey symbols): (◄) (Kawamura *et al.* 1999; Abe *et al.* 2004; Tsukahara *et al.* 2005), (▲) (Iwamoto *et al.* 2002) and (►) (del Álamo & Jiménez 2003; del Álamo *et al.* 2004; Hoyas & Jiménez 2006).

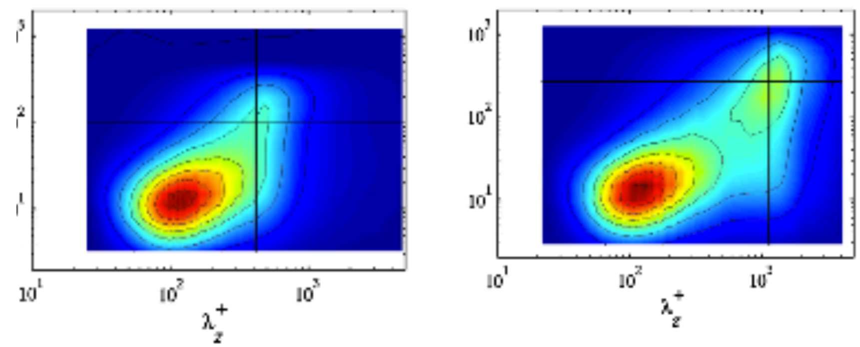

Re_θ = 1400 & 4300

Schlatter, Li, Brethouwer, Johansson & Henningson (2009)
Int. Jour. Heat & Fluid Flow 31

Schlatter & Örlü (2010) JFM 659

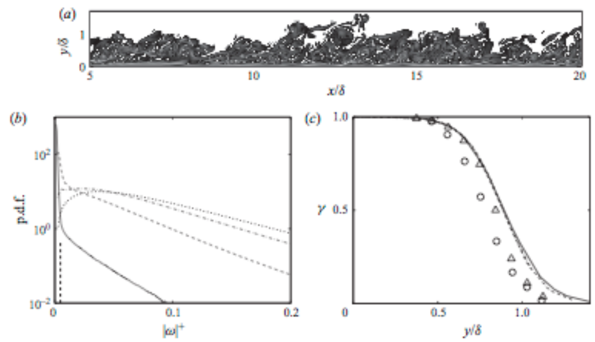

FIGURE 3. (*a*) Typical section of $|\omega'|$ in the boundary layer, showing intermittent potential flow deep into the vortical region. $Re_\theta \approx 700$–900. (*b*) Probability density functions of the vorticity magnitude in section BLS2, showing the development away from the wall of the irrotational delta at $|\omega| \approx 0$. ·······, $y/\delta_{99} = 0.44$; — · —, 0.59; - - - -, 0.88; ———, 1.31. The dashed vertical line is the limit used to define irrotational flow, slightly larger than a single histogram bin. (*c*) Intermittency factor. ———, BLS1 in the present simulation; - - - -, BLS2; — · —, BLS3; ○, from experimental velocity measurements at $Re_\theta = 3000$ (Kovasznay, Kibens & Blackwelder 1970); △, from temperature measurements at $Re_\theta = 1100$–4800 (Murlis, Tsai & Bradshaw 1982).

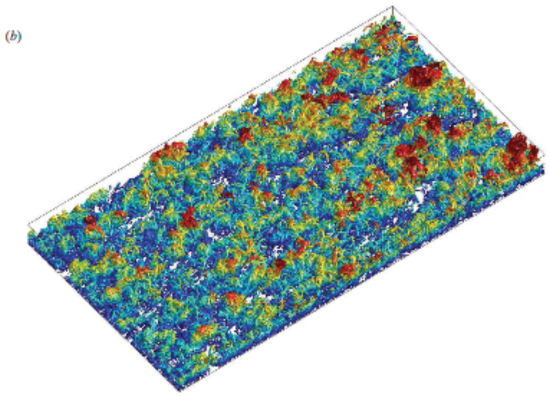

FIGURE 11. Isosurface of the discriminant of the velocity gradient tensor of the present simulation. (*a*) Top view. (*b*) Perspective view. In both cases the flow is from left to right, and the wall-parallel dimensions of the box are approximately 18×9 times the boundary-layer thickness at the centre of the box, spanning $Re_\theta \approx 1420$–1900. The isosurface is coloured by the distance to the wall, from $y/\delta \approx 0.3$–0.4 for the deepest blue, to $y \approx \delta$ for the brightest red.

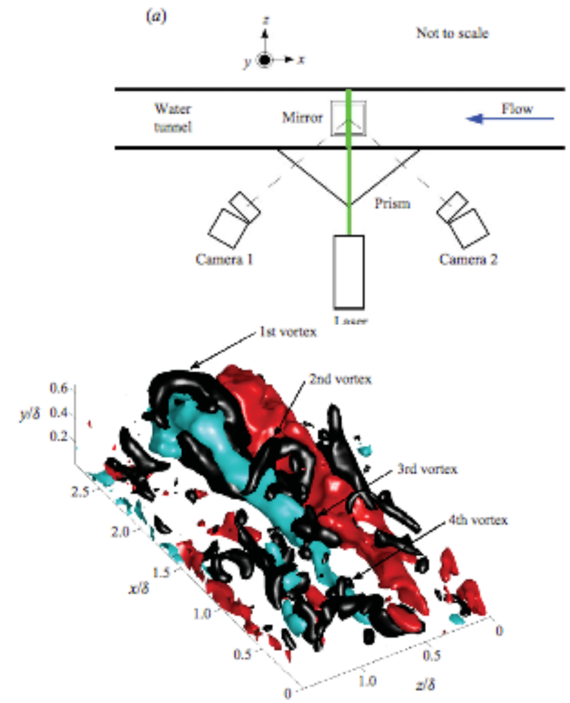

FIGURE 6. (Colour online) Visualisation of vortices with high- and low-speed structures. Black iso-surface: $|\lambda_{ci}|_{iso} = 0.18|\lambda_{ci}|_{max}$. Blue iso-surface: $u_{iso} = -0.1\overline{U}$. Red iso-surface: $u_{iso} = 0.1\overline{U}$.

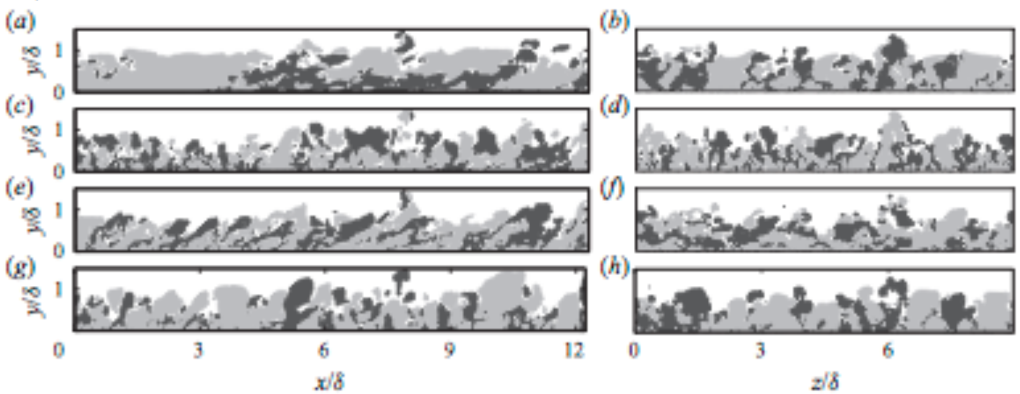

FIGURE 9. Instantaneous sections of the fluctuations in the boundary layer: u (*a*, *b*), v (*c*, *d*), w (*e*, *f*), p (*g*, *h*). (*a*, *c*, *e*, *g*) The x–y sections, in $Re_\theta = 1670$–2000, and (*b*, *d*, *f*, *h*) the z–y sections at $Re_\theta = 1670$. All the fluctuations are normalized with the x-dependent friction velocity, and the coordinates are normalized with δ_{99} at $Re_\theta = 1670$. In all the sections the dark areas are below -0.5 wall units, and the lighter ones above $+0.5$.

Dennis & Nickels (2011) JFM 673

Stereo PIV

Re_θ ~ 4700

Jimenez, Hoyas, Simens and Mizuno (2010) JFM 657

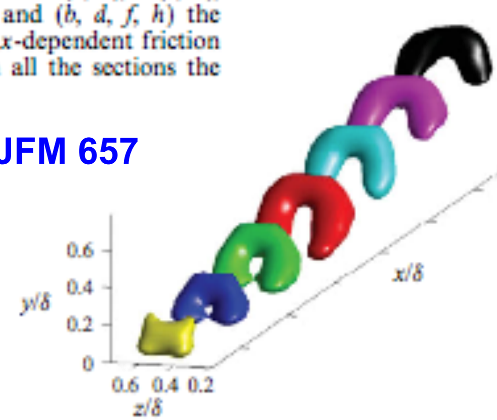

FIGURE 16. (Colour online) Conditionally averaged swirling

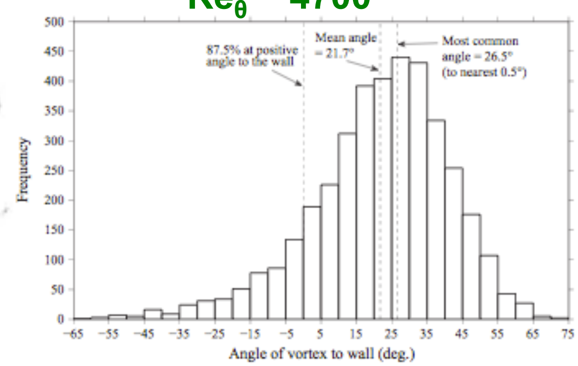

RE 23. Histogram showing the number of vortices binned according to their angle to the wall. Sample size of 3821.

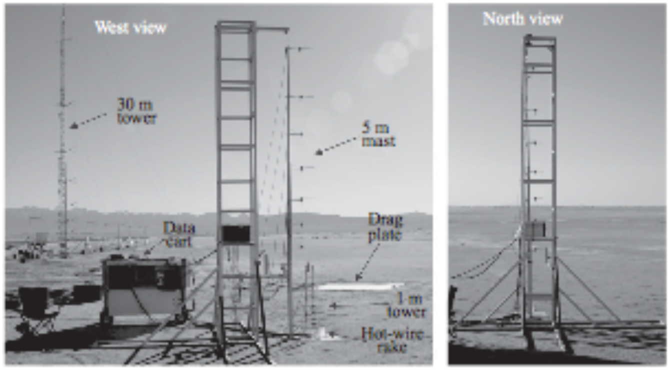

FIGURE 1. Experimental set-up, showing the hot-wire array in the foreground with the 30 m tower and sonic anemometers in the background.

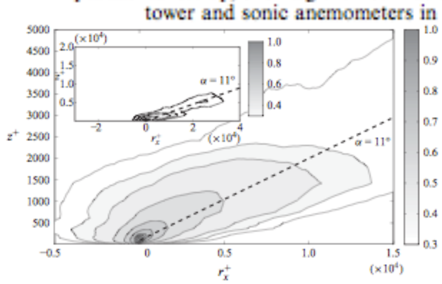

FIGURE 7. Isocontours of the two-point correlation function $\rho_{uu}(r_x^+, z^+, z^+_{ref})$ at $z^+_{ref} = 120$. The same contours are plotted in the inset to compare with ρ_{uu} at $z^+_{ref} = 4032$ plotted in figure 8.

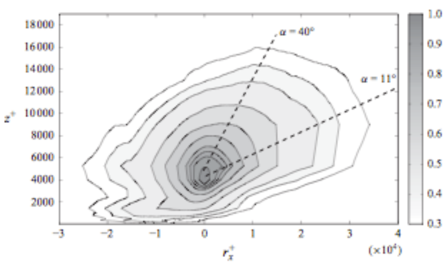

FIGURE 8. Isocontours of the two-point correlation function $\rho_{uu}(r_x^+, z^+, z^+_{ref})$ at $z^+_{ref} = 4032$.

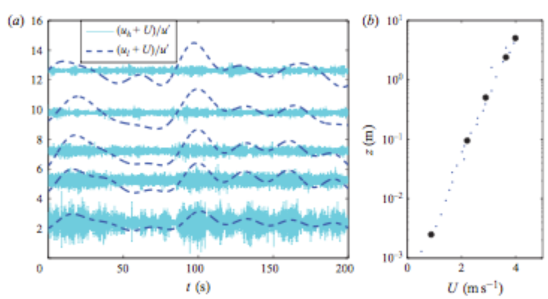

FIGURE 14. (Colour online) (*a*) Wall-normal variation of the low- (f_{c1}) and high- (f_{c1}) pass fluctuating velocities normalized with the r.m.s. velocity, $(u_h+U)/u'$ and $(u_l+U)/u'$ respectively, at $z^+ = 20, 762, 4033, 19\,296$ and $40\,547$. (*b*) Actual wall-normal locations and local mean velocities for the selected wires (•) and other hot-wire probes (·).

Guala, Metzger & McKeon (2011) JFM 666

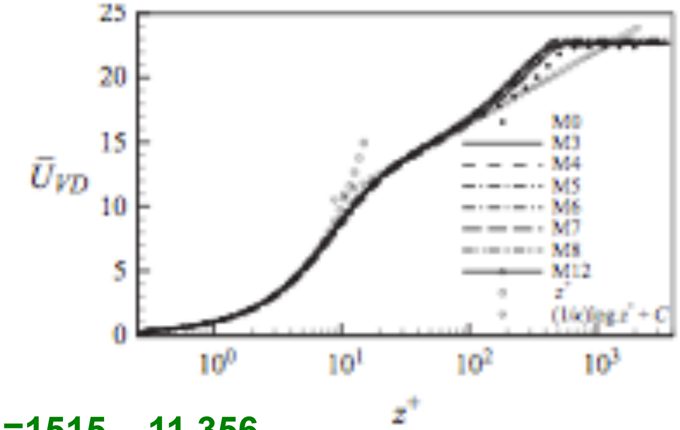

Re_θ =1515 – 11,356
Mach = 0. 3 – 11.9

Duan, Beekman & Martin (2011) JFM 672

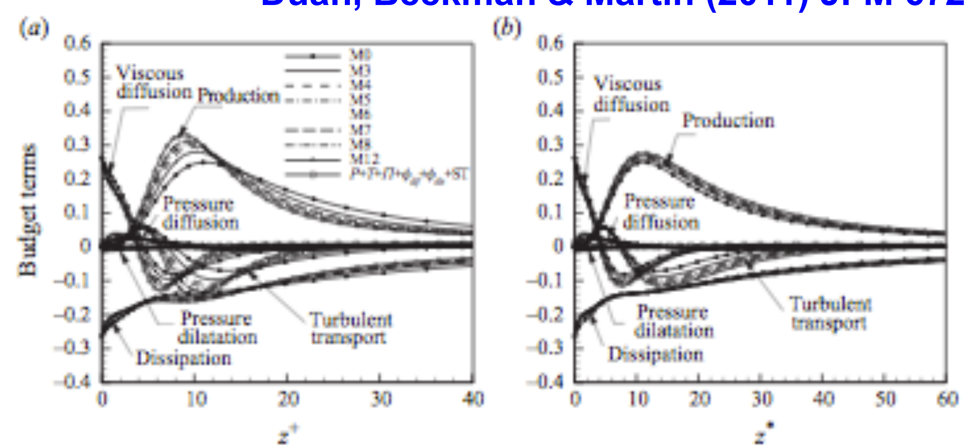

FIGURE 13. TKE budget for cases with different free-stream Mach numbers, non-dimensionalized with (*a*) wall units and (*b*) semi-local units, respectively. Variables in wall units are normalized by $\bar{\rho}_w u_\tau^3/z_\tau$ and $z^+ = z/z_\tau$, and variables in semi-local units are normalized by $\bar{\rho} u_\tau^{*3}/z_\tau^*$ and $z^* = z/z_\tau^*$.

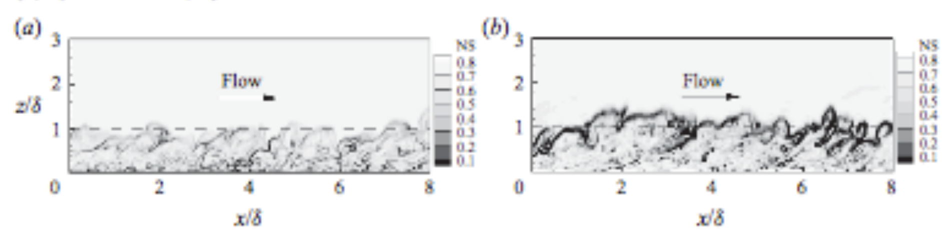

FIGURE 21. (*a*, *b*) Numerical Schlieren visualization in a (x, z) plane for Mach 3 and Mach 12.

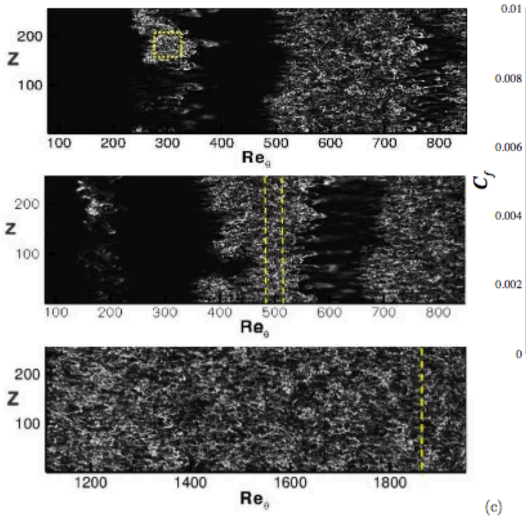

FIG. 2: Examples of (a) an individual turbulent spot at $Re_\theta \approx 300$, (b) merged turbulent sp
at $Re_\theta \approx 500$ and (c) developed turbulence at $Re_\theta = 1840$ in the boundary layer near the v
marked by isosurfaces of enstrophy. The yellow dashed lines demarcate the parts of the flow fr
which data was used to calculate the statistics.

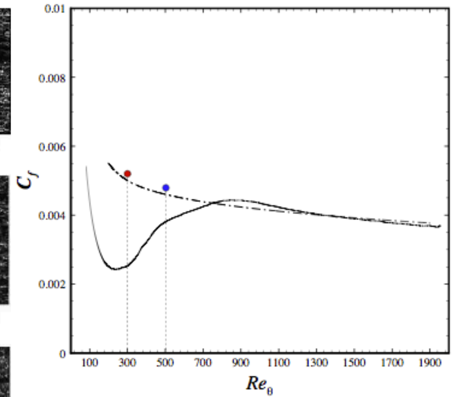

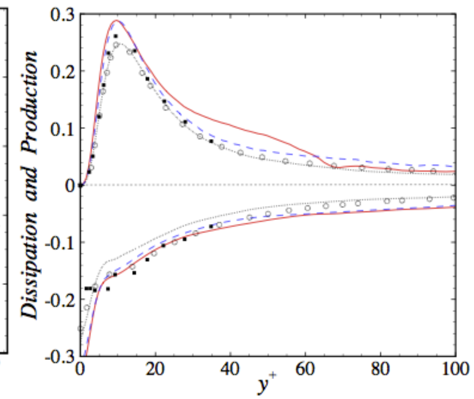

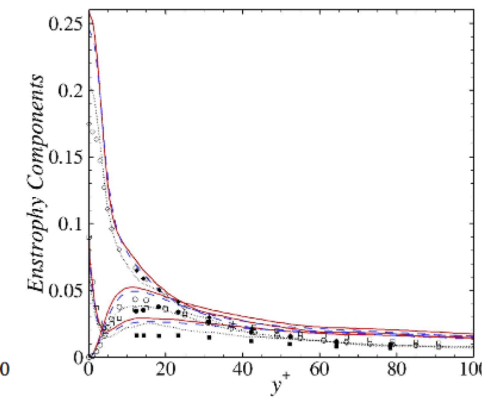

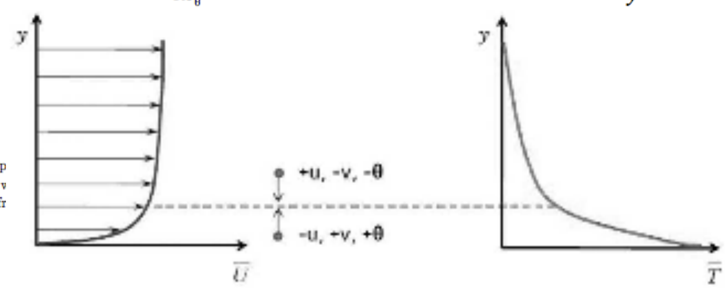

Octant	1	2	3	4	5	6	7	8
u	+	-	-	+	+	-	-	+
v	+	+	+	+	-	-	-	-
θ	+	+	-	-	+	+	-	-

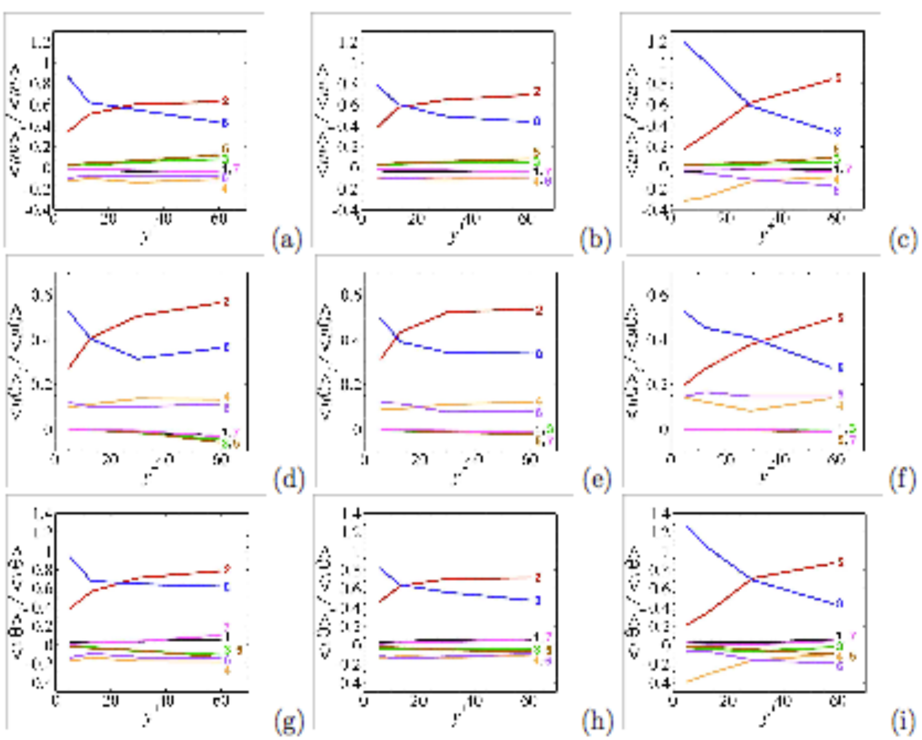

Park, Wallace, Wu & Moin (2011) TBP

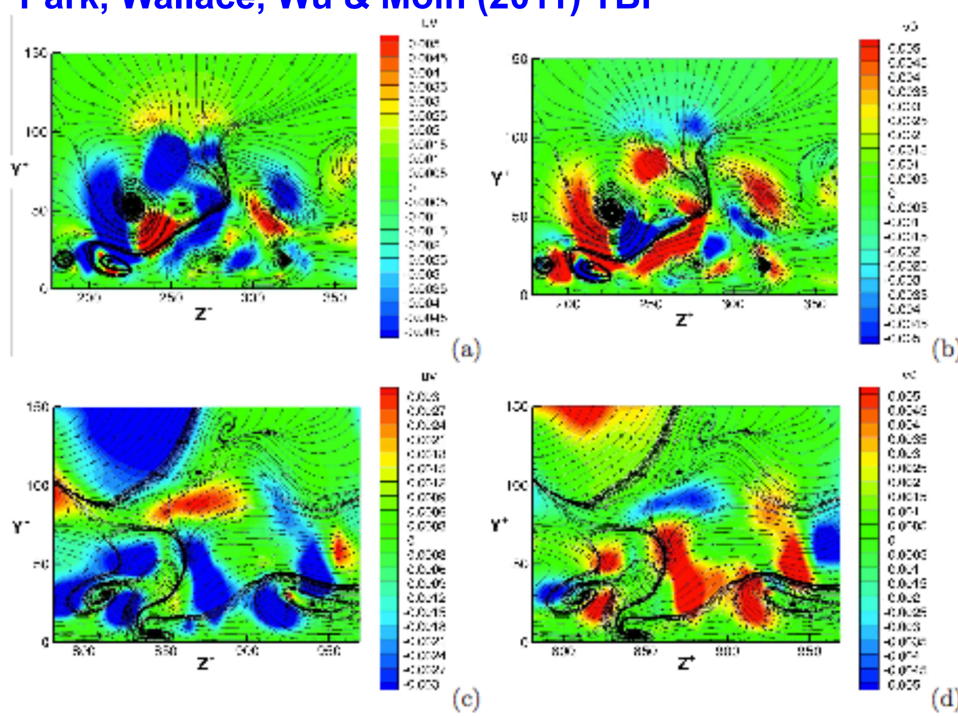

Summary

- There has been remarkable progress in turbulent boundary layer research in the past 50 years, particularly in understanding the structural organization of the flow. Consensus exists that vortices drive momentum transport but not about the exact form of the vortices or how they are created and sustained.

- This progress has been fueled by developments in experimental instrumentation (multi-sensor hot-wire anemometry and PIV) but most of all with the advent of DNS in the 1980s and its subsequent advances.

- Further progress has been made by the development of high Reynolds number laboratory facilities and the use of field sites to study the very high Reynolds number atmospheric surface layer under near neutral stability conditions.

- Challenges for the future:
  - Incorporating the knowledge of the structure of turbulent boundary layers into models, including RANS and subgrid scale LES models.

  - Further extending the knowledge gained for zero pressure gradient, smooth wall boundary layers to the complexities of accelerating and decelerating boundary layers and flows with rough walls.

  - Continuing to develop and implement methods to control turbulent boundary layers that occur in real engineering applications.

Highlights of Fifty Years of Turbulent Boundary Layer Research

Pre – 1961

SLIDE 1
Title

SLIDE 2
Summary of periods and highlights by decades

SLIDE 3
Early hot-wire measurements. Some done in Delft by Burgers and co-workers even earlier in the 20s.

SLIDE 4
Similarity laws for "overlap" and "wake" regions.

Millikan: "Law of the wall"

Coles: "Law of the wake"

SLIDE 5
Townsend: RMS distributions of velocity fluctuations and estimate of the TKE balance from hot-wire measurements.

Corrsin & Kistler: "Superlayer" properties and intermittency function in TBL

Klebanoff: TKE production and dissipation rate estimates. All the determinations of the dissipation rate from this period were crudely estimated as the residue of the other terms.

SLIDE 6
Favre et al: Space-time isocorrelation contours with optimum time delay. Probes were separated in both the streamwise and wall normal directions. Fixed probe at about $y+ = 40$. Note high aspect ratio of correlation in x-y plane compared to y-z plane. Note also that a small correlation remains all the way out to $y = 0.3\delta$.

Grant: Spatial correlation tensor components at several locations of the fixed probe in the boundary layer. He inferred structure from these correlations.

SLIDE 7
Willmarth & Wooldridge: Wall pressure space-time correlation function with two probes of varying separation in the streamwise direction. One horizontal axis is time and the other is downstream distance. The vertical axis is the correlation level. The ridge flowing out to the lower right of the figure shows the cumulative effect of

eddies of different scale on the wall pressure with increasing time and distance. The decay in correlation is interpreted as the increasing loss of the effect of smaller eddies.

Bakewell & Lumley: Streamlines in the cross-stream plane of a pipe flow of glycerin as revealed by proper orthogonal decomposition of hot-film data and their suggested eddy structure.

SLIDE 8
Visual experiments that excited the research community about organized coherent motions in wall bounded flows.

Kline et al.: Low-speed streaks revealed by hydrogen bubbles and their "bursting".

Corino & Brodkey: "Ejection" and "sweep" coherent events revealed by particle motion near the wall in a pipe flow viewed in a moving frame of reference.

1970 – 1986: Conditional Processing of Measurements & Further Visualization

SLIDE 9
Kovasznay et al.: Intermittency function, point averages of "fronts" and "backs" of potential flow bulges and a sketch of them.

SLIDE 10
Wallace et al.: Quadrant analysis of the Reynolds shear stress in a channel flow. Plot of covariance integrand, uv dudv, by quadrant and as function of distance from wall.

Willmarth and Lu: Quadrant analysis for boundary layer with "hole" of constant Re Stress to accentuate large amplitude events.

SLIDE 11
Several hundred small holes covered with a mirrored silicone rubber foil. Using interferometry and a high speed movie camera, the instantaneous fringes on each element were used to determine local wall pressure after calibration.

Figure shows pressure pulses being convected downstream over one row of transducers. Patterns persist for more than 1100 viscous length scales (1½ the boundary layer thickness). Convection velocities are about ¾ of the freestream velocity.

SLIDE 12
Blackwelder and Kaplan: Intention was to detect turbulent "bursts" using Variable Integral Time Averages (VITA) of conditionally sampled data. Condition was that the local square of the streamwise velocity fluctuation minus the square of the local mean be larger than some chosen threshold. This detected events with large du/dt.

The double peaks in the conditional averaged Re stress are roughly related to the Q2 and Q4 quadrants. Simultaneous rake measurements show that these events have great coherence in the wall normal direction.

Chen & Blackwelder: Passively heated wall and a rake of X-array hot-wires. Highly coherent ramps in the temperature fluctuations were observed. Conditioning on these ramps, conditional velocity fluctuation averages were obtained that show the outward motion of warmer, lower momentum fluid downstream of the front followed by inward motion of cooler, higher momentum flow upstream.

Antonia et al.: Similar study using heat as a passive scalar marker. Fig. shows conditional averages of u, v and theta and the momentum and heat fluxes in the inner layer of the TBL.

SLIDE 13
Head & Bandyopadhyay: Smoke visualization of boundary layer structure viewed in inclined planes and interpreted as hairpin vortices.

Balint et al.: A similar study with wall layer and potential flow separately marked by smoke and the tripping of the boundary layer varied. Photo shows the evolution and growth of wall layer structures which eventually penetrate the potential flow. The potential flow is also ingested deeply into the turbulent boundary layer.

Townsend: Proposed the attached eddy model

Perry et al.: Used this conceptual model of attached hairpin eddies, rolling up and lifting up out of near wall sheets of vorticity, to construct a theoretical model that attempts to explain many of the statistical features of the boundary layer, including the log layer.

1986 – 2011: DNS, Multi-Sensor Hot-Wire Probes & PIV Measurement

SLIDE 14
Kim & Moin: Vorticity (vortex lines) showing hairpin and Ω-like shapes in a turbulent channel flow DNS. Cross-stream plane cut through the leg of the vorticity line bundle in the upper right figure shows that this is truly a vortex as revealed by the velocity vector projections on this plane.

SLIDE 15
Kim Moin & Moser: Their DNS was accepted by experimental researchers in part because of the flow visualization they did of simulated hydrogen bubbles that revealed the same structure as in physical experiments.

In this paper, they showed the first DNS distribution of the rms vorticity components and other statistics of the vorticity field.

Balint et al.: We published our rms vorticity component distributions and other vorticity field statistics, experimentally measured with our minature 9-sensor probe, that year in the Proceedings of the 1st European Turbulence Conference.

SLIDE 16
Spalart: A year later, in 1988, he published the first DNS of a turbulent boundary layer where he employed the so-called "fringe" method to rescale the flow allowing him to employ periodic boundary conditions in the streamwise direction. The figures are of the TKE budget and contours of vorticity projected onto streamwise and cross-stream inclined planes of the flow.

Balint et al.: Experimental values of the turbulent production and dissipation rates are compared to Spalart's DNS values and the Kim, Moin and Moser DNS channel flow values in the figure on the right.

SLIDE 1
Balint et al.: Vorticity fluctuation component spectra compared to Spalart's DNS.

Distribution of the terms of the transport of total enstrophy equation.

SLIDE 18
Aubry et al.: Expansion of the wall region using POD to obtain low-dimensional sets of ODEs. Streamwise rolls are revealed that have intermittent Reynolds stress "burst" characteristics. This was one of the first applications of low-dimensional chaotic dynamical systems theory to realistic turbulent open flows.

Antonia et al.: A rake made up of an array of 8 X-array hot-wires was used to construct sectional streamlines and contours of the large-scale vorticity in streamwise planes at several Reynolds numbers. Large-scale vortices (foci) and saddle points of high strainrate are evident in this frame of reference traveling to the left at 0.8 of the freestream velocity. Variation with Reynolds number is seen in the figure in the lower right.

SLIDE 19
Bernard et al.: Lagrangian analysis of the Reynolds shear stress that decomposes it exactly into (1) the correlation of u at the terminal point, a, with v at the set of initial points, b, (2) a "displacement transport" term and (3) an "acceleration transport" term. For large enough mixing times, this u_a v_b_bar correlation goes to zero, as seen in the distribution on the right. The displacement transport term is simply a sort of mixing length/ mean gradient type effect. The acceleration transport term produces a significant fraction of the Reynolds stress, having a positive or negative contribution depending on position relative to the wall.

The upper right figure shows the pdfs of the particle displacements sorted by the quadrants of quadrant analysis as a function of y+.

Their group also identified quasi-streamwise vortices with a recognition algorithm and studied particle displacements and Reynolds stress creation in relation to these vortices as seen in the middle lower figure.

SLIDE 20
Spina et al: Studied the structure of supersonic turbulent boundary layers adopting methods used in subsonic, low Reynolds number flows such as the VITA technique and quadrant analysis.

SLIDE 21
Robinson: Analyzed the Spalart DNS to study the structure of the flow. Low pressure was used as a criterion to detect vortices. Few complete hairpins were observed, but this could have been a result of the threshold values set. The relation of low-speed streaks and Q2 and Q4 Reynolds stress to the vortices is clearly seen. Robinson believed that hairpin-shaped vorticity lines are simply a result of their distortion by quasi-streamwise vortices, and that they do not necessarily, themselves, indicate the presence of true hairpins.

SLIDE 22
Tsinober et al.: Use of a 12-sensor hot-wire probe to demonstrate, experimentally, the most probable alignment of the vorticity vector with the intermediate eigenvector of the rate of strain tensor. This had previously been seen in DNS of both isotropic and shear flow turbulence and is now known to be a general characteristic of all turbulent flows.

Durbin: Tensorially consistent 2^{nd} order closure modelling of the Reynolds stress transport equation. Applied to channel and boundary layer turbulent flows with and without pressure gradients and to flows around 90 deg. bends. Figures show model values of turbulence intensities and friction coefficient distributions compared to experimental values.

SLIDE 23
Choi et al.: Active control for drag reduction using (1) v control at the surface with suction and blowing based on detection in the flow of sweep and ejection events, (2) w control at the surface, (3) combinations of the two types of control, etc. The figures show the effects of control compared to no control on TKE production and dissipation rates and on the vorticity component rms distributions.

SLIDE 24
Saddoughi & Veeravalli: Performed a highly regarded experiment in the NASA AMES huge wind tunnel with its 80’ x 120’ test section to examine indicators of local isotropy in turbulent boundary layers. They documented the effects of Reynolds number and proximity to the wall. The figures here show examples of (1) compensated streamwise and cross-stream spectra rather far from the wall and at a

rather high Reynolds numbr (Re_λ = 1450) and (2) compensated second-order structure functions for streamwise and cross-stream velocity fluctuations. Both plots provide evidence of local isotropy under these conditions.

Wallace & Ong: We were kindly allowed to piggyback on their experiment to use our 12-sensor probe to examine local isotropy of the vorticity field. The figure shows evidence of it in the inertial subrange as seen in the ratio of the two cross-stream vorticity components computed from the streamwise component under isotropic assumptions to their measured values. This ratio should be unity for isotropic flow, and it is in the inertial subrange. Experimental error takes over in the dissipation range of this figure.

Mestayer had carried out an earlier and similar study in the high Reynolds number IMST Air-Sea Interation Simulation tunnel at Re_λ = 616 in the dissipative range but not in the inertial subrange.

Slide 25
Nagano & Tagawa: Trajectory analysis based on uv plane quadrants illustrated in upper left. In lower right the number of types of types of trajectories are shown as a function of the Willmarth & Lu "hole" size. The figure on the right shows auto regressive (AR) model predictions of time series of temperature for various trajectory patterns.

SLIDE 26
Klewicki et al.: Developed field site southwest of Salt Lake City, Utah, on the Salt Flats, where measurements in the atmospheric surface layer could be carried out. At sundown, neutral stability occurs giving conditions similar to those in a laboratory boundary layer but at the very high Reynolds numbers, Re_θ , of $O(10^6)$. The figures show: (1) the histogram of spanwise low-speed stream spacing obtained from flow visualization, (2) distribution of the rms streamwise velocity distribution showing how the peak increases with Reynolds number, (3)) the joint pdf of the u and v fluctuations at low and high Reynolds numbers and (4) the space-time auto-correlation of u at low and high Reynolds number.

Folz & Wallace: They have invited many research groups to work there over the years. We were there the first year, and, among other things, measured the contributions of all the terms to the dissipation rate.

SLIDE 27
Jeong et al.: Used method of detecting vortices with $-\lambda_2$, the second invariant of the velocity gradient tensor which indicates dominance of rotation over strain. Found quasi-streamwise vortices that are not in the form of hairpins. Vortices, of opposite sign, slightly inclined to the wall and skewed in the x-z plane, exist in staggered overlapping arrays. They state that a phase difference in space accounts for nearly

all of the Q2 and Q4 Reynolds stress as well as counter-gradient Q1 and Q3 Reynolds stress.

Schoopa & Hussain: Carried out a transient growth stability analysis to show how the vortices emerge out of instabilities of low-speed streaks under certain conditions.

SLIDE 28
Honkan & Andreopolous: Used a 12-sensor probe to obtain the angular orientation of the projection of the vorticity vector near the wall in wall normal and wall parallel planes of the flow.

Ong & Wallace: Obtained these orientations for the vorticity filaments that most contribute to the vorticity covariances from weighted vorticity component joint pdfs (covariance integrand plots).

SLIDE 29
Barenblatt et al.: Proposed a Reynolds number dependent power law alternative to the log law to describe the mean velocty in the overlap region. The figure shows many different data sets plotted as evidence to support this theory. The debate about the veracity of this partial similarity law compared to the complete similarity log law still continues.

SLIDE 30
Guarini et al.: Carried out a supersonic Mach 2.5 DNS that showed very little difference from subsonic turbulent boundary layer statistics. The figures show the distributions of the rms vorticity components and the TKE budget.

Kholmyanshy et al.: Carried out a study using a 20-sensor probe to measure both velocity and velocity gradient as well as temperature fluctuations. The measured many different properties of these fields including the joint pdf of the enstrophy production vs. production of strain shown in the figure.

SLIDE 31
Adrian et al.: Used planar PIV in numerous studies to reveal many features of the structure of turbulent boundary layers. Fig. in upper center compares rms spanwise vorticity to DNS and hot-wire values. The figures in the center and on the right show large scale zones of coherent momentum, high shear in ramps inclined to the wall and vortices that are interpreted as “heads” of hairpins. Their hairpin model, like those of others, accounts for Q2 and Q4 Reynolds stress. They also describe the hairpins as occuring in “packets” and account for the creation of new hairpins.

SLIDE 32
Chacin & Cantwell: Used critical point theory, primarily developed by Perry and Chong, to analyse the Spalart turbulent boundary layer DNS. The top middle figure shows regions of postitive discriminant in association with Reynolds stress events.

The top right figure shows the characteristic "tear drop" shape of the Q-R plane joint pdf with superimposed regions of Q2 and Q4 Reynolds stress. The regions in this plane with respect to the Villefosse line of zero discriminant are described by the flow categories in the figure to the lower left.

Andreopolous & Honkan: Obtained this teardrop shape jpdf from 12-sensor hot-wire measurements in the buffer layer of their experimental turbulent boundary layer. It is now believed to be a universal feature of turbulence.

SLIDE 33
Carlier & Stanislas: Used planar PIV to investigate structure in various planes, including planes tilted upstream and downstream across the flow, to study the eddy structure in the boundary layer at R_θ = 7,500. They used a pattern recognition technique that involved convolving a model vortex with the 2D flow field to educt the actual vortices. Instantaneous and average vortices are shown in the figures in the upper right. They studied Q2 and Q4 events in spatial relationship to these vortices.

SLIDE 34
Kim & Adrian: Observed very large scale motions (VLSMs) in a turbulent pipe flow that were 12 – 14 times as long as the pipe radius.

Del Alamo et al: Also observed these VLSMs in their channel flow DNS.

Hutchins & Maurusic: Observed VLSMs as long as 20δ in the log and lower wake regions in their experiment in the Utah desert, and studied how they affect premultiplied 1D spectra of the streamwise velocity fluctuations. The rising plateau in the rms distribution further from the wall is related to the second peak in the spectrum coming from these VLSMs.

SLIDE 35
Ringuette et al.: Carried out a DNS at $Re_\theta \sim 2600$ and Mach ~ 3 in which they observed most of the same types of structures as in subsonic flow.

Pirozzoli et al.: Also carried out a supersonic DNS at Mach = 2 and Re_θ = 950 – 1350. They studied the statistical properties of quasi-streamwise vortices near the wall and of hairpins and hairpin packets further from the wall. In the outer layer they state that these statistical properties are consistent with noninteracting closed loop vortices. In their later study they conclude that sheet-like structures have a greater influence on the statistical properties of the TBL than the vortices.

SLIDE 36
Mathis et al.: Studied the modulating effect that large scale motions in the outer flow have on the fluctuations in the inner region of the flow. They did this by filtering the streamwise velocity signals and correlating them. They examine how the degree of correlation depends on wall normal distance and how it is related to the 1D spectra.

SLIDE 37
Wu & Moin: Carried out a spatially developing DNS of the TBL which goes through bypass transition to turbulence. It exhibits a forest of hairpins. When the wall is passively heated, the temperature field also exhibits hairpins.

SLIDE 38
Sheng et al.: Used digital holography to study the wall layer structure in a square duct at Re_τ = 1470 and obtained conditionally averaged hairpin structures that emerge from the spanwise vorticity sheets near the wall and are related to high wall shear stress occurances.

Elsinga et al: Found hairpin packets using tomographic PIV at Re_θ =34,000 and Mach = 2

SLIDE 39
Schlatter et al.: Carried out boundary layer DNS up to $Re_\theta \sim$ 4,300. They carefully studied statistical properties, and have also compared the consistency of various DNS studies. They don't observe hairpins in their highest Reynolds number DNS.

SLIDE 40
Jimenez et al.: Carried out a TBL DNS up to Re_θ = 2100. They don't observe hairpins, but they do observe the large scale coherent momentum events.

SLIDE 41
Guala et al.: Observations in the atmospheric surface layer quantifying interactions between the VLSMs and the turbulence from the energy containing to the dissipative scales.

Duan et al.: DNS of TBL up to hypersonic cases. Flow structure doesn't change much.

SLIDE 42
Park et al. : Showed that statistics, including those of the fine scale properties, enstrophy and dissipation rate, are very similar in transitional turbulence spots and in developed turbulence. This implies that the structure is likely to be similar. Octant analysis showed that motions consistent with mean gradient transport of momentum and heat are the dominant contributors to the fluxes for both transitional spots and developed turbulence. The transport of momentum and heat is strongly associated with vortices as shown in the cross-stream cuts through the instantaneous fields for the transition and developed cases.

SLIDE 43

Summary

Review Articles and Special Volumes on Turbulent Boundary Layers and Turbulent Wall Layers (send additions to wallace@umd.edu)

50 Jahre Grenzschichtforschung [Festshrift for Ludwig Prandtl]
Eds. H. Goetler and W. Tollmein
Vieweg & Son (1955), Braunschweig

The Structure of Turbulent Shear Flow
A. A. Townsend
Cambridge Univ. Press (1956) 1st Edition, (1970) 2nd Edition,

The Turbulent Boundary Layer
L. S. K. Kovasznay
Ann. Rev. Fl. Mech. (1971) **2**, 95 – 112

Pressure Fluctuations Beneath Turbulent Boundary Layers
W. W. Willmarth
Ann. Rev. Fl. Mech. (1975) **7**, 13 – 38

Structure of Turbulence in Boundary Layers
W. W. Willmarth
Adv. in Appl. Mech. (1976) **15**, 159 – 254.

The Vortical Structure of Bounded Turbulent Shear Flow
J. M. Wallace
Flow of Real Fluids: Lect. Notes in Physics (1985) **235**, 253 – 258, Eds. G. Meier and F. Obermeier, Springer, Berlin

Turbulence Control in Wall Flows
D. M. Bushnell & C. B. McGinley
Ann. Rev. Fl. Mech. (1989) **21**, 1 – 20

The Turbulent Boundary Layer
K. R. Sreenivasan
Frontiers in Experimental Fluid Mechanics: Lect. Notes in Engr. **46** (1989) 189 – 209, Ed. M. Gad-el-Hak

Coherent Motions in the Turbulent Boundary Layer
S. K. Robinson
Ann. Rev. Fl. Mech. (1991) **23**, 601 – 639

The Physics of Supersonic Turbulent Boundary Layers
E. F. Spina, A. J. Smits & S. K. Robinson
Ann. Rev. Fl. Mech. (1994) **26**, 287 – 319

Reynolds Number Effects in Wall-Bounded Turbulent Flows
M. Gad-el-Hak & P. R. Bandyopadhyay
Appl. Mechanics Reviews (1994) **47**, 307 – 365
ASME Reprint No. AMR148

Advances in Fluid Mechanics: Self-Sustaining Mechanisms of Wall Turbulence
Ed. R. L. Panton
Comp. Mech. Pub. (1997), Southhampton and Boston

Boundary Layer Theory (Part IV)
H. Schlichting (revised by Klaus Gersten)
Springer Verlag (2000), Berlin, 8^{th} Edition

Turbulent Flows over Rough Walls
Javier Jiménez
Ann. Rev. Fl. Mech. (2004) **36**, 173 – 196

Wall-bounded turbulent flows at high Reynolds numbers: Recent advances and key issues
I. Marusic, B. J. McKeon, P. A. Monkewitz, H. M. Nagib, A. J. Smits, and K. R. Sreenivasan
Phys. Fluids 22, 065103 (2010)

High-Reynolds Number Wall Turbulence
A. J. Smits, B. J. McKeon & I. Marusic
Ann. Rev. Fl. Mech. (2011) **43**, 353 – 375

Selected Articles on Two-Dimensional, Zero-Pressure Gradient, Smooth Flat Plate Turbulent Boundary Layers and on Turbulent Wall Layers

Journal of Fluid Mechanics (1956 – Present)

Coles, D.
The law of the wake in the turbulent boundary layer,
1 (Issue 2) , 1956, 191 - 226

Favre, A.J., Gaviglio, J.J. & Dumas, R.
Space-time double correlations and spectra in a turbulent boundary layer,
2 (Issue 4) , 1957, 313 - 342

Favre, A.J., Gaviglio, J.J. & Dumas, R.
Further space-time correlations of velocity in a turbulent boundary layer,
3 (Issue 4) , 1958, 344 - 356

Grant, H.L.
The large eddies of turbulent motion,
4 (Issue 2) , 1958, 149 - 190

Townsend, A.A.
Equilibrium layers and wall turbulence,
11 (Issue 1) , 1961, 97 - 120

Willmarth, W.W. & Wooldridge, C.E.
Measurements of the fluctuating pressure at the wall beneath a thick turbulent boundary layer,
14 (Issue 2) , 1962, 187 - 210

Willmarth, W.W. & Roos, F.W.
Resolution and structure of the wall pressure field beneath a turbulent boundary layer,
22 (Issue 1) , 1965, 81 - 94

Townsend, A.A.
Self-preserving flow inside a turbulent boundary layer,
22 (Issue 4) , 1965, 773 - 797

Fiedler, H. & Head, M.R.
Intermittency measurements in the turbulent boundary layer,
25 (Issue 4) , 1966, 719 – 735

Mitchell, J.E. & Hanratty, T.J.
A study of turbulence at a wall using an electrochemical wall shear-stress meter,
26 (Issue 1) , 1966, 199 - 221

Tritton, D.J.
Some new correlation measurements in a turbulent boundary layer,
28 (Issue 3) , 1967, 439 - 462

Bull, M.K. Wall-pressure fluctuations associated with subsonic turbulent boundary layer flow,
28 (Issue 4) , 1967, 719 - 754

Schubert, G. & Corcos, G.M.
The dynamics of turbulence near a wall according to a linear model,
29 (Issue 1) , 1967, 113 - 135

Bradshaw, P.
`Inactive' motion and pressure fluctuations in turbulent boundary layers,
30 (Issue 2) , 1967, 241 - 258

Kline, S.J., Reynolds, W.C., Schraub, F.A. & Runstadler, P.W.
The structure of turbulent boundary layers,
30 (Issue 4) , 1967, 741 - 773

Kline, S.J., Moffatt, H.K. & Morkovin, M.V.
Report on the AFOSR-IFP-Stanford conference on computation of turbulent boundary layers,
36 (Issue 3) , 1969, 481 - 484

Corino, E.R. & Brodkey, R.S.
A visual investigation of the wall region in turbulent flow,
37 (Issue 1) , 1969, 1 - 30

Townsend, A.A.
Entrainment and the structure of turbulent flow,
41 (Issue 1) , 1970, 13 - 46

Kovasznay, L.S.G., Kibens, V. & Blackwelder, R.F.
Large-scale motion in the intermittent region of a turbulent boundary layer,
41 (Issue 2) , 1970, 283 - 325

Sirkar, K.K. & Hanratty, T.J.
The limiting behaviour of the turbulent transverse velocity component close to a wall,
44 (Issue 3) , 1970, 605 - 614

Blake, W.K.
Turbulent boundary-layer wall-pressure fluctuations on smooth and rough walls,
44 (Issue 4) , 1970, 637 - 660

Wills, J.A.B.
Measurements of the wave-number/phase velocity spectrum of wall pressure beneath a turbulent boundary layer,
45 (Issue 1) , 1971, 65 - 90

Kim, H.T., Kline, S.J. & Reynolds, W.C.
The production of turbulence near a smooth wall in a turbulent boundary layer,
50 (Issue 1) , 1971, 133 - 160

Grass, A.J.
Structural features of turbulent flow over smooth and rough boundaries,
50 (Issue 2) , 1971, 233 - 255

Owen, F.K. & Horstman, C.C.
On the structure of hypersonic turbulent boundary layers,
53 (Issue 4) , 1972, 611 - 636

Wallace, J.M., Eckelmann, H. & Brodkey, R.S.
The wall region in turbulent shear flow,
54 (Issue 1) , 1972, 39 - 48

Willmarth, W.W. & Lu, S.S.
Structure of the Reynolds stress near the wall,
55 (Issue 1) , 1972, 65 - 92

Antonia, R.A.
Conditionally sampled measurements near the outer edge of a turbulent boundary layer,
56 (Issue 1) , 1972, 1 - 18

Antonia, R.A. & Atkinson, J.D.
High-order moments of Reynolds shear stress fluctuations in a turbulent boundary layer,
58 (Issue 3) , 1973, 581 - 593

Lu, S.S. & Willmarth, W.W.
Measurements of the structure of the Reynolds stress in a turbulent boundary layer,
60 (Issue 3) , 1973, 481 - 511

Offen, G.R. & Kline, S.J.
Combined dye-streak and hydrogen-bubble visual observations of a turbulent boundary layer,
62 (Issue 2) , 1974, 223 - 239

Brodkey, R.S., Wallace, J.M. and Eckelmann, H.
Some Properties of Truncated Turbulence Signals in Bounded Shear Flows,
63 (Issue 2) , 1974, 209 - 224

Eckelmann, H.
The structure of the viscous sublayer and the adjacent wall region in a turbulent channel flow,
65 (Issue 3) , 1974, 439 - 459

Lee, M.K., Eckelman, L.D. & Hanratty, T.J.
Identification of turbulent wall eddies through the phase relation of the components of the fluctuating velocity gradient,
66 (Issue 1) , 1974, 17 - 33

Ueda, H. & Hinze, J.O.
Fine-structure turbulence in the wall region of a turbulent boundary layer,
67 (Issue 1) , 1975, 125 - 143

Offen, G.R. & Kline, S.J.
A proposed model of the bursting process in turbulent boundary layers,
70 (Issue 2) , 1975, 209 - 228

Bark, F.H.
On the wave structure of the wall region of a turbulent boundary layer,
70 (Issue 2) , 1975, 229 - 250

Blackwelder, R.F. & Kaplan, R.E.
On the wall structure of the turbulent boundary layer,
76 (Issue 1) , 1976, 89 - 112

Fulachier, L. & Dumas, R.
Spectral analogy between temperature and velocity fluctuations in a turbulent boundary layer,
77 (Issue 2) , 1976, 257 – 277

Wallace, J.M., Brodkey, R.S. & Eckelmann, H.
Pattern Recognized Structures in Bounded Shear Flows,
83 (Issue 1) , 1977, 673 - 693

Chen, C.-H.P. & Blackwelder, R.F.
Large-scale motion in a turbulent boundary layer: a study using temperature contamination,
89 (Issue 1) , 1978, 1 - 31

Kreplin, H.-P. & Eckelmann, H.
Propagation of perturbations in the viscous sublayer and adjacent wall region,
95 (Issue 2) , 1979, 305 - 322

Hatziavramidis, D.T. & Hanratty, T.J.
The representation of the viscous wall region by a regular eddy pattern,
95 (Issue 4) , 1979, 655 - 679

Head, M.R. & Bandyopadhyay, P.
New aspects of turbulent boundary layer structure ,
107 (Issue 4) , 1981, 297 - 337

Raupach, M.R.
Conditional statistics of Reynolds stress in rough-wall and smooth-wall turbulent boundary layers,
108 , 1981, 363 - 382

Pullin, D.I.
The nonlinear behaviour of a constant vorticity layer at a wall,
108 , 1981, 401 - 421

Perry, A.E. & Chong, M.S.
On the mechanism of wall turbulence,
119 , 1982, 173 - 217

Antonia, R.A., Rajagopalan, S., Subramanian, C.S. & Chambers, A.J.
Reynolds-number dependence of the structure of a turbulent boundary layer,
121 , 1982, 123 - 140

Murlis, J., Tsai, H.M. & Bradshaw, P.
The structure of turbulent boundary layers at low Reynolds numbers,
122 , 1982, 13 - 56

Subramanian, C.S., Rajagopalan, S., Antonia, R.A. & Chambers, A.J.
Comparison of conditional sampling and averaging techniques in a turbulent boundary layer,
123 , 1982, 335 - 362

Hogenes, J.H.A. & Hanratty, T.J.
The use of multiple wall probes to identify coherent flow patterns in the viscous wall region,
124 , 1982, 363 - 390

Mestayer, P.
Local isotropy and anisotropy in a high-Reynolds-number turbulent layer,
125 , 1982, 475 - 503

Thomas, A.S.W. & Bull, M.K.
On the role of wall-pressure fluctuations in deterministic motions in the turbulent boundary layer,
128 , 1983, 283 - 322

Smith, C.R. & Metzler, S.P.
The characteristics of low-speed streaks in the near-wall region of a turbulent boundary layer,
129 , 1983, 27 - 54

Nikolaides, C., Lau, K.K. & Hanratty, T.J. A study of the spanwise structure of coherent eddies in the viscous wall region,
130 , 1983, 91 - 108

Blackwelder, R.F. & Haritonidis, J.H.
Scaling of the bursting frequency in turbulent boundary layers,
132 , 1983, 87 - 103

Kaneda, Y. & Leslie, D.C. Tests of subgrid models in the near-wall region using represented velocity fields,
132 , 1983, 349 - 373

Schewe, G. On the structure and resolution of wall-pressure fluctuations associated with turbulent boundary-layer flow,
134 , 1983, 311 - 328

Johansson, A.V. & Alfredsson, P.H.
Effects of imperfect spatial resolution on measurements of wall-bounded turbulent shear flows,
137 , 1983, 409 - 421

Moin, P. & Kim, J.
The structure of the vorticity field in turbulent channel flow: Analysis of instantaneous fields and statistical correlations,
155 , 1985, 441 - 464

Savas, O. & Coles, D.
Coherence measurements in synthetic turbulent boundary layers,
160 , 1985, 421 - 446

Kim, J. & Moin, P.
The structure of the vorticity field in turbulent channel flow: Part 2. Study of ensemble-averaged fields,
162 , 1986, 339 - 363

Talmon, A.M., Kunen, J.M.G. & Ooms, G.
Simultaneous flow visualization and Reynolds-stress measurement in a turbulent boundary layer,
163 , 1986, 459 - 478

Perry, A.E., Henbest, S.M. & Chong, M.S.
A theoretical and experimental study of wall turnbulence,
165 , 1986, 163 - 199

Jang, P.S., Benney, D.J. & Gran, R.L.
On the origin of streamwise vortices in a turbulent boundary layer,
169 , 1986, 109 - 123

Johansson, A.V., Her, J.-Y. & Haritonidis, J.H.
On the generation of high-amplitude wall-pressure peaks in turbulent boundary layers and spots,
175 , 1987, 119 - 142

Krishnamoorthy, L.V. & Antonia, R.A.
Temperature-dissipation measurements in a turbulent boundary layer,
176 , 1987, 265 - 281

Kim, J., Moin P. & Moser, R.J.
Turbulence statistics in fully developed channel flow at low Reynolds number,
177 , 1987, 133 - 166

Perry, A.E., Lim, K.L. & Henbest, S.M.
An experimental study of the turbulence structure in smooth- and rough- wall boundary layers,
177 , 1987, 437 - 466

Maruyama, S. & Tanaka, H.
The effect of spatial restriction on the inner-layer structure of wall turbulence,
177 , 1987, 485 - 500

Spina, E.F. & Smits, A.J.
Organized structures in a compressible, turbulent boundary layer,
182 , 1987, 85 - 109

Swearingen, J.D. & Blackwelder, R.F.
The growth and breakdown of streamwise vortices in the presence of a wall,
182 , 1987, 255 - 290

Spalart, P.R.
Direct simulation of a turbulent boundary layer up to R_theta=1410,
187 , 1988, 61 - 98

Aubry, N., Holmes, P., Lumley, J.L. & Stone, E.
The dynamics of coherent structures in the wall region of a turbulent boundary layer,
192 , 1988, 115 - 173

Antonia, R.A. & Fulachier, L.
Topology of a turbulent boundary layer with and without wall suction,
198 , 1989, 429 - 451

Asai, M. & Nishioka, M.
Origin of the peak-valley wave structure leading to wall turbulence,
208 , 1989, 1 - 23

Antonia, R.A. & Bisset, D.K.
Spanwise structure in the near-wall region of a turbulent boundary layer,
210 , 1990, 437 - 458

Antonia, R.A., Bisset, D.K. & Browne, L.W.B.
Effect of Reynolds number on the topology of the organized motion in a turbulent boundary layer,
213 , 1990, 267 - 286

Perry, A.E. & Li, J.D.
Experimental support for the attached-eddy hypothesis in zero-pressure- gradient turbulent boundary layers,
218 , 1990, 405 - 438

Klewicki, J.C. & Falco, R.E.
On accurately measuring statistics associated with small-scale structure in turbulent boundary layers using hot-wire probes,
219 , 1990, 119 - 142

Bernard, P.S. & Handler, R.A.
Reynolds stress and the physics of turbulent momentum transport,
220 , 1990, 99 - 124

Lai, Y.G. & So, R.M.C.
On near-wall turbulent flow modelling,
221 , 1990, 641 - 673

Spina, E.F., Donovan, J.F. & Smits, A.J.
On the structure of high-Reynolds-number supersonic turbulent boundary layers,
222 , 1991, 293 - 327

Johansson, A.V., Alfredsson, P.H. & Kim, J.
Evolution and dynamics of shear-layer structures in near-wall turbulence,
224 , 1991, 579 - 599

Jimenez, J. & Moin, P. The minimal flow unit in near-wall turbulence,
225 , 1991, 213 - 240

Vukoslavcevic, P., Wallace, J.M. & Balint, J.-L.
The velocity and vorticity vector fields of a turbulent boundary layer. Part 1. Simultaneous measurement by hot-wire anemometry,
228 , 1991, 25 - 51

Balint, J.-L., Wallace, J.M. & Vukoslavcevic, P.
The velocity and vorticity vector fields of a turbulent boundary layer. Part 2. Statistical properties,
228 , 1991, 53 - 86

Erm, L.P. & Joubert, P.N.
Low-Reynolds-number turbulent boundary layers,
230 , 1991, 1 - 44

Berkooz, G., Holmes, P. & Lumley, J.L.
Intermittent dynamics in simple models of the turbulent wall layer,
230 , 1991, 75 - 95

Wark, C.E. & Nagib, H.M.
Experimental investigation of coherent structures in turbulent boundary layers,
230 , 1991, 183 - 208

Lu, L.J. & Smith, C.R .
Use of flow visualization data to examine spatial-temporal velocity and burst-type characteristics in a turbulent boundary layer,
232 , 1991, 303 - 340

Morrison, J.F., Subramanian, C.S. & Bradshaw, P.
Bursts and the law of the wall in turbulent boundary layers,
241 , 1992, 75 - 108

Tsinober, A, Kit, E. & Dracos, T.
Experimental investigation of the field of velocity gradients in turbulent flows
242 , 1992, 169 - 192

Naguib, A.M. & Wark, C.E. An investigation of wall-layer dynamics using a combined temporal filtering and correlation technique,
243 , 1992, 541 - 560

Sanghi, S. & Aubry, N.
Mode interaction models for near-wall turbulence,
247 , 1993, 455 - 488

Jimenez, J. & Orlandi, P..,
The rollup of a vortex layer near a wall,
248 , 1993, 297 - 313

Durbin, P.A.
A Reynolds stress model for near-wall turbulence,
249 , 1993, 465 - 498

Bernard, P.S., Thomas, J.M. & Handler, R.A.
Vortex dynamics and the production of Reynolds stress,
253 , 1993, 385 - 419

Choi, H., Moin, P. & Kim, J.
Direct numerical simulation of turbulent flow over riblets,
262 , 1993, 503 - 110

Choi, H., Moin, P. & Kim, J.
Active turbulence control for drag reduction in wall-bounded flows,
262 , 1994, 75 - 110

Saddoughi, S.G. & Veeravalli, S.V.
Local isotropy in turbulent boundary layers at high Reynolds number,
268 , 1994, 333 - 372

Antonia, R.A. & Kim, J.
Low-Reynolds-number effects on near-wall turbulence,
276 , 1994, 61 - 80

Krogstad, P.-A. & Antonia, R.A .
Structure of turbulent boundary layers on smooth and rough walls,
277 , 1994, 1 - 21

Hamilton, J.M., Kim, J. & Waleffe, F.
Regeneration mechanisms of near-wall turbulence structures,
287 , 1995, 317 - 348

Jovanovic, J., Ye, Q.-Y. & Durst, F.
Statistical interpretation of the turbulent dissipation rate in wall-bounded flows,
293 , 1995, 321 - 347

Perot, B. & Moin, P.
Shear-free turbulent boundary layers. Part 1. Physical insights into near-wall turbulence,
295 , 1995, 199 - 227

Perot, B. & Moin, P.
Shear-free turbulent boundary layers. Part 2. New concepts for Reynolds stress modelling of inhomogeneous flows,
295 , 1995, 229 - 245

Durst, F., Jovanovic, J. & Sender, J.
LDA measurements in the near-wall region of a turbulent pipe flow,
295 , 1995, 305 - 335

Perry, A.E. & Marusic, I.
A wall-wake model for the turbulence structure of boundary layers. Part 1. Extension of the attached eddy hypothesis,
298 , 1995, 361 - 388

Marusic, I. & Perry, A.E.
A wall-wake model for the turbulence structure of boundary layers. Part 2. Further experimental support,
298 , 1995, 389 - 407

Nagano, Y. & Tagawa, M.
Coherent motions and heat transfer in a wall turbulent shear flow,
305 , 1995, 127 - 157

Andreopoulos, J. & Agui, J.H .
Wall-vorticity flux dynamics in a two-dimensional turbulent boundary layer,
309 , 1996, 45 - 84

Jeong, J., Hussain, F., Schoppa, W. & Kim, J.
Coherent structures near the wall in a turbulent channel flow,
332 , 1997, 185 - 214

Aronson, D., Johansson, A.V. & Lofdahl, L.
Shear-free turbulence near a wall,
338 , 1997, 363 - 385

Honkan, A. & Andreopoulos, Y.
Vorticity, strain-rate and dissipation characteristics in the near-wall region of turbulent boundary layers,
350 , 1997, 29 - 96

Hartel, C. & Kleiser, L.
Analysis and modelling of subgrid-scale motions in near-wall turbulence,
356 , 1998, 327 - 352

Chong, M. ., Soria, J., Perry, A.E., Chacin, J., Cantwell, B. J. & Na, Y.
Turbulence structures of wall-bounded shear flows found using DNS data,
357 , 1998, 225 - 248

Ong, L. & Wallace, J.M.
Joint probability density analysis of the structure and dynamics of the vorticity field of a turbulent boundary layer,
367 , 1998, 291 - 328

Jimenez, J. & Pinelli, A.
The autonomous cycle of near-wall turbulence,
389 , 1999, 335 - 359

Seal, C.V. & Smith, C.R.
Visualization of a mechanism for three-dimensional interaction and near-wall eruption,
394 , 1999, 193 - 203

Chacin, J.M. & Cantwell, B.J.
Dynamics of a low Reynolds number turbulent boundary layer,
404 , 2000, 87 - 115

Barenblatt, G.I., Chorin, A.J. & Prostokishin, V.M.
Self-similar intermediate structures in turbulent boundary layers at large Reynolds numbers,
410 , 2000, 263 - 283

Guarini, S.E., Moser, R.D., Shariff, K. & Wray, A.
Direct numerical simulation of a supersonic turbulent boundary layer at Mach 2.5,
414 , 2000, 1 - 33

Adrian, R.J. , Meinhart, C.D. & Tomkins, C.D.
Vortex organization in the outer region of the turbulent boundary layer,
422 , 2000, 1 - 54

DeGraff, D.B. & Eaton, J.K.
Reynolds-number scaling of the flat-plate turbulent boundary layer,
422 , 2000, 319 - 346

Christensen, K.T. & Adrian, R.J.
Statistical evidence of hairpin vortex packets in wall turbulence,
431 , 2001, 433 - 443

Jimenez, J. & Simens, M.P.
Low-dimensional dynamics in a turbulent wall,
435 , 2001, 81 - 91

Andreopoulos, Y. & Honkan, A.
An experimental study of the dissipative and vortical motion in turbulent boundary layers,
439 , 2001, 131 - 163

Nickels, T.B. & Marusic, I.
On the different contributions of coherent structures to the spectra of a turbulent round jet and a turbulent boundary layer,
448 , 2001, 367 - 385

Schoppa, W. & Hussain, F.
Coherent structure generation in near-wall turbulence,
453 , 2002, 57 - 108

Ganapathisubramani, B., Longmire, E.K. & Marusic, I.
Characteristics of vortex packets in turbulent boundary layers,
478 , 2003, 35 - 46

Tomkins, C.D. & Adrian, R. J.
Spanwise structure and scale growth in turbulent boundary layers,
490 , 2003, 37 - 74

Dunn, D.C. & Morrison, J.F.
Anisotropy and energy flux in wall turbulence,
491 , 2003, 353 - 378

Rathnasingham, R. & Breuer, K.S.
Active control of turbulent boundary layers,
495 , 2003, 209 - 233

Lindgren, B., Osterlund, J.M. & Johansson, A.V.
Evaluation of scaling laws derived from Lie group symmetry methods in zero-pressure-gradient turbulent boundary layers,
502 , 2004, 127 - 152

Ferrante, A. & Elghobashi, S.
On the physical mechanisms of drag reduction in a spatially developing turbulent boundary layer laden with microbubbles,
503 , 2004, 345 - 355

Jimenez, J., del Alamo, J.C. & Flores, O.
The large-scale dynamics of near-wall turbulence
505 , 2004, 179 - 199

Delo, C.J., Kelso, R.M. & Smits, A.J.
Three-dimensional structure of a low-Reynolds-number turbulent boundary layer,
512 , 2004, 47 - 83

Carlotti, P. & Drobinski, P.
Length scales in wall-bounded high-Reynolds-number turbulence,
516 , 2004, 239 - 264

Marati, N., Casciola, C.M. & Piva, R.
Energy cascade and spatial fluxes in wall turbulence,
521 , 2004, 191 - 215

Wei, T., Fife, P., Klewicki, J. & McMurtry, P.
Properties of the mean momentum balance in turbulent boundary layer, pipe and channel flows,
522 , 2005, 303 - 327

Ganapathisubramani, B., Hutchins, N., Hambleton, W.T, Longmire, E.K. & Marusic, I.
Investigation of large-scale coherence in a turbulent boundary layer using two-point correlations,
524 , 2005, 57 - 80

Fife, P., Wei, T., Klewicki, J. & McMurtry, P.
Stress gradient balance layers and scale hierarchies in wall-bounded turbulent flows,
532 , 2005, 165 - 189

Carlier, J. & Stanislas, M.
Experimental study of eddy structures in a turbulent boundary layer using particle image velocimetry,
535 , 2005, 143 - 188

Hutchins, N., Hambleton, W.T. & Marusic, I.
Inclined cross-stream stereo particle image velocimetry measurements in turbulent boundary layers,
541 , 2005, 21 - 54

Ferrante, A. & Elghobashi, S.
Reynolds number effect on drag reduction in a microbubble-laden spatially developing turbulent boundary layer,
543 , 2005, 93 - 106

Chernyshenko, S.I. & Baig, M.F.
The mechanism of streak formation in near-wall turbulence ,
544 , 2005, 99 - 131

Tomkins, C.D. & Adrian, R.J.
Energetic spanwise modes in the logarithmic layer of a turbulent boundary layer,
545 , 2005, 141 - 162

Kunkel, G.J. & Marusic, I.
Study of the near-wall-turbulent region of the high-Reynolds-number boundary layer using an atmospheric flow,
548 , 2006, 375 - 402

Davidson, P.A., Nickels, T.B. & Krogstad, P.-A.
The logarithmic structure function law in wall-layer turbulence,
550 , 2006, 51 - 60

Ganapathisubramani, B., Clemens, N.T. & Dolling, D.S.
Large-scale motions in a supersonic turbulent boundary layer,
556 , 2006, 271 - 282

Hambleton, W.T., Hutchins, N. & Marusic, I.
Simultaneous orthogonal-plane particle image velocimetry measurements in a turbulent boundary layer,
560 , 2006, 53 - 64

Wu, Y. & Christensen, K.T.
Population trends of spanwise vortices in wall turbulence,
568 , 2006, 55 - 76

Martin, M.P.
Direct numerical simulation of hypersonic turbulent boundary layers. Part 1. Initialization and comparison with experiments,
570 , 2007, 347 - 364

Natrajan, V.K. & Christensen, K.T.
Spatial signatures of retrograde spanwise vortices in wall turbulence,
574 , 2007, 155 - 167

Hutchins, N. & Marusic, I.
Evidence of very long meandering features in the logarithmic region of turbulent boundary layers,
579 , 2007, 1 - 28

Morris, S.C., Stolpa, S.R., Slaboch, P.E. & Klewicki, J.
Near surface particle image velocimetry measurements in a transitionally rough-wall atmospheric boundary layer,
580 , 2007, 319 - 338

Tsuji, Y., Fransson, J.H.M., Alfredsson, P.H. & Johansson, A.V.
Pressure statistics and their scaling in high-Reynolds-number turbulent boundary layers,
585 , 2007, 1 - 40

Gulitski, G., Kholmyansky, M., Kinzelbach, W., Luthi, B., Tsinober, A. & Yorish, S.
Velocity and temperature derivatives in high-Reynolds-number turbulent flows in the atmospheric surface layer.
Part 1. Facilities, methods and some general results,
589 , 2007, 57 – 81
Part 2. Accelerations and related matters,
589 , 2007, 83 – 102
Part 3. Temperature and joint statistics of temperature and velocity derivatives.,
589 , 2007, 103 - 123

Volino, R.J., Schultz, M.P. & Flack, K.A. Turbulence structure in rough- and smooth-wall boundary layers,
592 , 2007, 263 - 293

Ringuette, M.J., Wu, M. & Martin, M.P.
Coherent structures in direct numerical simulation of turbulent boundary layers at Mach 3,
594 , 2008, 59 - 69

Stanislas, M., Perret, L. & Foucaut, J.-M.
Vortical structures in the turbulent boundary layer: a possible route to a universal representation,
602 , 2008, 327 - 382

Ganapathisubramani, B.
Statistical structure of momentum sources and sinks in the outer region of a turbulent boundary layer,
606 , 2008, 225 - 237

Klewicki, J.C., Priyadarshana, P.J.A. & Metzger, M.M.
Statistical structure of the fluctuating wall pressure and its in-plane gradients at high Reynolds number,
609 , 2008, 195 - 220

Jimenez, J. & Hoyas, S.
Turbulent fluctuations above the buffer layer of wall-bounded flows,
611 , 2008, 215 - 236

Pirozzoli, S., Bernardini, M. & Grasso, F.
Characterization of coherent vortical structures in a supersonic turbulent boundary layer,
613 , 2008, 205 - 231

Dennis, D.J.C. & Nickels, T.B.
On the limitations of Taylor's hypothesis in constructing long structures in a turbulent boundary layer,
614 , 2008, 197 - 206

Jones, M.B., Nickels, T.B. & Marusic, I.
On the asymptotic similarity of the zero-pressure-gradient turbulent boundary layer,
616 , 2008, 195 - 203

Camussi, R., Robert, G. & Jacob, M.C.
Cross-wavelet analysis of wall pressure fluctuations beneath incompressible turbulent boundary layers,
617 , 2008, 11 - 30

Gerashchenko, S., Sharp, N.S., Neuscamman, S. & Warhaft, Z.
Lagrangian measurements of inertial particle accelerations in a turbulent boundary layer,
617 , 2008, 255 - 281

Cossu, C., Pujals, G. & Depardon, S.
Optimal transient growth and very large-scale structures in turbulent boundary layers,
619 , 2009, 79 - 94

Mathis, R., Hutchins, N. & Marusic, I.
Large-scale amplitude modulation of the small-scale structures in turbulent boundary layers,
628 , 2009, 311 - 337

Marusic, I.
Unravelling near walls turbulence,
630 , 2009, 1 - 4

Wu, X. & Moin, P.
Direct numerical simulation of turbulence in a nominally-zero-pressure-gradient flat-plate boundary layer,
630 , 2009, 5 - 41

Chung, D. & Pullin, D.I. Large-eddy simulation and wall modelling of turbulent channel flow,
631 , 2009, 281 - 309

Sheng, J., Malkiel, E. & Katz, J.
Buffer layer structures associated with extreme wall stress events in a smooth wall turbulent boundary layer,
633 , 2009, 17 - 60

Grosse, S. & Schroder, W.
Wall-shear stress patterns of coherent structures in turbulent duct flow,
633 , 2009, 147 - 158

Hutchins, N., Nickels, T.B., Marusic, I. & Chong, M.S.
Hot-wire spatial resolution issues in wall-bounded turbulence.,
635 , 2009, 103 - 136

Elsinga, G.E., Adrian, R.J., van Oudheusden, B.W. & Scarano, F. Three-dimensional vortex organization in a high-Reynolds-number supersonic turbulent boundary layer,
644 , 2010, 35 - 60

Pirozzoli, S., Bernardini, M. & Grasso, F.
On the dynamical relevance of coherent vortical structures in turbulent boundary layers,
648 , 2010, 325 - 349

Hultmark, M., Bailey, S.C.C. & Smits, A.J.
Scaling of near-wall turbulence in pipe flow,
649 , 2010, 103 - 113

Ahn, B.-K., Graham, W.R. & Rizzi, S.A.
A structure-based model for turbulent-boundary-layer wall pressures,
650 , 2010, 443 - 478

Jakirlic, S. & Jovanovic, J.
On unifed boundary conditions for improved predictions of near-wall turbulence,
656 , 2010, 530 - 539

Yeo, K., Kim, B.-G. & Lee, C.
On the near-wall characteristics of acceleration in turbulence,
659 , 2010, 405 - 419

Jimenez, J., Hoyas, S., Simens, M.P. & Mizuno, Y.
Turbulent boundary layers and channels at moderate Reynolds numbers,
657 , 2010, 335 - 360

Schlatter, P. & Orlu, R Assessment of direct numerical simulation data of turbulent boundary layers,
659 , 2010, 116 - 126

Wu, X.
Establishing the generality of three phenomena using a boundary layer with free-stream passing wakes,
664 , 2010, 193 - 219

Oweis, G.F., Winkel, E.S, Cutbrith, J.M., Ceccio, S.L., Perlin, M. & Dowling, D.R.
The mean velocity profile of a smooth-flat-plate turbulent boundary layer at high Reynolds number,
665 , 2010, 357 - 381

Guala, M., Metzger, M. & McKeon, B.J.
Interactions within the turbulent boundary layer at high Reynolds number,
666 , 2011, 573 - 604

Duan, L., Beekman, I. & Martin, M.P.
Direct numerical simulation of hypersonic turbulent boundary layers. Part 3: Effect of Mach number,
672 , 2011, 245 - 267

Lee, J.H. & Sung, H.J.
Very-large-scale motions in a turbulent boundary layer,
673 , 2011, 80 – 120

Dennis, D.J.C. & Nickels, T.B.
Experimental measurement of large-scale three-dimensional structures in a turbulent boundary layer. Part 1: Vortex packets,
673 , 2011, 180 - 217

Dennis, D.J.C. & Nickels, T.B.
Experimental measurement of large-scale three-dimensional structures in a turbulent boundary layer. Part 2: Long structures,
673 , 2011, 218 - 244

Hutchins, N., Monty, J.P., Ganapathisubramani, B., Ng, H.C.H. & Marusic, I.
Three-dimensional conditional structure of a high-Reynolds-number turbulent boundary layer,
673 , 2011, 255 - 285

Smits, A.J., Monty, J., Hultmark, M., Bailey, S.C.C., Hutchins, N. & Marusic, I.
Spatial resolution correction for wall-bounded turbulence measurements,
676 , 2011, 41 - 53

Physics of Fluids and Physics of Fluids A (1959 – Present)

Turbulent Boundary Layer Measurements at Mach Numbers from 8 to 10
F. K. Hill
Phys. Fluids **2**, 668 (1959)

Patterns in Turbulent Flow in the Wall-Adjacent Region
F. M. Richardson and K. O. Beatty
Phys. Fluids **2**, 718 (1959)

Spectral Energy Budget in Wall Turbulence
J. L. Lumley
Phys. Fluids **7**, 190 (1964)

The Turbulent Boundary Layer in a Compressible Fluid
Donald Coles
Phys. Fluids **7**, 1403 (1964)

Structure of the Turbulent Boundary Layer
Leslie S. G. Kovasznay
Phys. Fluids **10**, S25 (1967)

Study of Turbulence Close to a Solid Wall
Thomas J. Hanratty
Phys. Fluids **10**, S126 (1967)

Statistical Theory of Wall Turbulence
Michio Ohji
Phys. Fluids **10**, S153 (1967)

Joint Density Functions of Turbulent Variables in the Atmospheric Boundary Layer

J. Z. Holland
Phys. Fluids **10**, S220 (1967)

Structure of the Turbulent Boundary Layer on a Smooth Wall

S. J. Kline and W. C. Reynolds
Phys. Fluids **10**, S304 (1967)

Correlation Measurements and the Large Eddies of a Turbulent Boundary Layer

D. J. Tritton
Phys. Fluids **10**, S308 (1967)

Viscous Sublayer and Adjacent Wall Region in Turbulent Pipe Flow

Henry P. Bakewell and John L. Lumley
Phys. Fluids **10**, 1880 (1967)

Mean Period of the Turbulent Production Mechanism in a Boundary Layer

John Laufer and M. A. Badri Narayanan
Phys. Fluids **14**, 182 (1971)

Statistical Characteristics of Reynolds Stress in a Turbulent Boundary Layer

A. K. Gupta and R. E. Kaplan
Phys. Fluids **15**, 981 (1972)

Time Scales and Correlations in a Turbulent Boundary Layer

Ron F. Blackwelder and Leslie S. G. Kovasznay
Phys. Fluids **15**, 1545 (1972)

Measurements of Reynolds Shear Stress Fluctuations in a Turbulent Boundary Layer

R. A. Antonia
Phys. Fluids **15**, 1669 (1972)

Turbulent energy production, dissipation, and transfer

Robert S. Brodkey, Stavros G. Nychas, Joseph L. Taraba, and James M. Wallace
Phys. Fluids **16**, 2010 (1973)

Comment on “Statistical characteristics of Reynolds stress in a turbulent boundary layer”
S. Corrsin
Phys. Fluids **16**, 341 (1973)

Comments on “Statistical characteristics of Reynolds stress in a turbulent boundary layer”
J. C. Wyngaard and Y. Izumi
Phys. Fluids **16**, 455 (1973

Probability distributions and correlations in a turbulent boundary layer
François N. Frenkiel and Philip S. Klebanoff
Phys. Fluids **16**, 725 (1973)

Comments on “Statistical characteristics of Reynolds stress in a turbulent boundary layer”
R. A. Antonia, J. D. Atkinson, and R. E. Luxton
Phys. Fluids **16**, 956 (1973)

Mean velocity and shear stress distributions in turbulent boundary layers
A. E. Perry and W. H. Schofield
Phys. Fluids **16**, 2068 (1973)

Pressure perturbation of a turbulent boundary layer
R. F. Blackwelder and H. H. W. Woo
Phys. Fluids **17**, 515 (1974)

Reply to comments by P. Bradshaw
Robert S. Brodkey, Joseph L. Taraba, Stavros G. Nychas, and James M. Wallace
Phys. Fluids **17**, 2150 (1974)

’’Bursting’’ frequencies obtained from wall shear stress fluctuations in a turbulent boundary layer
J. H. Strickland and Roger L. Simpson
Phys. Fluids **18**, 306 (1975)

High frequency wall‐pressure fluctuations in turbulent boundary layers
M. K. Bull and A. S. W. Thomas
Phys. Fluids **19**, 597 (1976)

Local anisotropy in heated and cooled turbulent boundary layers
Patrice G. Mestayer, Carl H. Gibson, Michel F. Coantic, and Anandkumar S. Patel
Phys. Fluids **19**, 1279 (1976)

Reynolds stress and joint probability density distributions in the u-v plane of a turbulent channel flow
James M. Wallace and Robert S. Brodkey
Phys. Fluids **20**, 351 (1977)

Structure of temperature fluctuations in a turbulent boundary layer
R. A. Antonia and H. Q. Danh
Phys. Fluids **20**, 1050 (1977)

Temperature dissipation fluctuations in a turbulent boundary layer
K. R. Sreenivasan, R. A. Antonia, and H. Q. Danh
Phys. Fluids **20**, 1238 (1977)

Survey and new measurements of turbulent structure near the wall
William W. Willmarth and Thomas J. Bogar
Phys. Fluids **20**, S9 (1977)

Turbulent fluctuations in the viscous wall region for Newtonian and drag reducing fluids
Thomas J. Hanratty, Larry G. Chorn, and Dimitrios T. Hatziavramidis
Phys. Fluids **20**, S112 (1977)

Coherent motions in the outer region of turbulent boundary layers
R. E. Falco
Phys. Fluids **20**, S124 (1977)

Investigation of pressure fluctuations beneath a turbulent boundary layer by means of an optical method
A. Dinkelacker, M. Hessel, G. E. A. Meier, and G. Schewe
Phys. Fluids **20**, S216 (1977)

Vorticity and turbulence production in pattern recognized turbulent flow structures
Helmut Eckelmann, Stavros G. Nychas, Robert S. Brodkey, and James M. Wallace
Phys. Fluids **20**, S225 (1977)

Large structure in a turbulent boundary layer
Garry L. Brown and Andrew S. W. Thomas
Phys. Fluids **20**, S243 (1977)

Temperature dissipation fluctuations in a turbulent boundary layer
K. R. Sreenivasan, H. Q. Danh, and R. A. Antonia
Phys. Fluids **20**, S288 (1977)

Log-normality of temperature dissipation in a turbulent boundary layer
R. A. Antonia and K. R. Sreenivasan
Phys. Fluids **20**, 1800 (1977)

Behavior of the three fluctuating velocity components in the wall region of a turbulent channel flow
Hans-Peter Kreplin and Helmut Eckelmann
Phys. Fluids **22**, 1233 (1979)

Skewness of spatial derivatives of temperature in a turbulent boundary layer
R. A. Antonia and C. W. Van Atta
Phys. Fluids **22**, 2430 (1979)

Large structure with a characteristic upstream interface in turbulent boundary layers
Promode Bandyopadhyay
Phys. Fluids **23**, 2326 (1980)

Turbulent boundary layer at low Reynolds number
L. P. Purtell, P. S. Klebanoff, and F.T. Buckley
Phys. Fluids **24**, 802 (1981)

Use of a quadrant analysis technique to identify coherent structures in a turbulent boundary layer
S. Rajagopalan and R. A. Antonia
Phys. Fluids **25**, 949 (1982)

A model for the skewness of the temperature derivative in a turbulent boundary layer
C. S. Subramanian and R. A. Antonia
Phys. Fluids **25**, 957 (1982)

Spanwise correlation of temperature in a turbulent boundary layer
S. Rajagopalan, C. S. Subramanian, R. A. Antonia, and A. J. Chambers
Phys. Fluids **25**, 1144 (1982)

Period between bursting in turbulent boundary layers
Promode R. Bandyopadhyay
Phys. Fluids **25**, 1751 (1982)

Observation of streamwise rotation in the near-wall region of a turbulent boundary layer
C. R. Smith and S. P. Schwartz
Phys. Fluids **26**, 641 (1983)

Asymptotic near-wall stress dissipation rates in a turbulent flow
B. E. Launder and W. C. Reynolds
Phys. Fluids **26**, 1157 (1983)

On the structure of wall-bounded turbulent flows
John Kim
Phys. Fluids **26**, 2088 (1983)

Analogies between transitional and turbulent boundary layers
Ron F. Blackwelder
Phys. Fluids **26**, 2807 (1983)

Conditional averages associated with the fine structure in a turbulent boundary layer
S. Rajagopalan and R. A. Antonia
Phys. Fluids **27**, 1966 (1984)

Turbulent normal velocity fluctuations close to a wall
Douglas S. Finnicum and Thomas J. Hanratty
Phys. Fluids **28**, 1654 (1985)

Second‐order modeling of near‐wall turbulence
T-H. Shih and J. L. Lumley
Phys. Fluids **29**, 971 (1986)

Coherent structures in a turbulent boundary layer. Part 1: Generation of ‘‘artificial’’ bursts
Mohamed Gad-el-Hak and A. K. M. Fazlé Hussain
Phys. Fluids **29**, 2124 (1986)

The wall region of a turbulent boundary layer
W. R. C. Phillips
Phys. Fluids **30**, 2354 (1987)

Modeling the viscous wall region
Karam Anwar Azab and John B. McLaughlin
Phys. Fluids **30**, 2362 (1987)

Scaling of the bursting frequency in turbulent boundary layers at low Reynolds numbers
John Kim and Philippe R. Spalart
Phys. Fluids **30**, 3326 (1987)

Scaling of the ‘‘bursting’’ period in turbulent boundary layer and duct flows
D. A. Shah and R. A. Antonia
Phys. Fluids A **1**, 318 (1989)

Reynolds number scaling of turbulent diffusivity in wall flows
Victor Yakhot
Phys. Fluids **31**, 709 (1988)

The fluctuating wall‐shear stress and the velocity field in the viscous sublayer
P. Henrik Alfredsson, Arne V. Johansson, Joseph H. Haritonidis, and Helmut Eckelmann
Phys. Fluids **31**, 1026 (1988)

A model for near‐wall turbulence
Joseph H. Haritonidis
Phys. Fluids A **1**, 302 (1989)

On the validity of Taylor's hypothesis for wall‐bounded flows
Ugo Piomelli, Jean-Louis Balint, and James M. Wallace
Phys. Fluids A **1**, 609 (1989)

On the shape and dynamics of wall structures in turbulent channel flow
Yann G. Guezennec, Ugo Piomelli, and John Kim
Phys. Fluids A **1**, 764 (1989)

Stochastic estimation of coherent structures in turbulent boundary layers
Y. G. Guezennec
Phys. Fluids A **1**, 1054 (1989)

Velocity–vorticity correlations related to the gradients of the Reynolds stresses in parallel turbulent wall flows
J. C. Klewicki
Phys. Fluids A **1**, 1285 (1989)

Forces acting on a low‐velocity region within a turbulent boundary layer
Alan L. Kistler and Theodore Markis
Phys. Fluids A **1**, 1883 (1989)

The outer region of a turbulent boundary layer
W. R. C. Phillips and J. T. Ratnanather
Phys. Fluids A **2**, 427 (1990)

On the asymmetry of structures in turbulent boundary layers
W. C. Choi and Y. G. Guezennec
Phys. Fluids A **2**, 628 (1990)

On the space‐time characteristics of wall‐pressure fluctuations
Haecheon Choi and Parviz Moin
Phys. Fluids A **2**, 1450 (1990)

On the sign of the instantaneous spanwise vorticity component in the near-wall region of turbulent boundary layers
J. C. Klewicki, C. P. Gendrich, J. F. Foss, and R. E. Falco
Phys. Fluids A **2**, 1497 (1990)

Similarity between turbulent kinetic energy and temperature spectra in the near-wall region
R. A. Antonia and J. Kim
Phys. Fluids A **3**, 989 (1991)

Is intermittent motion of outer flow in the turbulent boundary layer deterministic chaos?
Yoshiyuki Tsuji, Katsuya Honda, Ikuo Nakamura, and Shinichi Sato
Phys. Fluids A **3**, 1941 (1991)

Spectral features of wall pressure fluctuations beneath turbulent boundary layers
Theodore M. Farabee and Mario J. Casarella
Phys. Fluids A **3**, 2410 (1991)

Convection velocity in supersonic turbulent boundary layers
Eric F. Spina, John F. Donovan, and Alexander J. Smits
Phys. Fluids A **3**, 3124 (1991)

Coherence and chaos in a model of turbulent boundary layer
Xiang Zhou and L. Sirovich
Phys. Fluids A **4**, 2855 (1992)

Structure of the velocity field associated with the spanwise vorticity in the wall region of a turbulent boundary layer
S. Rajagopalan and R. A. Antonia
Phys. Fluids A **5**, 2502 (1993)

Zero crossings of velocity fluctuations in turbulent boundary layers
P. Kailasnath and K. R. Sreenivasan
Phys. Fluids A **5**, 2879 (1993)

Statistical analysis of the dynamic equations for higher-order moments in turbulent wall bounded flows
J. Jovanović, F. Durst, and T. G. Johansson
Phys. Fluids A **5**, 2886 (1993)

Normalization based on the active motion in a turbulent boundary layer
R. A. Antonia, F. Anselmet, and L. Fulachier
Phys. Fluids A **5**, 3007 (1993)

Turbulent transport in wall-bounded flows. Evaluation of model coefficients using direct numerical simulation
J. B. Cazalbou and P. Bradshaw
Phys. Fluids A **5**, 3233 (1993)

A note on turbulent energy dissipation in the viscous wall region
Peter Bradshaw and J. Blair Perot
Phys. Fluids A **5**, 3305 (1993)

On the relation of near-wall streamwise vortices to wall skin friction in turbulent boundary layers
Arthur G. Kravchenko, Haecheon Choi, and Parviz Moin
Phys. Fluids A **5**, 3307 (1993)

Vortical motion contributions to stress transport in turbulent boundary layers
J. C. Klewicki, J. A. Murray, and R. E. Falco
Phys. Fluids **6**, 277 (1994)

Flow visualization of the three-dimensional, time-evolving structure of a turbulent boundary layer
José E. Goldstein and Alexander J. Smits
Phys. Fluids **6**, 577 (1994)

On the generation of turbulent wall friction
Paolo Orlandi and Javier Jiménez
Phys. Fluids **6**, 634 (1994

On the structure and control of near wall turbulence
Javier Jiménez
Phys. Fluids **6**, 944 (1994)

Interaction of adjacent bursts in the wall region
B. D. Coller, P. Holmes, and J. L. Lumley
Phys. Fluids **6**, 954 (1994)

Fluctuation spectra and variances in convective turbulent boundary layers: A reevaluation of old models
A. M. Yaglom
Phys. Fluids **6**, 962 (1994)

Streamwise structures in a turbulent supersonic boundary layer
M. Samimy, S. A. Arnette, and G. S. Elliott
Phys. Fluids **6**, 1081 (1994)

Wall turbulence closure based on classical similarity laws and the attached eddy hypothesis
A. E. Perry, I. Marušić, and J. D. Li
Phys. Fluids **6**, 1024 (1994)

Energy transfer in numerically simulated wall‐bounded turbulent flows
J. Andrzej Domaradzki, Wei Liu, Carlos Härtel, and Leonhard Kleiser
Phys. Fluids **6**, 1583 (1994)

Reply to ''Observations regarding 'Coherence and chaos in a model of turbulent boundary layer' by X. Zhou and L. Sirovich [Phys. Fluids A 4, 2855 (1992)]''
L. Sirovich and X. Zhou
Phys. Fluids **6**, 1579 (1994)

Observations regarding ''Coherence and chaos in a model of turbulent boundary layer'' by X. Zhou and L. Sirovich [Phys. Fluids A 4, 2855 (1992)]
G. Berkooz, P. Holmes, J. L. Lumley, N. Aubry, and E. Stone
Phys. Fluids **6**, 1574 (1994)

A comparison study of conditional‐sampling methods used to detect coherent structures in turbulent boundary layers
Y. M. Yuan and M. R. Mokhtarzadeh‐Dehghan
Phys. Fluids **6**, 2038 (1994)

Anisotropy of the dissipation tensor in a turbulent boundary layer
R. A. Antonia, L. Djenidi, and P. R. Spalart
Phys. Fluids **6**, 2475 (1994)

Reynolds number similarity of orthogonal decomposition of the outer layer of turbulent wall flow
Z.-C. Liu, R. J. Adrian, and T. J. Hanratty
Phys. Fluids **6**, 2815 (1994)

Funnel‐shaped vortical structures in wall turbulence
D. Kaftori, G. Hetsroni, and S. Banerjee
Phys. Fluids **6**, 3035 (1994)

The enstrophy equation budget of bounded turbulent shear flows
Joseph J. Gorski, James M. Wallace, and Peter S. Bernard
Phys. Fluids **6**, 3197 (1994)

The fractal aspect of an isovelocity set and its relationship to bursting phenomena in the turbulent boundary layer
Yoshiyuki Tsuji and Ikuo Nakamura
Phys. Fluids **6**, 3429 (1994)

Quadrant analysis in a heated‐wall supersonic boundary layer
J. Deleuze, N. Audiffren, and M. Elena
Phys. Fluids **6**, 4031 (1994)

On the existence of uniform momentum zones in a turbulent boundary layer
Carl D. Meinhart and Ronald J. Adrian
Phys. Fluids **7**, 694 (1995)

Viscous sublayer flow visualizations at $R\theta \approx 1\,500\,000$
J. C. Klewicki, M. M. Metzger, E. Kelner, and E. M. Thurlow
Phys. Fluids **7**, 857 (1995)

Comparative measurements in the canonical boundary layer at $Re\delta 2 \leq 6\times 104$ on the wall of the German–Dutch windtunnel
H. H. Fernholz, E. Krause, M. Nockemann, and M. Schober
Phys. Fluids **7**, 1275 (1995)

Subgrid‑scale energy transfer and near‑wall turbulence structure
Ugo Piomelli, Yunfang Yu, and Ronald J. Adrian
Phys. Fluids **8**, 215 (1996)

A low‑shear turbulent boundary layer
Jennifer Hamelin and Amy E. Alving
Phys. Fluids **8**, 789 (1996)

Hierarchical order in wall‑bounded shear turbulence
Fernando Carbone and Nadine Aubry
Phys. Fluids **8**, 1061 (1996)

Probability density function and Reynolds‑stress modeling of near‑wall turbulent flows
Thomas D. Dreeben and Stephen B. Pope
Phys. Fluids **9**, 154 (1997)

System identification and control of a turbulent boundary layer
Ruben Rathnasingham and Kenneth S. Breuer
Phys. Fluids **9**, 1867 (1997)

Coherent vortex model for surface pressure fluctuations induced by the wall region of a turbulent boundary layer
Manhar R. Dhanak, Ann P. Dowling, and Chao Si
Phys. Fluids **9**, 2716 (1997)

On the existence of uniform momentum zones in a turbulent boundary layer Similarity law for the streamwise turbulence intensity in zero-pressure-gradient turbulent boundary layers
I. Marusic, A. K. M. Uddin, and A. E. Perry
Phys. Fluids **9**, 3718 (1997)

Convection velocities in a turbulent boundary layer
P.-Å. Krogstad, J. H. Kaspersen, and S. Rimestad
Phys. Fluids **10**, 949 (1998)

Scaling of the intermediate region in wall-bounded turbulence: The power law
G. I. Barenblatt and Alexandre J. Chorin
Phys. Fluids **10**, 1043 (1998)

A large-scale control strategy for drag reduction in turbulent boundary layers
Wade Schoppa and Fazle Hussain
Phys. Fluids **10**, 1049 (1998)

Reconstructing the flow in the wall region from wall sensors
Bérengère Podvin and John Lumley
Phys. Fluids **10**, 1182 (1998)

Observed mechanisms for turbulence attenuation and enhancement in opposition-controlled wall-bounded flows
E. P. Hammond, T. R. Bewley, and P. Moin
Phys. Fluids **10**, 2421 (1998)

Very large-scale motions in the outer layer
K. C. Kim and R. J. Adrian.
Phys. Fluids **11**, 417 (1999)

Probability density function in the log-law region of low Reynolds number turbulent boundary layer
Yoshiyuki Tsuji and Ikuo Nakamura
Phys. Fluids **11**, 647 (1999)

Intermittency and scaling laws for wall bounded turbulence
R. Benzi, G. Amati, C. M. Casciola, F. Toschi, and R. Piva
Phys. Fluids **11**, 1284 (1999)

Space–time characteristics of the wall shear-stress fluctuations in a low-Reynolds-number channel flow
Sejeong Jeon, Haecheon Choi, Jung Yul Yoo, and Parviz Moin
Phys. Fluids **11**, 3084 (1999)

Relationship between wall pressure and velocity-field sources
Peter A. Chang, Ugo Piomelli, and William K. Blake
Phys. Fluids **11**, 3434 (1999)

A note on the overlap region in turbulent boundary layers
Jens M. Österlund, Arne V. Johansson, Hassan M. Nagib, and Michael H. Hites
Phys. Fluids **12**, 1 (2000)

Turbulent boundary layer control utilizing the Lorentz force
Timothy W. Berger, John Kim, Changhoon Lee, and Junwoo Lim
Phys. Fluids **12**, 631 (2000)

A linear process in wall-bounded turbulent shear flows

John Kim and Junwoo Lim
Phys. Fluids **12**, 1885 (2000)

Comment on "A note on the intermediate region in turbulent boundary layers" [Phys. Fluids 12, 2159 (2000)]

Jens M. Österlund, Arne V. Johansson, and Hassan M. Nagib
Phys. Fluids **12**, 2360 (2000)

A note on the intermediate region in turbulent boundary layers

G. I. Barenblatt, A. J. Chorin, and V. M. Prostokishin
Phys. Fluids **12**, 2159 (2000)

Direct numerical simulation of turbulent thermal boundary layers

Hojin Kong, Haecheon Choi, and Joon Sik Lee
Phys. Fluids **12**, 2555 (2000)

Velocity derivatives in the atmospheric surface layer at $Re_\lambda = 10^4$

M. Kholmyansky, A. Tsinober and S. Yorish
Phys. Fluids 13, 311 (2001)

A comparative study of near-wall turbulence in high and low Reynolds number boundary layers

M. M. Metzger and J. C. Klewicki
Phys. Fluids **13**, 692 (2001)

On the role of large-scale structures in wall turbulence

Ivan Marusic
Phys. Fluids **13**, 735 (2001)

Scaling the near-wall axial turbulent stress in the zero pressure gradient boundary layer

M. M. Metzger, J. C. Klewicki, K. L. Bradshaw, and R. Sadr
Phys. Fluids **13**, 1819 (2001)

Reynolds number effects in the near-wall region of turbulent channel flows

M. Fischer, J. Jovanović, and F. Durst
Phys. Fluids **13**, 1755 (2001)

Stochastic estimation and flow sources associated with surface pressure events in a turbulent boundary layer
A. M. Naguib, C. E. Wark, and O. Juckenhöfel
Phys. Fluids **13**, 2611 (2001)

Experimental assessment of a new form of scaling law for near-wall turbulence
B. Jacob, A. Olivieri, and C. M. Casciola
Phys. Fluids **14**, 481 (2002)

Relationship between wall pressure fluctuations and streamwise vortices in a turbulent boundary layer
Joongnyon Kim, Jung-Il Choi, and Hyung Jin Sung
Phys. Fluids **14**, 898 (2002)

Evaluation of the Barenblatt–Chorin–Prostokishin power law for turbulent boundary layers
Ronald L. Panton
Phys. Fluids **14**, 1806 (2002)

Varicose instabilities in turbulent boundary layers
M. Skote, J. H. Haritonidis, and D. S. Henningson
Phys. Fluids **14**, 2309 (2002)

Viscous effects in control of near-wall turbulence
Yong Chang, S. Scott Collis, and Srinivas Ramakrishnan
Phys. Fluids **14**, 4069 (2002)

Some dynamical properties of a differential model for the bursting cycle in the near-wall turbulence
A. Porporato and L. Ridolfi
Phys. Fluids **14**, 4278 (2002)

Contribution of Reynolds stress distribution to the skin friction in wall-bounded flows
Koji Fukagata, Kaoru Iwamoto, and Nobuhide Kasagi
Phys. Fluids **14**, L73 (2002)

Power laws for turbulent boundary layer flow
Joseph B. Keller
Phys. Fluids **14**, L89 (2002)

Analysis of the small-scale structure of turbulence on smooth and rough walls
D. Poggi, A. Porporato, and L. Ridolfi
Phys. Fluids **15**, 35 (2003)

Control of turbulent boundary layers
John Kim
Phys. Fluids **15**, 1093 (2003)

Direct numerical simulation and analysis of a spatially evolving supersonic turbulent boundary layer at M = 2.25
S. Pirozzoli, F. Grasso, and T. B. Gatski
Phys. Fluids **16**, 530 (2004)

Probability density function computation of turbulent flows with a new near-wall model
Marta Wacławczyk, Jacek Pozorski, and Jean-Pierre Minier
Phys. Fluids **16**, 1410 (2004)

Publisher's Note: "Probability density function computation of turbulent flows with a new near-wall model" [Phys. Fluids 16, 1410 (2004)]
Marta Wacławczyk, Jacek Pozorski, and Jean-Pierre Minier
Phys. Fluids **16**, 2143 (2004)

Universality of probability density distributions in the overlap region in high Reynolds number turbulent boundary layers
Björn Lindgren, Arne V. Johansson, and Yoshiyuki Tsuji
Phys. Fluids **16**, 2587 (2004)

Assessment of inflow boundary conditions for compressible turbulent boundary layers
Sheng Xu and M. Pino Martin
Phys. Fluids **16**, 2623 (2004)

On turbulent energy production in wall bounded flows
R. Gurka, G. Hetsroni, A. Liberzon, N. Nikitin, and A. Tsinober
Phys. Fluids **16**, 2704 (2004)

Flow field properties local to near-wall shear layers in a low Reynolds number turbulent boundary layer
J. C. Klewicki and C. R. Hirschi
Phys. Fluids **16**, 4163 (2004)

Study of the motions contributing to the Reynolds stress in high and low Reynolds number turbulent boundary layers
P. J. A. Priyadarshana and J. C. Klewicki
Phys. Fluids **16**, 4586 (2004)

Characterization of near-wall turbulence in terms of equilibrium and “bursting” solutions
Javier Jiménez, Genta Kawahara, Mark P. Simens, Masato Nagata, and Makoto Shiba
Phys. Fluids **17**, 015105 (2005)

Statistical properties of vortical structures with spanwise vorticity in zero pressure gradient turbulent boundary layers
R. Camussi and F. Di Felice
Phys. Fluids **18**, 035108 (2006)

Experimental investigation of vortex properties in a turbulent boundary layer
Bharathram Ganapathisubramani, Ellen K. Longmire, and Ivan Marusic
Phys. Fluids **18**, 055105 (2006)

The role of coherent structures in subgrid-scale energy transfer within the log layer of wall turbulence
V. K. Natrajan and K. T. Christensen
Phys. Fluids **18**, 065104 (2006)

A refined interpretation of the logarithmic structure function law in wall layer turbulence
P. A. Davidson, P.-Å. Krogstad, and T. B. Nickels
Phys. Fluids **18**, 065112 (2006)

Stochastic simulation of Lagrangian trajectories in near-wall turbulence
A. M. Reynolds
Phys. Fluids **18**, 075107 (2006)

The spatial relationships between dissipation and production rates and vortical structures in turbulent boundary and mixing layers
James Diorio, Douglas H. Kelley, and James M. Wallace
Phys. Fluids **19**, 035101 (2007)

Reynolds number effect on the dissipation function in wall-bounded flows
F. Laadhari
Phys. Fluids **19**, 038101 (2007)

Hairpin vortex organization in wall turbulence
Ronald J. Adrian
Phys. Fluids **19**, 041301 (2007)

The effect of subgrid-scale models on the near wall vortices: A priori tests
Gwenaël Hauët, Carlos B. da Silva, and José C. F. Pereira
Phys. Fluids **19**, 051702 (2007)

Asymptotic analysis of the constant pressure turbulent boundary layer
Thomas S. Lundgren
Phys. Fluids **19**, 055105 (2007)

Statistical properties of streamwise velocity in a supersonic turbulent boundary layer
B. Ganapathisubramani
Phys. Fluids **19**, 098108 (2007)

Dissipation equals production in the log layer of wall-induced turbulence
J. J. H. Brouwers
Phys. Fluids **19**, 101702 (2007)

Response of a spatially developing turbulent boundary layer to active control strategies in the framework of opposition control
Mathieu Pamiès, Eric Garnier, Alain Merlen, and Pierre Sagaut
Phys. Fluids **19**, 108102 (2007)

Self-consistent high-Reynolds-number asymptotics for zero-pressure-gradient turbulent boundary layers
Peter A. Monkewitz, Kapil A. Chauhan, and Hassan M. Nagib
Phys. Fluids **19**, 115101 (2007)

Scaling of mixed structure functions in turbulent boundary layers
Boris Jacob, Carlo Massimo Casciola, Alessandro Talamelli, and P. Henrik Alfredsson
Phys. Fluids **20**, 045101 (2008)

Local isotropy of the velocity and vorticity fields in a boundary layer at high Reynolds numbers
James M. Wallace and Lawrence Ong
Phys. Fluids **20**, 101506 (2008)

Comparison of mean flow similarity laws in zero pressure gradient turbulent boundary layers
Direct intervention of hairpin structures for turbulent boundary-layer control
Yong-Duck Kang, Kwing-So Choi, and Ho Hwan Chun
Phys. Fluids **20**, 101517 (2008)

A filtered-wall formulation for large-eddy simulation of wall-bounded turbulence
Amitabh Bhattacharya, Arup Das, and Robert D. Moser
Phys. Fluids **20**, 115104 (2008)

A proper-orthogonal-decomposition–based model for the wall layer of a turbulent channel flow
Bérengère Podvin
Phys. Fluids **21**, 015111 (2009)

Turbulent boundary layers up to Reθ = 2500 studied through simulation and experiment
P. Schlatter, R. Örlü, Q. Li, G. Brethouwer, J. H. M. Fransson, A. V. Johansson, P. H. Alfredsson, and D. S. Henningson
Phys. Fluids **21**, 051702 (2009)

Near-wall similarity between velocity and scalar fluctuations in a turbulent channel flow
Hiroyuki Abe and Robert Anthony Antonia
Phys. Fluids **21**, 025109 (2009)

Effects of large-scale free stream turbulence on a turbulent boundary layer
N. S. Sharp, S. Neuscamman, and Z. Warhaft
Phys. Fluids **21**, 095105 (2009)

Comparison of large-scale amplitude modulation in turbulent boundary layers, pipes, and channel flows
Romain Mathis, Jason P. Monty, Nicholas Hutchins, and Ivan Marusic
Phys. Fluids **21**, 111703 (2009)

Evolution and lifetimes of flow topology in a turbulent boundary layer
G. E. Elsinga and I. Marusic
Phys. Fluids **22**, 015102 (2010)

Designing large-eddy simulation of the turbulent boundary layer to capture law-of-the-wall scaling
James G. Brasseur and Tie Wei
Phys. Fluids **22**, 021303 (2010)

Transitional and turbulent boundary layer with heat transfer
Xiaohua Wu and Parviz Moin
Phys. Fluids **22**, 085105 (2010)

A numerical study of compressible turbulent boundary layers
M. Lagha, J. Kim, J. D. Eldredge, and X. Zhong
Phys. Fluids **23**, 015106 (2011)

On the fluctuating wall-shear stress in zero pressure-gradient turbulent boundary layer flows
Ramis Örlü and Philipp Schlatter
Phys. Fluids **23**, 021704 (2011)

Inner/outer layer interactions in turbulent boundary layers: A refined measure for the large-scale amplitude modulation mechanism
Matteo Bernardini and Sergio Pirozzoli
Phys. Fluids **23**, 061701 (2011)

Experiments in Fluids (1983 - Present)

Measurements of some features of turbulence in wall-proximity
R. S. Azad and S. Burhanuddin
Experiments in Fluids, 1983, Volume 1, Number 3, Pages 149-160

Influence of Reynolds number on characteristics of turbulent wall boundary layers
J. Andreopoulos, F. Durst, Z. Zaric and J. Jovanovic
Experiments in Fluids, 1984, Volume 2, Number 1, Pages 7-16

Wall pressure and its relation to turbulent structure of a boundary layer

Y. Kobashi and M. Ichijo

Experiments in Fluids, 1986, Volume 4, Number 1, Pages 49-55

Streamwise pseudo-vortical structures and associated vorticity in the near-wall region of a wall-bounded turbulent shear flow

N. Kasagi, M. Hirata and K. Nishino

Experiments in Fluids, 1986, Volume 4, Number 6, Pages 309-318

Three-component LDA measurements in a turbulent boundary layer

O. Özcan

Experiments in Fluids, 1988, Volume 6, Number 5, Pages 327-334

Comparison between outer regions of turbulent boundary layer and channel flows

M. Teitel and R. A. Antonia

Experiments in Fluids, 1991, Volume 11, Numbers 2-3, Pages 203-204

The structure of Reynolds stress in the near-wall region of a fully developed turbulent pipe flow

P. -A. Chevrin, H. L. Petrie and S. Deutsch

Experiments in Fluids, 1992, Volume 13, Number 6, Pages 405-413

RMS spanwise vorticity measurements in a turbulent boundary layer

S. Rajagopalan and R. A. Antonia

Experiments in Fluids, 1993, Volume 14, Numbers 1-2, Pages 142-144

The use of orthogonal X-wire arrays for structure investigation in a turbulent boundary layer

P-Å. Krogstad, R. A. Antonia and L. W. B. Browne

Experiments in Fluids, 1993, Volume 15, Numbers 4-5, Pages 231-239

Three-component, time-resolved velocity statistics in the wall region of a turbulent pipe flow

A. A. Fontaine and S. Deutsch

Experiments in Fluids, 1994, Volume 18, Number 3, Pages 168-173

Low-Reynolds-number effects in a turbulent boundary layer
C. Y. Ching, L. Djenidi and R. A. Antonia
Experiments in Fluids, 1995, Volume 19, Number 1, Pages 61-68

Analysis of two-point velocity measurements in near-wall flows
G. P. Romano
Experiments in Fluids, 1995, Volume 20, Number 2, Pages 68-83

Reynolds-number-dependence of the maximum in the streamwise velocity fluctuations in wall turbulence
S. Mochizuki and F. T. M. Nieuwstadt
Experiments in Fluids, 1996, Volume 21, Number 3, Pages 218-226

Effects of imperfect spatial resolution on turbulence measurements in the very near-wall viscous sublayer region
B. C. Khoo, Y. T. Chew and G. L. Li
Experiments in Fluids, 1996, Volume 22, Number 4, Pages 327-335

Advantages of using a power law in a low Rθ turbulent boundary layer
L. Djenidi, Y. Dubief and R. A. Antonia
Experiments in Fluids, 1996, Volume 22, Number 4, Pages 348-350

Near-wall structure of three-dimensional turbulent boundary layers
K. A. Flack
Experiments in Fluids, 1997, Volume 23, Number 4, Pages 335-340

Conditional correlation between a passive scalar and its dissipation in a turbulent boundary layer
A. Benaissa, J. Lemay and F. Anselmet
Experiments in Fluids, 1999, Volume 26, Number 6, Pages 488-496

Three-dimensional visualization of large structures in the turbulent boundary layer
J. W. Hoyt and R. H. J. Sellin
Experiments in Fluids, 2001, Volume 30, Number 3, Pages 295-301

Some Reynolds number effects on two- and three-dimensional turbulent boundary layers
Experiments in Fluids, 2001, Volume 31, Number 2, Pages 219-228

Quantitative visualization of the near-wall structures in a turbulent pipe flow by image correlation velocimetry
K. S. Hwang, G. X. Cui, Z. S. Zhang and B. C. Feng
Experiments in Fluids, 2002, Volume 32, Number 4, Pages 447-452

PIV study of the influence of large-scale streamwise vortices on a turbulent boundary layer
G. Di Cicca, G. Iuso, P. Spazzini and M. Onorato
Experiments in Fluids, 2002, Volume 33, Number 5, Pages 663-669

Propagation of shear-layer structures in the near-wall region of a turbulent boundary layer
L. Labraga, B. Lagraa, A. Mazouz and L. Keirsbulck
Experiments in Fluids, 2002, Volume 33, Number 5, Pages 670-676

Measurements and scaling of wall shear stress fluctuations
K. J. Colella and W. L. Keith
Experiments in Fluids, 2003, Volume 34, Number 2, Pages 253-260

Investigation of the spatio-temporal flow structure in the buffer region of a turbulent boundary layer by means of multiplane stereo PIV
C.J. Kähler
Experiments in Fluids, 2004, Volume 36, Number 1, Pages 114-130

Unsteady wall-shear measurements in turbulent boundary layers using MEMS
J.-D. Ruedi, H. Nagib, J. Österlund and P.A. Monkewitz
Experiments in Fluids, 2004, Volume 36, Number 3, Pages 393-398

Smooth and rough turbulent boundary layers at high Reynolds number
Luciano Castillo, Junghwa Seo, Horia Hangan and T. Gunnar Johansson
Experiments in Fluids, 2004, Volume 36, Number 5, Pages 759-774

Outer flow scaling of smooth and rough wall turbulent boundary layers
O. G. Akinlade, D. J. Bergstrom, M. F. Tachie and L. Castillo
Experiments in Fluids, 2004, Volume 37, Number 4, Pages 604-612

Investigation of a turbulent spot and a tripped turbulent boundary layer flow using time-resolved tomographic PIV
Andreas Schröder, Reinhard Geisler, Gerrit E. Elsinga, Fulvio Scarano and Uwe Dierksheide
Experiments in Fluids, 2008, Volume 44, Number 2, Pages 305-316

Stereoscopic PIV measurements of a turbulent boundary layer with a large spatial dynamic range
Sophie Herpin, Chong Yau Wong, Michel Stanislas and Julio Soria
Experiments in Fluids, 2008, Volume 45, Number 4, Pages 745-763

Quantitative characterization of coherent structures in the buffer layer of near-wall turbulence. Part 1: streaks
J. Lin, J. P. Laval, J. M. Foucaut and M. Stanislas
Experiments in Fluids, 2008, Volume 45, Number 6, Pages 999-1013

Double large field stereoscopic PIV in a high Reynolds number turbulent boundary layer
S. Coudert, J. M. Foucaut, J. Kostas, M. Stanislas and P. Braud, *et al*.
Experiments in Fluids, 2011, Volume 50, Number 1, Pages 1-12

Full 3D correlation tensor computed from double field stereoscopic PIV in a high Reynolds number turbulent boundary layer
Jean-Marc Foucaut, Sebastien Coudert, Michel Stanislas and Joel Delville
Experiments in Fluids, 2011, Volume 50, Number 4, Pages 839-846

Eulerian and Lagrangian views of a turbulent boundary layer flow using time-resolved tomographic PIV
A. Schröder, R. Geisler, K. Staack, G. E. Elsinga and F. Scarano, *et al*.
Experiments in Fluids, 2011, Volume 50, Number 4, Pages 1071-1091

A study of the three-dimensional spectral energy distribution in a zero pressure gradient turbulent boundary layer
J. LeHew, M. Guala and B. J. McKeon
Experiments in Fluids, Online First™, 23 May 2011

Journal of Turbulence (2000 – Present)

On coherent-vortex identification in turbulence
Yves Dubief & Franck Delcayre (2000) **1**

Active control of streak structures in wall turbulence using an actuator array producing inclined wavy disturbances
Takehiko Segawa , Yasuo Kawaguchi, Yoshihiro Kikushima & Hiro Yoshida (2002) **1**

The velocity and acceleration signatures of small-scale vortices in turbulent channel flow
Kenneth T Christensen & Ronald J Adrian (2002) **3**

The effects of the upstream conditions on a low Reynolds number turbulent boundary layer with zero pressure gradient
Luciano Castillo & T Gunnar Johansson (2002) **3**

Reynolds stress in turbulent boundary layers at high Reynolds number
Junghwa Seo, Luciano Castillo , T Gunnar Johansson & Horia Hangan (2004) **5**

Dynamics of fine scale eddy clusters in turbulent channel flows
Shin-Jeong Kang, Mamoru Tanahashi & Toshio Miyauchi (2007) **8**

Anisotropy of a turbulent boundary layer
Kunlun Liu & Richard H. Pletcher (2008) **9**

Experimental analysis of a turbulent boundary layer at high Reynolds numbers
Giovanni Aloisio, Fabio Di Felice & Giovanni P. Romano (2009) **10**

Two-point correlations in high Reynolds number flat plate turbulent boundary layers
M. Tutkun, W. K. George, J. Delville, M. Stanislas, P. B.V. Johansson, J.-M. Foucaut & S. Coudert (2009) **10**

Chasing eddies and their wall signature in DNS data of turbulent boundary layers
Clara O'Farrell & M. Pino Martín (2009) **10**

The organization of near-wall turbulence: a comparison between boundary layer SPIV data and channel flow DNS data
S. Herpin, M. Stanislas & J. Soria (2010) **11**

Multiscale edge detection and imperfect phase synchronization of the wall turbulence
Sedat Tardu (2011) **12**